Pancreatic Stellate Cells Promote Cancer Cell Proliferation, Glucose Transport, Lactate Secretion, and Gemcitabine Chemoresistance in PDAC

by

Miguel Garcia Skilbrei

Master thesis for the degree of: Master of Science
Molecular biology and biochemistry
60 points

Department of Biosciences
Faculty of Mathematics and Natural Sciences

UNIVERSITY OF OSLO

May 2021

2021

Pancreatic stellate cells promote cancer cell proliferation, glucose transport, lactate secretion, and gemcitabine chemoresistance in PDAC

Miguel Garcia Skilbrei

http://www.duo.uio.no/

Print: Reprosentralen, Universitetet i Oslo

Acknowledgements

This study was performed at the department of pharmacology and department of pathology, faculty of medicine at Rikshospitalet, Oslo University Hospital (OUS).

This study was funded by the following project: Norwegian Cancer Society (Kreftforeningen, project number: 212734-2019).

A special thanks to my supervisor Manoj Amrutkar for allowing me to be a part of this exciting project. Your teachings and guidance have been invaluable and encouraging. Thank you for your patience and for entrusting me with this study.

A huge thank you to Caroline Sophie Verbeke for allowing me to be a master student in the Pancreatic Pathology Research Group. Your kindness and feedback on presentations and paper writing have been most helpful.

Thank you, Anette Vefferstad Finstadsveen, for always being helpful with experimental setups and execution if needed. Also, a thank you to the pancreatic pathology research group (Verbeke group) for creating a good workspace and a fruitful learning environment.

A special thanks to Aina Balto, a friend and a fellow master student in the Verbeke group working on the same project, but with different cell lines. Thank you for all talks, discussions and help regarding experiments and writing

Finally, an enormous thanks to my family, first and foremost my mom Kate and grandmother Anne-Lise. Thank you for all mentally and financial help through this time. I would not be where I am today without you.

Abstract

Pancreatic ductal adenocarcinoma (PDAC) is currently one of the deadliest and most challenging cancers. PDAC has a 5-year survival of less than 10%, which is mostly due to its late detection, high metastatic potential, high degree of heterogeneity and profound resistance to existing treatment options. In recent years, pancreatic stellate cells (PSCs) were found to be a contributing factor to the development and progression of PDAC. Therefore, further knowledge on how PSCs affect cancer cells may result in better treatment options.

In this study, the conditioned medium from PSCs (PSC-CM), obtained from two different human PDACs - treatment naive (PSC-1) and neoadjuvantly treated (PSC-2) - and from a healthy donor (HPaSteC) was used. Pancreatic cancer cells (PCCs) - BxPC-3, Panc-1 and SW-1990 - exposed to the three PSC-CMs were investigated for phenotypic changes and alterations in metabolism and chemosensitivity. The cell viability and proliferation of the PCCs were investigated by MTT assays and BrdU assay, respectively. Furthermore, glucose transport experiments were performed with radioactively labeled glucose. Lactate secretion was measured using a glycolysis assay kit. Moreover, the effects of the small molecule glucose transport inhibitor NV-5440 and the chemotherapeutic agent gemcitabine on glucose transport were investigated. Lastly, western blot-based protein expression analysis and secretome analysis of the protein content of the PSC-CMs were performed.

The results show that viability and proliferation significantly increased following 72h incubation with PSC-CM compared to the control. However, glucose transport after PSC-CM exposure showed variable results. Furthermore, PSC-CM lactate secretion was increased following 72h incubation with PSC-CM as compared to nutrient-poor low glucose medium. The PCCs showed reduced chemosensitivity following incubation with PSC-CMs. Moreover, NV-5440 was successful in inhibiting glucose transport after PSC-CM exposure. Western blots and secretome analysis of PSC-CM further confirmed these results, showing that metabolic pathway proteins and carbon metabolism proteins were upregulated in PSC-CM, especially in PSC-CM from HPaSteC. Furthermore, we have demonstrated that the small molecule inhibitor NV-5440 is effective at inhibiting glucose transport in PCCs.

In conclusion, PSC-CM promotes induced viability, proliferation, glucose transport and lactate secretion in PCCs, while it reduced chemosensitivity for gemcitabine. However, marked variability is seen between the PCCs as well as between the PSC-CMs. Further research into

the impact of PSC-secreted proteins on cancer cell glucose metabolism and chemosensitivity of PCCs is needed.

Index

Acknowledgements ... 3
Abstract ... 5
1. Introduction ... 10
1.1 The pancreas: anatomy and function ... 10
1.2 Pancreatic cancer ... 11
1.3 Pancreatic ductal adenocarcinoma (PDAC) ... 12
1.4 Pancreatic tumor microenvironment ... 17
1.5 Pancreatic stellate cells (PSCs) ... 19
1.6 Cancer metabolism ... 21
1.7 Pancreatic cancer metabolism ... 23
1.8 Chemosensitivity ... 26
Aim of the study ... 29
2. Materials and methods ... 30
2.1 Aseptic conditions ... 30
2.2 Cells ... 30
2.2.1. Pancreatic cancer cell lines ... 30
2.2.2 Pancreatic stellate cell cultures (PSC-1, PSC-2 and HPaSteC) ... 30
2.3 Cell culture medium ... 31
2.3.1. Complete growth medium ... 31
2.3.2. Serum-free medium (SFM) ... 31
2.3.3 Freezing medium ... 32
2.3.4. Pancreatic stellate cell conditioned medium (PSC-CM) ... 32
2.4 Cell culture ... 32
2.4.1. Thawing / Seeding ... 32
2.4.2. Trypsinization ... 32
2.4.3. Counting ... 33
2.4.4. Passaging ... 33
2.4.5. Cryopreservation ... 33
2.5 Experimental procedures ... 34
2.5.1 Interactions between cancer cells and stellate cells. ... 34
2.5.2 H & E staining ... 34
2.5.3 Morphology assessment ... 35
2.5.4 MTT cell viability assay ... 35
2.5.5 BrdU cell proliferation assay ... 35

2.5.6 Glucose transport assay 36
2.5.7 Glycolysis assay (Lactate secretion) 37
2.5.8 Measurement of glucose in the cells 37
2.5.9 Measurement of protein concentration 38
2.5.10 Preparation of protein lysates 39
2.5.11 Gemcitabine sensitivity 40
2.5.12 Western Blot 41
2.5.13 Secretome analysis 41
3. Results 43
3.1 Morphology 43
3.2 Cell viability using MTT 45
3.3 BrdU cell proliferation assay 47
3.4 Basal glucose transport 49
3.5 Glucose transport after PSC-CM exposure 50
3.6 Lactate secretion following incubation with PSC-CM 51
3.7 Lactate secretion under nutrient-poor conditions 53
3.8 Gemcitabine sensitivity 54
3.9 NV-5440 dose-response 55
3.10 Glucose transport after PSC-CM exposure *plus* NV5440 and gemcitabine 56
3.11 Western blot 57
3.12 Secretome analysis 59
4. Discussion 64
5. References 78

1. Introduction

1.1 The pancreas: anatomy and function

The pancreas is an organ located deeply in the abdomen, behind the stomach, in close proximity to large blood vessels such as the portal vein and superior mesenteric vein and artery (Figure 1). The pancreas has an elongated shape. The left and thinnest part of the pancreas is called the tail which ends near the spleen. It has a thicker central section which is called the body. The right part of the pancreas is called the head and is located towards the center of the abdomen, in the junction where the stomach meets the duodenum (first part of the small intestine) [1].

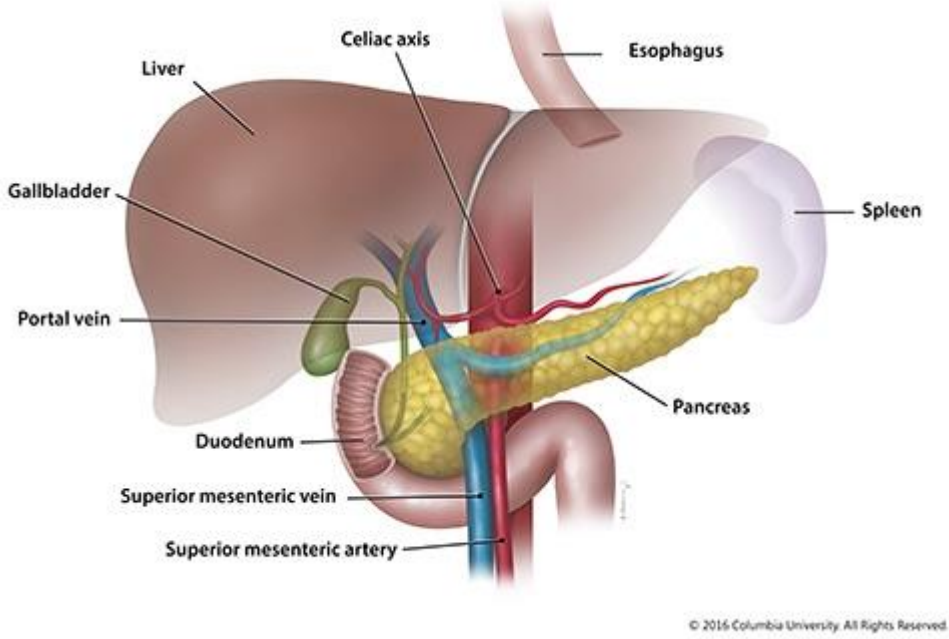

Figure 1: Anatomy of the pancreas [1].

The pancreas has two major functions: an exocrine function and an endocrine function. About 95% of the pancreas consists of the exocrine compartment, which is composed of cells from the pancreatic digestive enzymes. The latter are crucial to the body for digestion of the contents that is released from the stomach [1]. Proteins, carbohydrates and fats are digested by chymotrypsin and trypsin, amylase and lipase, respectively, which are all pancreatic digestive enzymes released by the exocrine cells in the pancreas. These enzymes are ultimately released into the pancreatic duct, which joins with the bile duct, which drains bile from the liver to the

duodenum. Here, the digestive enzymes can exert their functions by effectuating the breakdown of foodstuffs released from the stomach [1].

The remaining 5% of the pancreas consists of the endocrine compartment, which is composed of endocrine cells that form small cell clusters, the so-called *islets of Langerhans*. The two main cells in the islets of Langerhans are the alpha cells which produce the hormone glucagon and the beta cells which produce the hormone insulin [2]. Insulin is a crucial regulator of blood sugar and functions by inducing uptake of carbohydrates into cells, thus lowering the amount of carbohydrates in the blood. Glucagon serves the opposite function, raising blood sugar. Appropriate levels of blood sugar and oxygen are crucial to the normal functionality of organs such as the brain and kidneys. As a consequence of this, there are several major blood vessels in close proximity to the pancreas. These mainly to help with supply of oxygen and nutrients and the removal of metabolites, but also the secretion of insulin and glucagon [1-3].

1.2 Pancreatic cancer

Pancreatic cancer is the collective name for cancers originating in the pancreas. Pancreatic cancer is one of the deadliest cancers that humans can acquire. The relative 5-year survival rate for patients with pancreatic cancer was as low as 6% in 2016 [4], however, the recent advances in neoadjuvant and adjuvant therapies as well as earlier detection and improved management of the disease, have increased the 5-year survival rate to 9-10% in specialist pancreatic cancer centers [5]. Pancreatic cancer patients have the lowest 5-year survival rate of all cancers, reflecting the need for better treatment options and detection methods [6]. Pancreatic cancers are subdivided into endocrine pancreatic cancers and exocrine pancreatic cancer, depending on the origin of the tumor in the pancreas.

Endocrine pancreatic cancers, also called neuroendocrine tumors (NET) originate from the endocrine tissue of the pancreas, i.e., the islets cells and can be either benign or malignant [7]. Endocrine pancreatic cancers can be further classified, based on the function of the cells that the cancer originates in. Most of the NETs do not produce a functional hormone (so-called non-functioning NETs), while other NETs are associated with excessive secretion of one of the islet hormones and clinical signs and symptoms related to the abnormally elevated hormone levels. When a tumor originates in the insulin producing beta cells of the islets of Langerhans and produces in an uncontrolled fashion high levels of insulin, it is called an insulinoma.

Similarly, glucagonomas are the NETs that are characterized by excessive production of glucagon and the presence of related clinical signs and symptoms [7]. Other types of pancreatic NETs include somatostatinomas and gastrinomas [7].

Exocrine pancreatic cancers are the cancers that originate in the exocrine compartment of the pancreas, that is, the cells that secrete digestive enzymes or lines the ducts that drain the secreted enzymes. Exocrine pancreatic cancers account for about 95% of all pancreatic tumors [8]. The most common type of exocrine pancreatic tumor is the so-called ductal adenocarcinoma. As the name indicates, this cancer originates from the ducts of the pancreas. However, if the tumor starts in the acini of the pancreas, it is called acinar adenocarcinoma, which is a rare form of exocrine pancreatic cancer [8]. Ductal adenocarcinoma is the most common type of pancreatic cancer and accounts for 90% of all reported cases of pancreatic tumors [8]. Pancreatic ductal adenocarcinoma (PDAC) is the subject of this study and is discussed in detail in section 1.3

1.3 Pancreatic ductal adenocarcinoma (PDAC)

Background: PDAC is the most common type of pancreatic cancer and the deadliest of all cancers. It has a reported 5-year survival of under 10%, this is mostly due to its late detection, high metastasis potential and the lack of efficient treatment options [9]. PDAC is currently at the third place when it comes to cancer-related deaths in the United States and it is expected to become second within 10 years' time [4]. As of 2017, there were reported 448 000 new cases of pancreatic cancer and a total of 441 000 deaths globally [10]. In Norway, there were a total of 884 newly reported cases of pancreatic cancer in 2019, of which 496 male and 388 females [11]. In 2019, there were a total of 294 855 people living with cancer or that had survived a cancer in Norway. There were a total of 11 000 cancer related deaths in 2018 in Norway, of which approximately 800 were due to pancreatic cancer [12]. In 2019, there were a total of 884 patients diagnosed with pancreatic cancers, while 800 patients died of pancreatic cancer in 2018 [13]. The fact that the incidence and mortality is almost equal demonstrates that PDAC is a cancer with an extremely low survival rate.

Risk factors: Despite the recent advances in technology and detection methods, the causes of PDAC remain relatively unknown. However, there are several risk factors associated with PDAC, which can be grouped into **modifiable** and **non-modifiable** risk factors.

Modifiable risk factors include tobacco smoking, obesity, severe alcohol consumption, diet and exposure to toxic substances. Non-modifiable risk factors include diabetes mellitus, gender, age, genetics, family history of PDAC, ethnicity and chronic pancreatitis, to name a few [5]. Smoking remains the main risk factor for developing PDAC and the risk of developing PDAC is 2-times higher in smokers compared to non-smokers [5]. Obesity is another main risk for PDAC. Obesity is linked with body mass index (BMI) and a BMI of 25 or above is linked with a higher risk for developing PDAC compared to individuals with a normal BMI [5]. Physical inactivity is also a factor to consider when it comes to the increased risk of developing PDAC, as it is an indirect contributor to overweight [5]. Dietary factors also affect the risk of developing PDAC. Some foodstuffs present a higher risk, while others are protective towards the development of PDAC. For example, processed food, red meat, cholesterol, fried food and food containing nitrosamines greatly increase the risk for developing PDAC [5]. A meta-analysis showed that the consumption of red meat increased the PDAC risk by 48%, while the consumption of fruit and vegetables, in particular, citrus and antioxidant rich food decreased the risk of cancer development by 38% and 29%, respectively [5, 14].

Non-modifiable risk factors are factors that a person has to live with, for example gender and age. Studies confirm that the risk of PDAC increases with age and the risk for developing PDAC is higher in males than in females [15]. It is said that pancreatic cancer is a disease of the elderly, with most patients being above 50 years old. The incidence of pancreatic cancer peaks between ages 60 and 80 years and is hardly ever diagnosed before the age of 40 and the average age for detection of PDAC is 71 years in >50% of the cases [5]. The risk of PDAC is higher in the black population, compared to any other ethnic group. Both type I and type II diabetes have been reported to increase the risk of pancreatic cancer [16-20]. A 1.8-fold increased risk of developing PDAC could be seen in Hispanic and Asian men, compared to white and black men with diabetes mellitus. The risk of developing PDAC decreases with the duration of diabetes, which can correlate with oral anti-diabetic medications, which have been shown to associate with an decreased risk of developing PDAC [5]. Lastly, 5-10% of patients with PDAC report a familiar case of the disease in first degree family (parent, child, sibling), so-called familial pancreatic cancer. A first degree relative of a person with PDAC has a 9-fold increase of developing PDAC compared to the common population. This number increases to a 32-fold higher risk of developing PDAC, if the individual has 3 or more first degree relatives with PDAC [5]. Although there is a clear genetic predisposition due to family history, a germline mutation cannot be identified. This is in contrast to other PDAC patients, which have

a genetic predisposition due to an identifiable germline mutation. More of this in section 1.3: genetics.

Symptoms: The symptoms of PDAC are usually vague, which is one of the main reasons for the late detection of the disease. Abdominal pain, jaundice and weight loss are the main symptoms of PDAC [9]. However, other symptoms may present, which include itching, dark urine, pale faeces, nausea and vomiting, dyspepsia, early satiety anorexia, back pain, and newly diagnosed type II diabetes [9, 11]. Depression may also occur, but only in very rare cases. As the symptoms for PDAC are numerous and mostly non-specific, it is important to differentiate many diseases that occur due to these symptoms, thus avoiding false diagnoses. Because of these vague symptoms PDAC is often diagnosed very late in the disease progression. Therefore, at the time of diagnosis, most patients will have developed a metastatic disease or have a locally advanced and unresectable tumor, making treatment difficult [9]. After PDAC has been diagnosed, only 24% will survive for a year, while 9% survive for up to 5 years [5]. Therefore, it is critical that methods for the detection of PDAC become more efficient than they are today. This will allow for earlier detection, increasing the chance for effective treatment and delaying tumor progression.

Diagnosis: Most PDACs are diagnosed at an advanced stage, when about 85% of the patients have unresectable tumors, often with metastasis [5]. This makes surgical removal of the tumor nearly impossible. This is critical as surgery is the only potentially curative treatment option. Today, there are two main categories of methods of detecting pancreatic cancer: imaging techniques and biomarkers [21]. **Diagnosis using imaging techniques:** These tests can be used to diagnose pancreatic cancers by the detection of tumors in the pancreas. These tests include magnetic resonance imaging (MRI), computerized tomography (CT), positron emission tomography (PET) and endoscopic ultrasound (EUS). CT is the preferred diagnostic test for detecting PDAC whereas MRI and EUS are performed if deemed necessary. EUS has the advantage that it allows to extracts cells from tissue samples from the tumor, which can confirm the diagnosis microscopically [11, 22]. **Diagnosis using biomarkers:** Biomarkers are usually taken by non-invasive bio samples, such as blood, faeces and saliva. Today, blood tests are the most common and they are used to detect specific tumor markers, which are specific proteins that are shed by a pancreatic tumor. However, in isolation, blood tests are not sufficiently reliable for a diagnosis of pancreatic cancer, and they have to be combined with other diagnostic methods [21, 22]. Furthermore, other non-invasive molecular biomarker

detection methods are being developed, which would be the ideal way to detect pancreatic cancers. These methods include epigenetic markers, which include methylation-on-beads (MOB) technology to detect pancreatic cancer in serum, circulating tumor DNA (ctDNA) to detect ctDNA from a pancreatic tumor, and miRNA, that can distinguish serum from patients compared to control serum based on miRNA levels [21]. Other promising non-invasive biomarker methods that can diagnose pancreatic cancer in the future include screening of the faeces, examining the oral and gut microbiome as some oral and gut bacteria have been shown to increase the risk of pancreatic cancer, and saliva-based testing [21]. In the end, if a pancreatic cancer diagnosis is likely, a biopsy may be taken. A biopsy is the removal of a small piece of pancreatic tissue that is to be examined microscopically. This is to determine the type of pancreatic cancer (exocrine vs endocrine). The stage of pancreatic cancer ranks from 0 to IV, where 0 represents a cancer localized in the pancreas only, while stage IV indicates a metastatic pancreatic cancer [11, 22].

Genetics: As with most other types of diseases and cancers, genetics also plays a role in pancreatic cancer. In other cancers such as breast cancer (BRCA1/2) and melanoma (BRAF), there is one common mutation that drives disease progression [23, 24]. This makes treatment easier. However, pancreatic cancer possesses a broad range of different cancer-causing mutations, where each mutation can be found in a small number of patients. This further complicates the treatment options for pancreatic cancer [9]. The most common and key genetic mutations in PDAC occurs in the genes of *KRAS, TP53, CDKN2A/p16 and SMAD4 [9]*.

Furthermore, in 5-10% of all PDAC cases, hereditary genetics are shown to play a role and several genetic familial syndromes are thought to increase the risk of pancreatic cancer [21]. These familial genetic mutations include: *STK11*, which is a gene that encodes the STK11 protein, a tumor suppressor protein that regulates several processes including cell growth and metabolism via the AMPK/mTOR pathway in individuals with Peutz-Jeghers syndrome [25]. HNPCC or Lynch syndrome is characterized by certain germline mutations in genes that are involved in DNA mismatch repair such as *MLH1, MSH2, MSH6 and PMS2.* A large study on these genes in 147 families showed a 9-fold increase in risk of developing pancreatic cancer up to the age of 70 years [25]. Hereditary breast and ovarian cancer syndrome (HBOC) are characterized by germline mutations in the aforementioned *BRCA1/2* genes and an increased risk of pancreatic cancer. Several studies have identified a 4-6-fold increased risk of developing pancreatic cancer if the patient has mutations in the *BRCA2* gene which encodes tumor

suppressor proteins important for DNA repair and damage response [25]. Familial adenomatous polyposis (FAP) is another familial syndrome associated with increased risk of pancreatic cancer. Patients with FAP have mutations in the tumor suppressor gene APC, which is involved in the WNT pathway [25]. Another gene associated with increased risk of pancreatic cancers is the *PRSS1* gene, which encodes the digestive enzyme trypsin-1. A gain of function germline mutation in this gene is associated with hereditary pancreatitis (HP), which has been shown to increase the risk of developing pancreatic cancer by as much as a 69-fold increase [25]. Other genes such as *SPINK1*, *CFTR, CTRC* and *CASR* have been shown to influence the susceptibility to pancreatitis and thus, indirectly, pancreatic cancer [25]. Genetic heterogeneity is a hallmark of PDAC and is found both between patients and in a single primary tumor from one patient. Such an extent of genetic heterogeneity and mutational changes generates genetic instability, which plays a crucial role in PDAC growth and proliferation, as well as in PDACs resistance to treatment [9].

Treatment: The pancreatic cancer treatment is divided in three major categories; surgery, chemotherapy and radiotherapy; which are used alone or in combination [26]. **Surgery** is the preferred therapy method; however, treatment depends on the location and stage of the tumor (from 0 to IV). If the tumor is at stage 0, it is confined to the pancreas, without metastasis and surgery can be performed. The surgery performed on the head of the pancreas is called pancreatoduodenectomy (Whipple's procedure) [22]. This is an extensive and challenging surgical procedure that removes the head of the pancreas as well as a part of bile duct, the gallbladder, duodenum, lymph nodes, and in some cases, parts of the stomach [22]. A distal pancreatectomy is performed if the tumor is located in the tail or body of the pancreas, and a total pancreatectomy is performed if the whole pancreas needs to be removed [22]. As most cases of pancreatic cancers are diagnosed at an advanced stage, surgery is not often an option. Instead, patients must undergo chemotherapy and possibly radiotherapy. **Chemotherapy** uses cytotoxic drugs to destroy cancer cells. Chemotherapeutic agents can be administered orally or intravenously, alone (monotherapy) or in combination with one or more drugs (combination therapy) [22, 27]. The main chemotherapeutic drugs currently in use to treat pancreatic cancer include: gemcitabine (GEM), FOLFIRINOX (5-fluorouracil, folinic acid [leucovorin], irinotecan, and oxaliplatin) and gemcitabine plus nab-paclitaxel [28-31]. However, since 1997, gemcitabine remains the golden standard for treatment of patients with PDAC, even though it has been shown that it is less effective than FOLFIRINOX [32]. Gemcitabine can be administered in combination with nab-paclitaxel, or alone in monotherapy [33]. **Radiation**

therapy utilizes high energy beams/lasers/particles to kill cancer cells by radiation. It can both be administered neoadjuvant and adjuvant to surgery, alone or in combination with chemotherapy. External beam radiation therapy is the preferred method in pancreatic cancer treatment. This method applies high energy beams from a machine directed at specific points of the body to treat the pancreatic tumor and limiting damage to surrounding tissues and organs [22, 34-36]. In Norway, radiotherapy is used mainly to alleviate local complications (e.g., pain due to bone destruction) in inoperable PDAC.

1.4 Pancreatic tumor microenvironment

The tumor microenvironment (TME) is the environment generated first and foremost by stromal cells that are adjacent to the neoplastic cancer cells in a tumor. In other words, an environment created by stromal cells that affect the nearby cancer. The pancreatic TME is characterized by increased desmoplasia, that is, the presence of a prominent stroma and pancreatic stellate cells (PSCs; also known as CAFs, Cancer Associated Fibroblasts), which is activated by the surrounding cancer cells (Figure 2) [9, 37]. The composition of the pancreatic TME consists of several cell types and non-cellular components. Among the cellular components we find the PSCs and their recently described possible subtypes - inflammatory PSCs and myofibroblastic PSCs -, several immune cells such as macrophages, lymphocytes and neutrophils and endothelial cells that form the small blood vessels (Figure 2). Non-cellular components include the extracellular matrix (ECM), which consists mainly of hyaluronic acid, collagens, laminin, and fibronectin, as well as chemokines and cytokines released by immune cells [38]. The PSCs are responsible for producing excessive amounts of ECM components, which together create a dense and stiff stroma that surrounds the PCCs as a biophysical barrier and results in the collapse of a considerable part of the microvasculature [37]. It is the latter effect that makes the TME deeply hypoxic and nutrient-poor, attenuates drug delivery and results in evasion from the host's immune system. These mechanics induce rapid cancer progression due to the tumor’s ability to resist chemotherapeutic treatment by limiting the exposure of cancer cells to chemotherapeutic agents and by limiting immune cell infiltration of the tumor. Ultimately, pancreatic TME leads to PDAC being resistant to chemotherapeutic agents and has a low susceptibility for the host’s immune system. [9, 37, 39, 40]. Therefore, targeting of the TME may provide more efficient treatment for PDAC patients

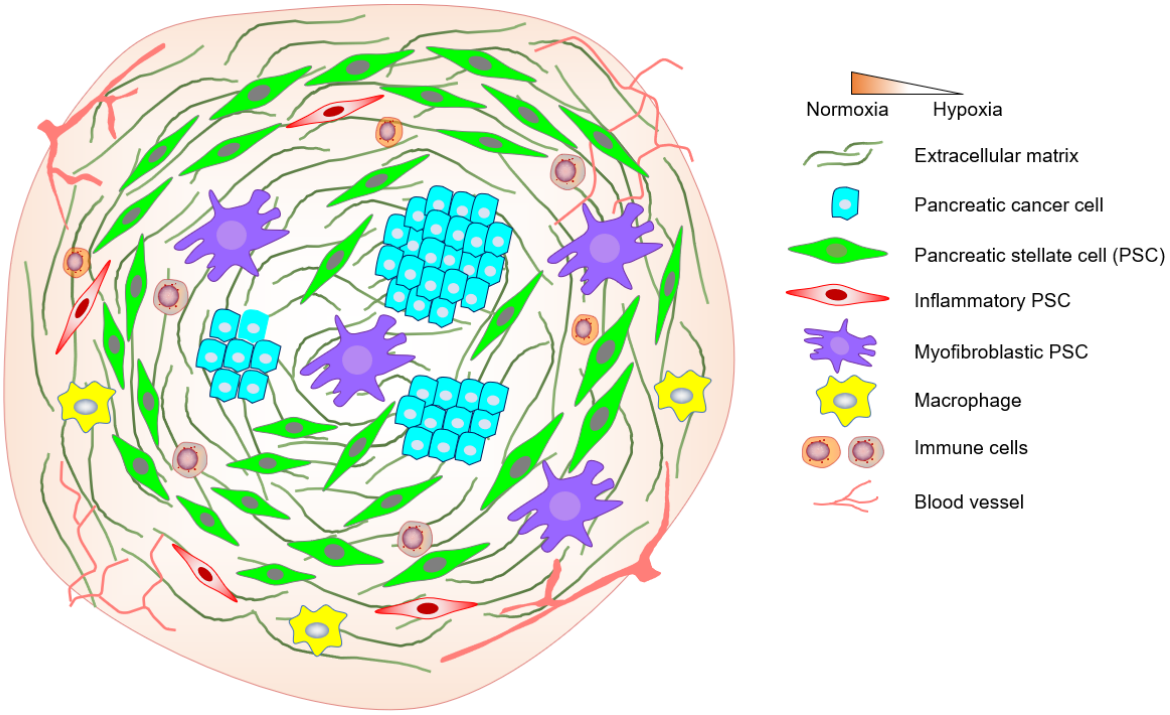

Figure 2: *The pancreatic tumor microenvironment. The picture was created by Amrutkar M. and a permission was obtained for its use in this thesis. Edited.*

However, a term called heterogeneity complicates things further. There are two main types of heterogeneity: Inter-tumor heterogeneity and intra-tumor heterogeneity. Inter-tumor heterogeneity refers to differences between the tumors of individual patients despite the fact that these patients suffer from the same cancer type (i.e. PDAC) [41]. Inter-tumor heterogeneity is the reason behind personalized medicine, in which patients receive the best-suited treatment based on their specific subtype of PDAC. The odds for two different individuals to have the "exact same tumor" are extremely low. Inter-tumor heterogeneity can manifest at multiple levels: histological, genomic, transcriptomic, metabolomic and stroma [41, 42]. Intra-tumor heterogeneity is more challenging and refers to diversity within the same tumor, and adds another level of complexity to the already complex inter-tumor heterogeneity of PDAC. Intra-tumor heterogeneity can occur within the primary tumor, in the metastases, and even between metastases [41]. A study by Nakamura et. al even showed that certain genes were upregulated in the periphery of a tumor, compared to the center of the tumor where other genes were upregulated. This is called zonal heterogeneity which further complicates the treatment for PDAC patients [43]. Ultimately, this will lead to a high degree of heterogeneity in pancreatic tumors, and especially regarding the TME, which can vary between the patients and within the same tumor, making the treatment further challenging. Therefore, it is necessary to gather data

and perform research on the TME, so that the best available treatment option can be given to the patient.

1.5 Pancreatic stellate cells (PSCs)

The pancreatic stellate cells, the PSCs (also called CAFs) are the main cellular component in PDAC stroma. Stroma can form up to about 90% of the total tumor mass in PDAC and the PSCs can constitute 50% of this stroma [44, 45]. They are derived from the PSCs that are present in the stroma of normal pancreas. It was not until 1982, that Watari discovered a star shaped (stellate-shaped) cell in the pancreas, later known as PSC [46]. PSCs were found to localize near the periacinar regions in the exocrine tissue of the pancreas [47]. Despite the fact that PSCs were discovered in the early 1980s, it was not until the end of the 1990s that they received the much-needed attention, in 1998, the first method for isolation and culturing of PSCs was developed [47]. Since these two discoveries, scientists have been able to characterize the biology of the PSCs.

PSCs appear in two different phenotypes: quiescent PSCs (qPSC) and activated PSC (aPSC) [46]. In normal pancreas, PSCs exist in quiescent form, are located around the enzyme-producing exocrine cells of the pancreas, have an elongated, fibroblastic stellate shaped appearance and are the main producers of ECM [46]. Quiescent PSCs can be identified by the presence of vitamin A containing lipid droplets in the cytoplasm, which in fact led to the discovery of PSCs in 1982 [46]. A further characteristic of qPSC is the high expression of vimentin, GFAP and desmin, and that they are alpha smooth muscle actin (αSMA) negative. qPSCs also have a high expression of nestin and nerve growth factor, they have a weak capacity to migrate, proliferate and produce ECM materials such as hyaluronic acid. Finally, qPSCs secrete a low number of factors, such as chemokines and cytokines [46]. qPSCs can be activated by several different mechanisms, first and foremost injury and inflammation, which are key causative factors of chronic pancreatitis, a chronic inflammatory disease of the pancreas that is characterized by excessive fibrosis, that is, deposition of ECM by the activated PSCs. PSCs can also be activated by micro-environmental factors such as hypoxia and elevated secretion of factors such as TGF-B, CTGF, Galectin-1, PDAF and IL-1 [46]. Activated PSCs have a myofibroblast-like appearance (that is, are less slender than the star-shaped form of qPSCs) and are characterized by the loss of their lipid droplets and the expression of αSMA [46]. In contrast to qPSCs, aPSCs show less expression of vimentin, GFAP and Desmin; increased ability in

migration, proliferation and secretion of ECM components, as well as increased ability to release cytokines, chemokines and growth factors [46].

Activation of PSCs also occurs during the development of PDAC and leads to the formation of the prominent stromal microenvironment that is so characteristic of PDAC. PSCs have the ability to crosstalk with PCCs and other stromal components (Figure 3) [46]. While PCCs stimulate migration, proliferation and collagen synthesis in PSCs, the PSCs stimulate EMT, proliferation, migration, metastasis and chemoresistance and downregulate programmed cell death in PCCs [47]. aPSCs interact with endothelial cells to promote proliferation and angiogenesis, with immune cells to increase immune suppression, and with nerve cells which together contribute to the aggressive nature of PDAC [46]. Furthermore, PSCs play a crucial role in the metabolic remodeling of PDAC. To fulfil the increased energy demand of PCCs and to drive tumor progression, a remodeling of the pancreatic TME has been shown to create a supportive niche and to assist the PDAC in its metabolic reprogramming [48].

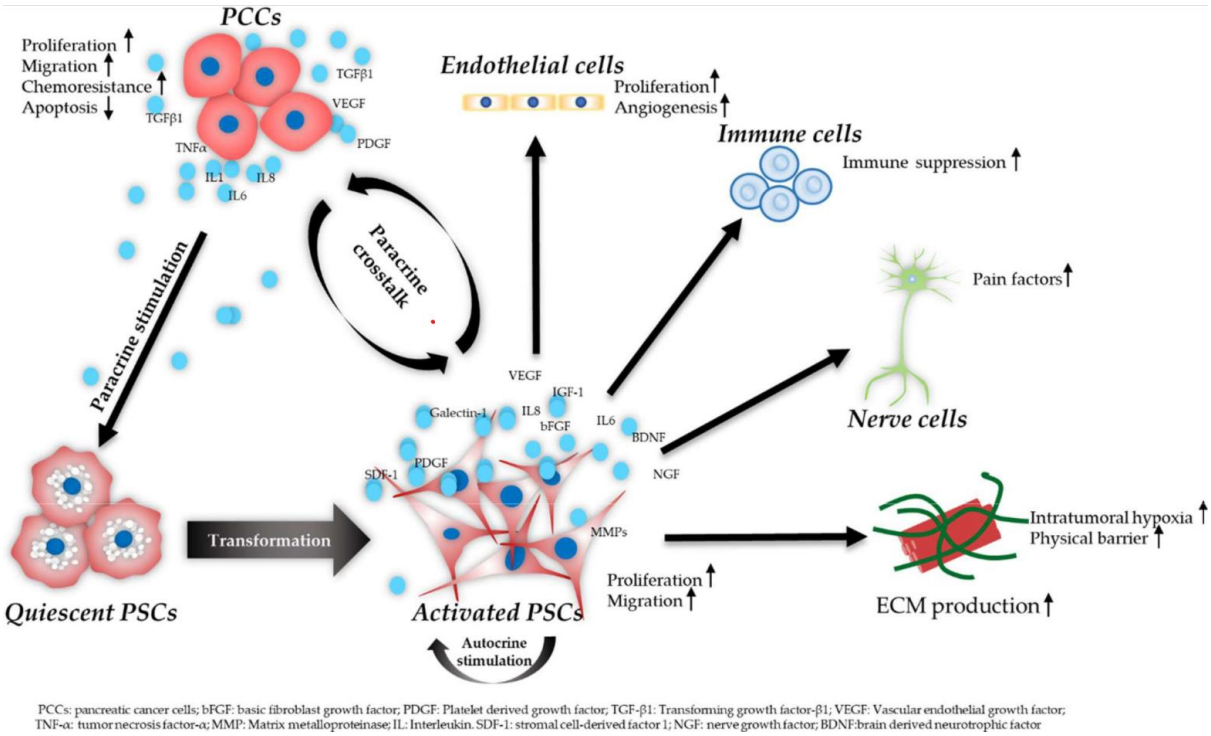

Figure 3: *The role of PSC in PDAC, how they are activated and its extensive crosstalk with other cellular components. From [46]*

1.6 Cancer metabolism

Metabolism is the sum of all catabolic and anabolic reactions. Metabolism is essential for all cells, as they need energy to perform their biological functions. All normal cells utilize the same metabolic pathways for acquisition of energy and other compounds important for metabolism [49]. Some major metabolic pathways used by normal cells include glycolysis, citric acid cycle, urea cycle, oxidative phosphorylation in mitochondria, pentose phosphate pathway and several other known pathways [49]. Compared to the healthy (normal) cells, in cancer cells, these pathways are dysregulated to meet the increased energy demand of cancerous cells to maintain their continuous proliferation and invasion [50].

In contrast to healthy cells, the cancer cells chose a different strategy for energy acquisition in order to meet their increased energy demand. In normal cells, adenosine triphosphate (ATP, the currency of energy) is obtained by catabolism of various energy sources, such as carbohydrates, proteins, and fat [51]. In short, under normal aerobic conditions, glucose is generated by the breakdown of carbohydrates, glucose is then converted to pyruvate and acetyl coenzyme-A (CoA). CoA enters the Krebs cycle (also called the tri-carboxylic acid cycle TCA) and is metabolized, generating ATP and high energy carriers such as nicotinamide adenine dinucleotide phosphate (NADPH) [51]. From here, the NADPH energy carriers enter the electron transport chain, also known as oxidative phosphorylation (OXPHOS) to generate high amounts of ATP with the help of respiratory oxygen (Figure 4) [52].

However, cancer cells employ a very different tactic than normal cells when it comes to acquiring energy. The main and fundamental differences between normal cells and cancer cells are found in the glycolysis pathway. Under normoxic conditions, normal cells opt not to metabolize glucose into lactate. However, in an environment where oxygen is limited or absent (hypoxia), normal cells will resort to anaerobic glycolysis, by metabolizing glucose to lactate by fermentation [51]. In total, anaerobic glycolysis yields a lower total amount of ATP than aerobic glycolysis, which is the preferred method in any circumstances. In contrast, cancer cells utilize anaerobic glycolysis, independent of oxygen availability [51]. Cancer cells metabolize glucose to lactate, even in the presence of oxygen and a functioning mitochondrion, although the yield is much lower. The ability of cancer cells to metabolize glucose into pyruvate and lactate, even in aerobic conditions is known as “The Warburg effect” [51].

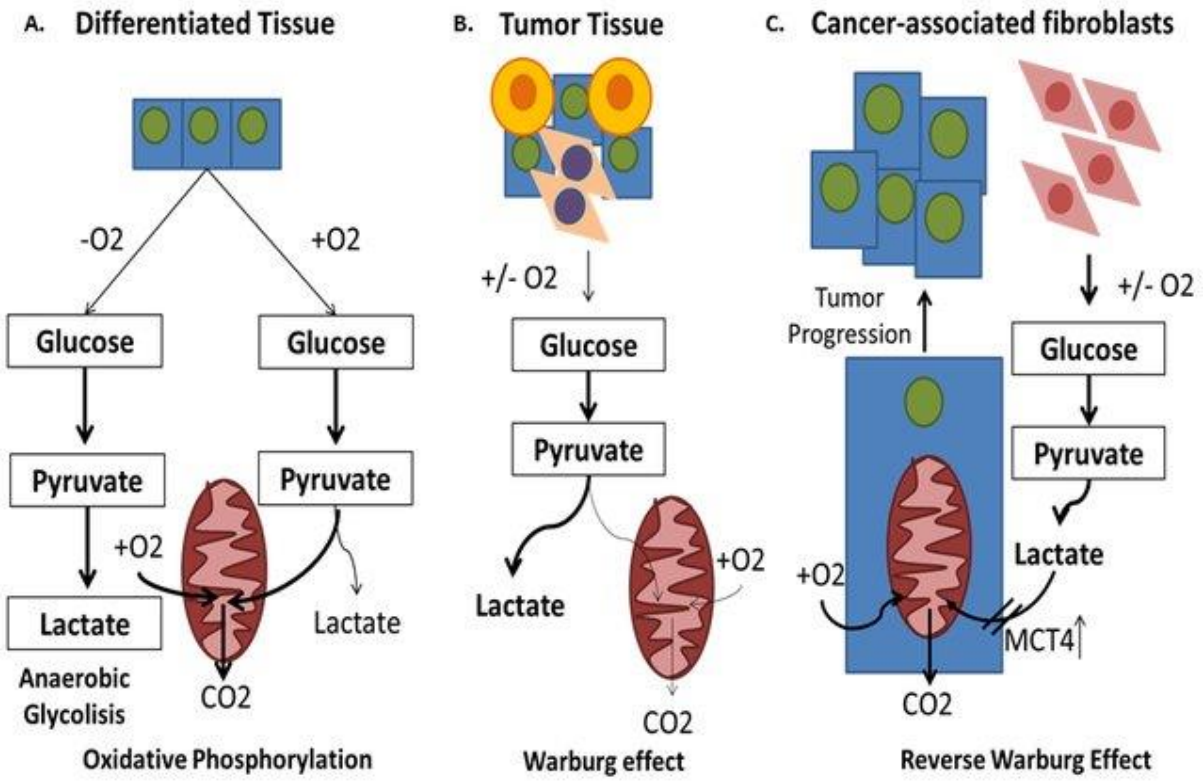

Figure 4: *The fate of glucose in the presence or absence of oxygen in regards to the OXPHOS pathway (4a), the Warburg effect (4b) and the reverse Warburg effect (4c)* [53].

The Warburg effect is named after Otto Warburg, who in the 1920s made the discovery that tumor tissue takes up considerably more glucose than surrounding tissue and that the cancer cells ferment glucose into lactate, even in the presence of oxygen [54]. However, there are certain limitations to the Warburg effect. Firstly, the Warburg effect is observed mainly in tumor cells, which is much more inefficient compared to glycolysis and oxidative phosphorylation of pyruvate by mitochondria, as observed in normal cells [48]. In normal healthy cells that perform mitochondrial respiration under normoxic conditions, the net yield of cellular energy carrying molecules is 36 molecules of ATP and a molecule of carbon dioxide (CO2) per glucose molecule [51]. However, in lactate producing cancer cells, the net yield is only 4 ATP molecules per glucose molecule [51]. This is a contradiction, as cancer cells require more energy, one would assume that they alter their metabolism to meet this increased energy demand. However, the Warburg effect does not describe why cancer cells prefer a less efficient energy-acquisition pathway that yields a lower amount of total ATP [54].

Secondly, the Warburg effect is only focused on metabolism in tumor cells and does not consider the impact from the TME [48]. To accommodate the impact of TME on cancer cell

metabolism, Pavlides et al. proposed a modified Warburg model, called *the reverse Warburg effect* [55]. According to the reverse Warburg effect, the stress-signals known as reactive oxygen species (ROS) from cancerous cells induce aerobic glycolysis (Warburg effect) in neighboring stromal fibroblast cells (CAFs), or in the case of PDAC, PSCs, subsequently leading to secretion of pyruvate and lactate, the main metabolic products of the Warburg effect [55, 56]. The original cancer cells that induced the Warburg effect in the PSCs can now take up the secreted high energy compounds pyruvate and lactate. However, now the pyruvate and lactate are instead funneled into the Krebs cycle in mitochondria, resulting in a higher and more efficient energy production, due to generation of ATP via OXPHOS. This ultimately leads to a higher proliferative and growth capability of the cancer cells [48, 55]. The reverse Warburg effect can also provide some insight as to why cancer cells prefer the less efficient method. By utilizing this method, cancer cells can induce aerobic glycolysis in several PSCs, which generates pyruvate and lactate in large amounts, which can immediately be used by the cancer cells to promote growth and proliferation at a higher rate, compared to the normal metabolic pathway. This ultimately leads to rapid invasion, tumor development and disease progression.

1.7 Pancreatic cancer metabolism

One of the main characteristic features of PDAC is the extensively altered metabolism, a phenomenon known as metabolic reprogramming [48]. This can in general be described as modifications to the ordinary metabolic pathways to an extent that activities will either be suppressed or enhanced in cancer cells, compared to healthy cells and tissue, due to the effect of tumor promoting mutations or other factors [48]. The metabolic reprogramming seen in PDAC is influenced by multiple factors [57]. However, above all, oncogenic *KRAS* mutations in PDAC ultimately drives and regulates metabolism in PDAC cells. Oncogenic *KRAS* mutations regulate glucose and glutamine metabolism, resulting in increased levels of pyruvate, which ultimately leads to cell proliferation and survival by enhancing characteristics such as invasiveness, acidification and increased energy production (ATP) [58].

Firstly, PDAC are able to reprogram metabolism at an intracellular level by altering the pathways for glucose, lipids and amino acids [57]. Here, the Warburg effect is central as described earlier. However, there are also some advantages to using the Warburg effect over the OXPHOS pathway. Aerobic glycolysis generates a higher glycolytic flux, which in turn generates a higher production rate of ATP, tumor cells acquire more intermediates important

for rapid biosynthesis, it maintains redox balance and the state of chromatin, and it provides a low immunity microenvironment as well as improved invasion abilities [57]. Furthermore, PDAC tumor cells display a vast array of heterogeneous metabolic phenotypes, driven by the TME, stromal cues and genetic mutations, which include Warburg effect, the reverse Warburg effect and pathways affecting the lipid and glutamine metabolism [57]. This results in the marked presences of highly heterogeneous metabolic phenotypes.

Secondly, PDAC tumors employ scavenging and recycling mechanisms for nutrient acquisition called autophagy and micropinocytosis [48, 57]. Macropinocytosis is a form of "cell drinking" that takes place in the cell membrane. Extracellular fluids are taken up by endocytic vacuoles by the cell membrane and released into the cytosol of the cancer cell where it is digested and degenerated. This form of cell drinking is essential for the maintenance of the amino acid supply to the pancreatic cancer cells [57]. Autophagy is a form of self-eating. Autophagy is a cellular process which recycles intracellular components by degrading organelles and macromolecules that already exist in the cell. Autophagy is thus a key regulator of energy homeostasis and metabolic fuel in the pancreatic tumor [57]. Ultimately, both of these nutrient acquisition processes result in degradation of its contents in the lysosome to regenerate and recycle nutrients to promote cell proliferation and growth of the pancreatic tumor [57].

Finally, there is evidence of extensive crosstalk between the pancreatic cells and the TME, especially the PSCs with regards to metabolism [57]. PDACs are very heterogeneous in its composition and consists of cancer cells, extracellular matrix (ECM) and PSCs, and crosstalk occurs between all these components [57]. The role of PSCs in pancreatic cancer metabolism will be discussed below.

The influx of glucose is the cornerstone of carbon metabolism in all cells, including PCCs, providing ATP and biomass for anabolic processes that ultimately leads to cell proliferation [59]. The expression of glucose transporters (GLUTs) and the rate limiting enzymes hexokinase 2 (HK2), phosphofructokinase-1 (PFK1) and lactate dehydrogenase A (LDHA) control the breakdown of glucose which in turn controls and regulates the rate of glycolytic influx [59]. The main parts of the glycolytic pathway in PDAC are the uptake of glucose, breakdown/processing and the secretion of lactate. Glucose is taken up by GLUT transporters in the cell membrane. Glucose then encounters the first key glycolytic enzyme HK2, which converts glucose to glucose-6-phosphate (G6P) [59]. G6P are then converted to

fructose-6-phosphate (F6P), which is converted to fructose-1,6-bisphosphate (F1,6BP) by the help of the PFK1. After a series of more enzymatic steps, pyruvate is generated and converted to lactate by LDHA. Lastly, lactate is secreted via the MCT1/4 (monocarboxylate transporters) transporters [59]. From here, lactate can be used as energy by cancer cells, but it can also be used by other cells, such as the PSCs.

Enhanced glucose metabolism in the form of the reverse Warburg effect and the Warburg effect cannot single-handedly compensate for the highly increased energy demand of the tumor cells [48]. It has been conceptualized that PSCs function as a supplier of energy for PDAC tumor cells. Furthermore, PSCs are thought to reprogram the metabolic pathways in PDAC to a significant extent. This occurs by crosstalk between the PSCs and the tumor cells [48, 60]. This crosstalk is orchestrated in several ways and is bidirectional.

One such example is the following: PCCs can release ROS' into the PDAC TME, which will be taken up by the PSCs and raises the intracellular levels of hypoxia-inducible factor 1a (HIF-1α) in the PSCs. Increased levels of HIF-1α in PSCs promotes a higher rate glycolysis and subsequent increased secretion of nutrients such as lactate via the MCTs from the PSCs, that ultimately fuels the increased energy demand of cancer cells [48]. PSCs also secrete insulin-like growth factors (IGFs), which increase OXPOS respiration in the PCC mitochondria via the PI3K/AKT pathway. These two mechanisms are a result of *KRAS*-dependent crosstalk between PSCs and cancer cells [48].

However, there is also *KRAS*-independent crosstalk that affect pathways that mediate metabolic reprogramming in the tumor cells. As mentioned earlier, recent studies have shown that PSCs support the metabolism of the cancer cells by alanine secretion [60]. The cancer cells induce autophagy in the PSCs, which ultimately leads to alanine secretion by the PSCs [48]. Alanine is a so-called non-essential amino acid (NEAA), that the cancer cells can use as an alternative source of fuel. Sousa et al. describe that the NEAA alanine even outcompetes carbon derived glutamine and glucose in PDAC as fuel in the Krebs cycle, which in turn will regulate NEAA and the lipid biosynthesis for the cancer cell [60]. Another form of KRAS-independent crosstalk is the transport of exosomes from PSCs to the cancer cells. Exosomes are a further provider of alanine, which cancer cells can use as fuel, resulting in metabolic remodeling [48]. A returning concept is macropinocytosis. PSCs can secrete NEAAs and lipids which, along with extracellular proteins, will be taken up by the cancer cells through macropinocytosis and

stored in macropinosomes. The macropinosomes will fuse with lysosomes, where the contents will be degraded and funneled into the mitochondria for energy extraction [48]. Furthermore, growth factors released by PSCs have been found to be important in KRAS-independent signaling in the reprogramming of the PDAC metabolism [48].

1.8 Chemosensitivity

All topics covered so far have implications for the chemosensitivity of PDAC. Extensive chemoresistance is a known trait of PDAC and gemcitabine (2′,2′-difluoro-2′-deoxycytidine [dFdC], GEM) remains the gold standard for treatment of unresectable, locally advanced and metastatic PDAC tumors as well as for resectable PDAC following surgery (adjuvant therapy) [33]. After a study by Burris et al. in 1997, which reported that gemcitabine treatment in patients with advanced symptomatic pancreatic cancer increased the median survival time to 5.65 months, compared to 4.41 months with 5-fluorouracil (5-FU), which was the standard care at the time, the food and drug administration (FDA, in the US), approved the use of gemcitabine. Although only offering a slight increase in survival, some patients experienced an improvement in symptoms, weight gain and stabilization of tumor growth, which was enough for the FDA to approve the drug [32, 61].

Gemcitabine (dFdC) is a deoxynucleoside analog that needs to be intracellularly activated to its active form dFdCTP in order to exert its cytotoxic effect by inhibiting DNA synthesis and inducing apoptosis [48, 62]. In order to enter the cell, gemcitabine is transported across the cell membrane by the human equilibrative nucleoside transporters (hENTs), in both PSCs and cancer cells, although hENTs are downregulated in PSCs [33, 48]. Upon entry to the cell, most of the gemcitabine is deactivated to dFdU (2′,2′-difluoro-2′-deoxyuridine) by cytidine deaminase (CDA), which subsequently leads to the clearance of the inactivated gemcitabine from the cancer cell [48, 62]. The remaining small portion of gemcitabine is activated by deoxycytidine kinase (DCK) to the monophosphate form dFdCMP (2′,2′-difluoro-2′-deoxycytidine monophosphate) [48]. The dFdCMP form can subsequently either be reverted back to dFdC by the inactivating enzyme 5’ -nucleotidase cytosolic 1A (NT5C1A), converted to the inactive form 2′,2′-difluoro-2′-deoxyuridine monophosphate by deoxycytidylate deaminase (DCTD), or activated to its diphosphate form dFdCDP and further to its final active triphosphate form dFdCTP by DCK [48]. Although the uptake of gemcitabine is reduced in PSCs because of the downregulation of hENT1, gemcitabine suffers a similar fate, but with

reduced cytotoxic abilities. This was confirmed by Amrutkar et al. in 2020, who showed that PSCs are resistant to gemcitabine with a minimal uptake, while PCCs are chemosensitive to gemcitabine and have a significantly higher uptake of gemcitabine compared to PSCs [33].

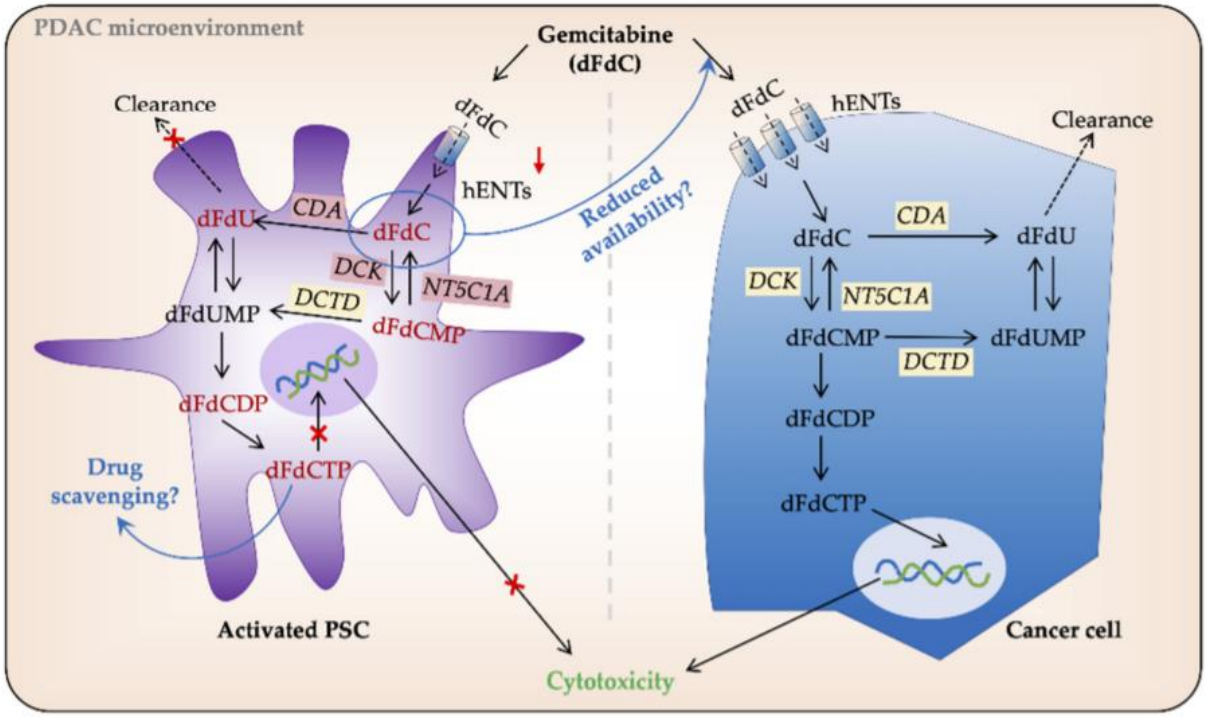

Figure 5: *Gemcitabine metabolic processing in PSCs (left) and PCCs (right)* [48].

The response to chemotherapy-induced cytotoxic activities seen in PCCs and the development of chemoresistance in PDAC are influenced by several factors that can be classified into four groups: 1. reduced intracellular transport, 2. increased drug efflux, 3. dysregulated drug metabolism, and 4. alterations in cellular signaling leading to inhibition or impairment of drug-induced cytotoxicity [48]. PSCs have recently been shown to promote chemoresistance to gemcitabine by several factors, including the physical barrier of the stroma, which prevents gemcitabine form reaching and entering the tumor, crosstalk between PSCs and PCCs, altered drug bioavailability and molecular changes to the tumor cells orchestrated by the PSCs [48, 62].

In addition, it is suggested that intracellular gemcitabine processing (drug metabolism) contributes significantly to the gemcitabine resistance in PDAC [63]. Altered expression of the deactivating (DCTD, NT5C1A and CDA) and activating (DCK) enzymes in the processing of gemcitabine may lead to chemoresistance by reducing the cytotoxicity of gemcitabine, while

downregulation of hENT1 itself causes chemosensitivity due to reduced uptake and intracellular transport [48].

As the triphosphate activated (dFdCTP) form of gemcitabine cannot travel through cell membranes, uptake of gemcitabine into PSCs will lead to accumulation of gemcitabine inside the PSCs (Figure 5), which then cannot be utilized by the PCCs. Hessman et al. suggested that increased intracellular levels of dFdCTP lead to a drug scavenging effect by the PSCs, which ultimately reduces the effect of gemcitabine on PCCs [63]. Hesler et al. showed that the protein cysteine-rich angiogenic inducer 61 (CYR61) is secreted by PSCs, which downregulates the expression of hENT1 in PCCs, thereby promoting gemcitabine resistance and sensitivity by reducing drug uptake through the hENT1 receptors [64]. Furthermore, loss of functional TP53 with subsequent activation of the JAK2-STAT3 signaling pathway has been shown to promote chemoresistance to gemcitabine in mice [62]. Moreover, a recent study by Amrutkar M. and colleagues showed that PSCs secrete fibronectin, which promotes chemoresistance to gemcitabine by activation of the ERK1/2 cellular pathway in PCCs [65]. These studies highlight the importance of PSCs in the regulation of gemcitabine chemoresistance in PDAC.

Both the broad range of mechanisms employed by PDAC tumors, especially by the PSCs, and the presence of profound tumor heterogeneity contribute to chemoresistance to gemcitabine. As described earlier, PSCs act as one of the main energy providers to PCCs and on other hand, the PSCs induce chemoresistance to gemcitabine. Therefore, it is of utmost importance to further understand the role of PSCs not only in the context of chemoresistance but also their contributions to the metabolic rewiring in PDAC, especially the glycolysis, which is a major metabolic alteration in pancreatic tumors.

Aim of the study

Pancreatic ductal adenocarcinoma (PDAC) is the most common type of pancreatic cancer and the deadliest of all cancers. With a reported 5-year survival rate of under 10%, improved treatment and new treatment targets could potentially increase the abysmal survival rate of PDAC. In recent years, the PSCs of pancreatic cancer have gained increased attention due to their key role in cancer progression. PSCs have been shown to both promote chemoresistance to certain drugs, especially gemcitabine, and contribute to the altered metabolism of PCCs, a process known as metabolic rewiring, Glycolysis is a major metabolic alteration in PDAC, however, the impact of PSCs on this process and its potential correlation with the development of gemcitabine chemoresistance in PDAC remain unclear. This study aims to investigate the impact of PSCs on pancreatic cancer cell metabolism and chemosensitivity in vitro by using BxPC-3, Panc-1 and SW-1990 cells.

2. Materials and methods

2.1 Aseptic conditions

To avoid contamination by microorganisms such as bacteria, fungi or viruses, all the cell culture work was done under aseptic conditions. All work regarding cell cultures was done inside a laminar flow hood (cell culture hood) to prevent contamination from aerosols and airborne particles. The hood bench and all equipment used inside the hood were sprayed with 70% ethanol before and after use. Moreover, the hood was regularly cleaned. Gloves used during cell culture experiments to protect the cells from human contamination were always sprayed with 70% ethanol. Furthermore, all reagents that were not provided sterile were sterilized using a 0.22 µm syringe filter or autoclaved depending upon the amount of reagent required. Lastly, pipette tips were always switched between handling of different cell lines and cell culture conditions.

2.2 Cells

2.2.1. Pancreatic cancer cell lines

The commercially available pancreatic cancer cell lines BxPC-3, Panc-1 and SW1990 were used in this study. The cell lines were obtained from American Type Culture Collection (ATCC, Manassas, VA, USA) [66]. The aliquots of the cells for each cell line were stored in a liquid nitrogen vapor container. Table 1 below provides some information on cell line characteristics and patient information from which these cell lines were originally derived from [67]. Additional information about these cell lines can be found on ATCC (website).

2.2.2 Pancreatic stellate cell cultures (PSC-1, PSC-2 and HPaSteC)

PSC-1 and -2: Human PDAC-derived primary cultures of PSCs, PSC-1 and PSC-2, were obtained from two individual tumor biopsies (3.5 mm^2) from two different patients. The PSCs were isolated by the outgrowth method, as described previously [68]. The PSC-1 cells were isolated from the tumor of a treatment-naive patient (not treated before surgery), whereas PSC-2 cells were isolated from the tumor of a neoadjuvantly treated patient who received 4-cycles of FOLFIRINOX before surgery.

Table 1: Overview of cell lines; Donor information and characteristics.

Cell Line	Age	Gender	Derivation	Metastasis	Proliferation	Differentiation
BxPC-3	61	Female	Primary tumor	No	48-60 h	Moderate to poor
Panc-1	56	Male	Primary tumor	Yes	52 h	Poor
SW-1990	56	Male	Spleen metastasis	Yes	64 h	-

HPaSteC: Human Pancreatic Stellate Cells (HPaSteC) were derived from normal human pancreas of a 22-week-old, fetal, non-diseased, male donor. Isolation of these cells was followed by purification and cryopreservation. HPaSteC cells are delivered frozen at passage one. Each cryovial contains 1 mL with a cell concentration of $>5.0*10^5$. Cells are, upon delivery, directly transferred and stored into a liquid nitrogen vapor container until further use. HPaSteC cells were cultured and maintained by other laboratory colleagues as described previously [68].

2.3 Cell culture medium

2.3.1. Complete growth medium

Dulbecco's modified Eagle's medium (DMEM) glutamax bottle (cat nr: 31966021, ThermoFisher, Waltham, MA, USA) was used to prepare a complete growth medium. Sterile filtered Amphotericin B (Amp, cat nr: 15290026, ThermoFisher), Penicillin-Streptomycin (PS, cat nr: 15140122, ThermoFisher) and fetal bovine serum (FBS, cat nr: 16000044, ThermoFisher) were warmed in a water bath (37℃). 50 mL FBS (10%) and 5 mL (1%) of each antibiotic was added to a 450 ml Dulbecco's modified Eagle's medium (DMEM) glutamax bottle and shaken to mix.

2.3.2. Serum-free medium (SFM)

Complete growth medium without FBS and antibiotics was used as serum-free medium (SFM).

2.3.3 Freezing medium

Freezing medium is used to cryopreserve cultured cells in liquid nitrogen vapor containers. Freezing medium consists of a complete growth medium mixed with a cryoprotective agent, in this case DMSO (Cat nr: D5879, Sigma-Aldrich), which reduces the freezing point and prevents the formation of ice crystals [69]. Furthermore, the freezing medium was made using DMEM-glutamax containing 1% antibiotics (PS and Amp) + 10% DMSO and 20% FBS. For example, to prepare 10 mL freezing media 1 mL of DMSO and 1 mL FBS was added to 8 mL of complete growth medium.

2.3.4. Pancreatic stellate cell conditioned medium (PSC-CM)

PSCs were cultured in complete growth media. The complete growth medium was removed from the plate when the cells were sub-confluent. The plate was washed four times with PBS (Cat nr: P4417, Sigma-Aldrich) to make sure all medium was removed. 10 mL SFM was added to the plate. The plate was incubated at 37°C for 48h. The medium was added to 15 mL tube and centrifuged at 5000 rpm for 5 min. The supernatant was sterile filtered and poured into a new 15 mL tube, and the pellet was discarded. Tubes were stored at -20°C degrees indefinitely or until further use.

2.4 Cell culture

2.4.1. Thawing / Seeding

Complete growth medium was pre-warmed to 37°C. Vials with corresponding cells were picked up from a liquid N_2 tank and held in a 37°C water bath until the sides were thawed but the center remained frozen. Thereafter, 10 mL of complete growth medium was added to a 100-mm tissue culture plate and the cells were poured onto the plate. The plate was then swirled lightly to achieve a homogenous mix of cells and placed in an incubator overnight. The following day, the medium was changed to a fresh complete growth medium and the cells were further grown until the plate was more than 70% confluent or needed for an experiment.

2.4.2. Trypsinization

Firstly, the complete growth medium was removed from the plate. Thereafter, the plates were washed 2x by adding 1 mL PBS to the side of the plate and light swirling. 550 µL trypsin (Trypsin-EDTA, cat nr: BE17-161, Thermo Fisher Scientific) were added directly on the cells

and the plate was swirled and incubated for 3-5 min. The cells were then examined in the microscope to observe if all had become detached. If not detached, the plate was lightly bashed against a table top. With most of the cells detached, 3 mL complete growth medium were added to stop the trypsinization process. The cell mix was transferred to a 15 mL Nunc tube and centrifuged for 3 min at 1000 rpm. The supernatant was discarded and the tube was hit with the fingers to detach the pellet and loosen the cells. Finally, the cells were re-suspended in culture medium and diluted accordingly, or in freezing medium (1 mL freezing medium per vial to be frozen), depending on the planned next activity.

Table 2: Overview of different plates used in seeding experiments.

Plate	Size	Plating volume	Seeding density	Cells at confluence
96-well plate	0.3 cm^2	100 µL	0.01 x 10^6	0.05 x 10^6
6-well plate	10 cm^2	2 mL	0.3 x 10^6	1.2 x 10^6
100 mm dish	60 cm^2	10 mL	5 x 10^6	20 x 10^6

2.4.3. Counting

Cells were counted using Invitrogen Countess II automated cell counters. Equal volumes of cell mixture and tryptan blue (Cat nr: T8154, Sigma-Aldrich) were mixed and 10 µL of this mixture were loaded onto a disposable Countess chamber slide (Cat nr: C10283, ThermoFisher). This slide was inserted into the Invitrogen Countess II automated cell counter.

2.4.4. Passaging

All cells were incubated in an incubator with 37°C and 5% CO_2. Medium was changed every 3-4 days. Cells were examined in a light microscope to inspect growth. When cells were approximately 80% confluent, they were split. Cells were split by trypsinization (see section 2.4.2 trypsinization) and added to a new plate with 10 mL complete growth medium.

2.4.5. Cryopreservation

Cryopreservation is a useful method for long term storage of cells while at the same time maintaining cell viability. This is very practical when doing several experiments on the same cell line, as it minimizes mutations and genetic changes so that the cells have the same

characteristics regardless of when you want to use them. For cryopreservation, cells were trypsinized (see 2.4.2 trypsinization) and resuspended in freezing medium. The re-suspended mixture was aliquoted in cryovials (1 mL per vial), and frozen overnight at -80°C. Then vials were transferred to a liquid N_2 tank at -196°C for indefinite storage.

2.5 Experimental procedures

2.5.1 Interactions between cancer cells and stellate cells.

For morphology, viability, proliferation and glucose metabolism experiments, the following common experimental setup was used. Around 10 000 cells/well, depending on the experiment, were seeded in 100 µL/well in DMEM in a 96-well plate and incubated overnight at 37°C. The following day, the plates were washed 2x with 1X PBS. The cells were incubated with 100 µL low glucose DMEM for 2h at 37°C to acclimatize the cells to a less optimal medium. After acclimatization, the cells were again washed 2xwith 1X PBS, and 100 µL new medium (either SFM or one of the following conditioned media from PSC-1, PSC-2 or HPaSteC) were added to the wells and the cells were incubated for 24, 48 and 72h at 37°C.

2.5.2 H & E staining

Cells were washed once with 1X PBS to get rid of any leftovers from culture medium. To achieve fixation, the cells were incubated with 100 µL 4% formaldehyde solution (Cat nr: 30525-89-4, Sigma-Aldrich) at 4°C for 15 min. Following fixation, the cells were washed 3x with a wash buffer, 0.1% Triton x-100 in 1X PBS (Cat nr: T-9284, Sigma-Aldrich), each wash for 3-5 min at room temperature (RT). Thereafter, cells were incubated with 100 µL/well of Hagens Hematoxylin solution for 5 min to stain the nucleus. To get rid of any leftover hematoxylin, the cells were washed 3x with tap water, each wash for 3-5 min at RT. To acidify the cells, cells were incubated with an acidified solution (0.1% acetic acid in distilled water) for 1-2 seconds and then washed once with tap water (100 µL/well). After acidification, cells were incubated with 100 µL/well of Eosin solution (Cat nr: ab246824, Abcam) for <1 min to obtain a cytoplasmic stain. After cytoplasmic staining, cells were washed 3x with tap water, each wash for 3-5 min at RT, and once with distilled water (100 µL/well). Lastly, 100 µL distilled water was added to each well. Photos were then taken immediately. The plate could also be stored in 4°C until use (max 1 week)

2.5.3 Morphology assessment

The H&E-stained cells were examined and pictures were captured using a light microscope (Zeiss) at 40X magnification. The cells were subsequently manually counted and the area % covered by the cells was measured using ImageJ.

2.5.4 MTT cell viability assay

3-[4,5-dimethylthiazol-2-yl]-2,5-diphenyltetrazolium bromide (MTT) is a water-soluble yellow tetrazolium salt that in actively respiring cells is converted to insoluble purple formazan crystals by the mitochondria [70]. The MTT assay is based on measuring the concentration of formazan to detect the number of viable cells. The assay was performed by trypsinizing the cells (see 2.4.2 Trypsinization) followed by the addition of 3 mL of complete growth media. The cell mixture was transferred to a 15 mL tube and centrifuged at 1000 rpm for 3 min. The supernatant was subsequently removed and the remaining pellet (cell pellet) was resuspended in 3 mL complete growth media. Following resuspension, the cells were diluted according to the automatic cell counter, to 100 000 cells. Thereafter, 100 µL of cells (10 000 cells/100 µL) were added into each representative well on a 96-well plate and incubated overnight. The following day, serial dilutions in a 1:10 ratio were prepared from stock of chosen drug and diluted in complete growth medium. Culture medium was replaced with the drug-media mix (100 µL/well) and incubated for 48h at 37℃. After the 48h incubation, a mixture of plain DMEM and MTT labelling reagent, 5 µL MTT per 100 µL (ratio 1:20), was prepared. Thereafter, the culture medium was replaced with 100 µL/well of the DMEM/MTT mix. Three replicates of wells containing MTT but no cells were included as a negative control. The plate was incubated for 4h at 37℃, allowing viable cells to convert MTT into the formazan crystals. Lastly, violet colored formazan crystals were observed under the light microscope. The medium was carefully removed and 100 µL/well DMSO was added to solubilize the purple formazan crystals. Finally, the absorbance was read at 570 nm by using a spectrophotometer.

2.5.5 BrdU cell proliferation assay

The “BrdU Cell Proliferation ELISA Kit (colorimetric, abcam)” was used. All reagents used were prepared according to the manual in this kit [71]. In short, 20 000 cells/well were seeded in 100 µL/well with DMEM in a 96-well plate. The plate was incubated overnight at 37°C, and the following day, the plates were washed 2x with 1X PBS. The cells were then incubated for 2h with 100 µL/well low glucose DMEM at 37°C to acclimatize the cells to a

suboptimal medium. The cells were subsequently washed 2x with 1X PBS, and 100 µL new medium (either SFM or CM) were added to the wells. The cells were incubated for 24h and 72h at 37°C. Following incubation, the medium was replaced with 100 µL/well of BrdU + DMEM mixture (1x BrdU), followed by an overnight incubation. The next day, the wells were incubated with 200 µL fixing Solution at RT for 30 min. Following fixation, the 96-well plates were washed 3x with 100 µL 1X Wash Buffer. Thereafter, 100 µL/well anti-BrdU monoclonal Detector Antibody was added to the wells and the plates were incubated 1h at RT. Following incubation, wells were washed 3x with 1X Wash Buffer. Subsequently, the cells were incubated with 100 µL/well of 1X Peroxidase Goat Anti-Mouse IgG Conjugate for 30 min at RT, followed by washing 3x with 1X Wash Buffer. A final water wash was performed by washing the entire plate with 200 µL/well distilled water. Afterwards, the plates were dried on absorbent paper towels to remove any remaining contamination. Finally, the cells were incubated with 100 µL/well TMB Peroxidase substrate for 30 min at RT in the dark. Wells containing actively proliferating cells will be visible by a turquoise color, the intensity of which is directly proportional to the amount of BrdU incorporated in the proliferating cells. The reaction was stopped by adding 100 µL/well of Stop Solution. A color change from turquoise to vibrant yellow could be seen in all wells. The plate was read at 450 nm by using a spectrophotometer.

2.5.6 Glucose transport assay

^{3}H-2-deoxy-D-glucose (^{3}H-2-deoxy-DG) is transported into the cells with the glucose transporters (GLUTs), the same transporters that transport glucose, however, ^{3}H-2-deoxy-DG is phosphorylated intracellularly and thus avoids further breakdown [72]. The ionizing radiation from ^{3}H-2-deoxy-DG encounters and collides with crystals in the scintillation solution, which emits light. The number of photons in the emitted light is directly proportional to the number of ionizing particles (radioactivity), in this case, the glucose. This signal can be read by a scintillation counter and quantified as a measure of glucose transport [73].

The 96-well plate was washed 2x with 1X PBS before adding 100 µL/well of KRH buffer, HEPES, (Sigma Aldrich H3375), NaCl (Sigma Aldrich 31434), KCl (Sigma Aldrich P9541), $CaCl_2$ (Sigma Aldrich 223506), $MgSO_4$(Merck 105886), BSA (#A4503, Sigma-Aldrich), pH: 7,4) followed by 10 µL/well of start solution (^{3}H-2-deoxy-DG, cat nr: NET238C001MC, Perkin Elmer, Waltham, MA, USA), (2-deoxy-DG, cat nr: D8375-1G, Sigma-Aldrich), and PBS). The plate was incubated at 37°C for 24h. After a day, 10 µL/well of stop solution (Phloretin, cat nr: P7912-100MG, Sigma-Aldrich), Methanol (Sigma-Aldrich,

#34860), and PBS) were added to the wells and the cells were incubated for 10 min to stop the uptake/transport. Thereafter, the plate was washed 3x with ice-cold PBS. This plate can be frozen down and used when required. When the experiment was to be performed, the cells were incubated with 100 µL/well of 0.2 M NaOH on a see-saw for 10 min to lyse the cells. 50 µL of the cell lysates were transferred to a scintillation tube along with 4 mL scintillation solution (Opti-Fluor, cat nr: 6013199, Perkin Elmer). A liquid scintillation counter was used to quantify the amount of radioactive glucose in the cell lysates. The amount of ^{3}H-2-deoxy-DG taken up by the cells is directly proportional to the radioactivity from the cell lysates.

2.5.7 Glycolysis assay (Lactate secretion)

The following assay is based on the principle of anaerobic glycolysis which produces lactate that is secreted by the cells. Lactate dehydrogenase is an enzyme which converts lactate and NAD+ to pyruvate and NADH. NADH has reducing power and reduces a tetrazolium salt in the reaction solution to a colored formazan that absorbs light between 490-520 nm. The amount of formazan present is directly proportional to the amount of lactate secreted by the cells into the medium. This can thus be used as an indirect measurement of glycolysis. To measure the activity of glycolysis or lactate content secreted by the cells in the medium, a "Glycolysis Cell-Based Assay" kit was used according to the manufacturer's instructions [74]. Briefly, the supernatant from BxPC-3, Panc-1 and SW-1990 treated with PSC-CMs or standards were added to a 96-well plate along with an assay buffer and enzyme mixture. The plate was incubated for 30 min on a see-saw before the absorbance was read at 490 nm using a spectrophotometer.

2.5.8 Measurement of glucose in the cells

The following assay is based on the concept of oxidation of glucose to δ-gluconolactone and the following reduction of the FAD-dependent enzyme glucose-oxidase to glucose-oxidase-$FADH_2$. Glucose-oxidase-$FADH_2$ is regenerated to its oxidized state using oxygen, with the formation of hydrogen peroxide (H_2O_2) in the process. A catalysator called horseradish peroxidase is used to force hydrogen peroxide to react with 3,5-Dichloro-2-hydroxybenzenesulfonic acid sodium salt and 4-aminoantipyrine to make a pink-colored product which absorbs light at 514 nm [75].

1. Glucose + Glucose-oxidase-FAD ←→ Gluconolactone + Glucose-oxidase-$FADH_2$.
2. Glucose-oxidase-$FADH_2$ + O_2 ←→ Glucose-oxidase-FAD + H_2O_2
3. $2H_2O_2$ + 3,5-Dichloro-2-hydroxybenzenesulfonic acid sodium salt and 4-aminoantipyrine → $4H_2O$ + HCl + Pink color [75]

To measure the remaining glucose in the media, a "Glucose Colorimetric Assay kit" was used according to the manufacturer's instructions [75]. Briefly, the supernatant from BxPC-3, Panc-1, SW-1990 treated with PSC-CM or standards were added to a 96-well plate along with an assay buffer and enzyme mixture. The plate was incubated for 10 min on a see-saw before the reading of absorbance at 520 nm using a spectrophotometer.

2.5.9 Measurement of protein concentration

Protein concentrations were measured to account for differences in cell numbers and to support the results. A standard dilution range with known concentrations was made by mixing BSA with a diluent (PBS) as shown in table 3. 10 µL of standards and 10 µL of each respective sample were transferred to a 96-well plate as pictured in table 4. 200 µL Bradford reagent was added to all wells to be assessed, standards included. The Bradford reagent starts off with a brown color when no protein is present and gradually changes to a deep blue color at very high protein concentrations. The intensity of the blue color is directly proportional to the protein concentration. Therefore, the Bradford reagent can be used as a measure to indicate how much protein is contained in a sample. To quantify the protein in a sample, the plate was read on a spectrophotometer at 595 nm.

Table 3: Dilution scheme for standard test tube protocol and microplate procedure for protein concentration with BSA. (Working Range = 20–2 000 µg/mL)

Vial	Volume of Diluent (µL)	Volume and Source of BSA (µL)	Final BSA Concentration (µg/mL)
A	0	300 of Stock	2000
B	125	375 of Stock	1500
C	325	325 of Stock	1000
D	175	175 of vial B dilution	750
E	325	325 of Vial C dilution	500
F	325	325 of vial E dilution	250
G	325	325 of vial F dilution	125
H	400	100 of vial G dilution	25
I	400	0	0=Blank

2.5.10 Preparation of protein lysates

A minimum confluence of 70% was required to perform this experiment. We used a microfuge tube (1.5mL) per replicate per condition. 5% Bromophenol blue (#B0126, Sigma-Aldrich), 5% of total lysis buffer, was added to the microfuge tube. The wells were washed 3x with 1X PBS, with subsequent addition of 150 µL lysis buffer to each well. Thereafter, the plate was swirled lightly and the creation of a viscous substance was observed. The plate rested for 5 min and then the wells were scraped completely of the viscous substance which subsequently was collected in a corresponding 1.5 mL microfuge tube. Two replicates were collected in the same tube. 10% 2-mercaptoethanol (Cat nr: M3148, Sigma-Aldrich), 10% of total volume of lysis buffer, was added (inside a fume hood) to each 1.5 mL tube and then heated on a heating block for 5 min at 95°C. While on the heating block, the tubes build up pressure. This pressure was expelled by opening the lid of the tube during the incubation time. Tubes were then stored in -20°C until needed.

Table 4: Setup for protein concentration experiments. Depending on the experiments, row 3-12 always contain the sample that belongs to the corresponding experiment, while row 1 and 2 contain the standards. The setup was modified for each experiment to best suit the protein concentration for the respective experiment. B-H is the concentration of BSA in (µg/mL)

	1 (standard	2 (standard)	3	4	5	6	7	8	9	10	11	12
A	**Blank**	**Blank**										
B	**31,25**	**31,25**										
C	**62,5**	**62,5**										
D	**125**	**125**										
E	**250**	**250**										
F	**500**	**500**										
G	**1000**	**1000**										
H	**2000**	**2000**										

2.5.11 Gemcitabine sensitivity

Two identical 96-well plates were utilized, one with gemcitabine and one control plate. In this experiment, the experimental setup is the same as stated in the section 2.5.1 until after the acclimatization part. After acclimatization, cells were washed 2x with PBS and 100 µL of new medium, SFM or PSC-CM were added to the respective wells. The plates were then incubated at 37°C for 72h. Following this, 100 µL of gemcitabine (10 µM) diluted in SFM was added to the gemcitabine plate, while only 100 µL SFM were added to the control plate. The plates were then incubated at 37°C for 24h. After 24h, a mixture of plain DMEM and MTT labelling reagent, 5 µL MTT per 100 µL (ratio 1:20), was prepared. Thereafter, the culture medium was replaced with 100 µL/well of the DMEM/MTT mix. Three replicates of wells containing MTT but no cells were included as negative controls. The plate was incubated for 4h at 37°C, allowing viable cells to convert MTT into the formazan crystals. Lastly, violet colored formazan crystals were observed under the light microscope. The medium was carefully

removed and 100 µL/well DMSO was added to solubilize the purple formazan crystals. Finally, the absorbance was read at 570 nm by using a spectrophotometer.

2.5.12 Western Blot

After reaching confluence, the cells were washed with PBS to get rid of growth medium. To obtain cell lysates, the cells were boiled with Laemmli buffer for 5 min (4% SDS, 20% glycerol, and 120 mM Tris-HCl, pH 6.8) with subsequent addition of 2% BPB and 5% β-mercaptoethanol. Electrophoresis (SDS-PAGE) was used to separate protein on 10% polyacrylamide gels. Proteins were then transferred to nitro-cellulose membranes by utilizing a semidry transfer system from BioRad. Tris-buffered saline containing 0.1% Tween 20 (TBST) with 5% non-fat dry milk solution was used to block the membranes. Thereafter, the membranes were incubated overnight with primary antibodies at 4°C. After incubation, the blots were washed 3x with TBST and incubated at RT with HRP-conjugated secondary antibodies for 1h. The blots were processed and visualized with LumiGLO® (KPL, Gaithersburg, MD, USA).

2.5.13 Secretome analysis

The CM samples from PSC-1, PSC-2 and HPaSteC (5 mL in triplicate for each culture) were subjected to a proteomics-based secretome analysis, as described previously [68]. Aliquots of 5 mL PSC-CM were concentrated down to 250 µL using a 10 kDa cut off Amicon Ultra centrifugal filter. The proteins were further reduced, alkylated and overnight digested with trypsin (Promega). The peptides were desalted and concentrated before being submitted to mass spectrometry (MS). Each peptide mixture was analyzed by nEASY-LC coupled to QExactive Plus (ThermoElectron, Bremen, Germany) with EASY Spray PepMap®RSLC column (C18, 2 µm, 100Å, 75 µm x 50 cm). Proteome Discoverer 2.1 (Thermo Fisher Scientific) and Mascot 2.6 (MatrixScience, London, UK) search engines were used to identify the proteins. The following search criteria were used for Mascot searches: trypsin digestion with two missed cleavage allowed, carbamidomethyl (C) as fixed modification and Acetyl (N-term), Gln->pyro-Glu (N-term Q), Oxidation (M) as dynamic modifications. The parent mass tolerance was 10 ppm and MS/MS tolerance 0.1 Da. The SwissProt database for human entries supplemented with known contaminants provided by MaxQuant was used for the database searches. All proteins identified that were statistically significant ($p<0.05$) in Mascot were further filtered in Proteome Discoverer for at least medium confidence identifications. The list of identified

proteins was subjected to the Kyoto Encyclopedia of Genes and Genomes (KEGG) database for pathway analysis [76] and Gene Ontology (GO) analysis was performed by using the DAVID Bioinformatics Database [77, 78].

3. Results

3.1 Morphology

To evaluate the impact of three different PSC-CMs (CM from PSC-1, PSC-2 and HPaSteC) on the morphology of the PCC lines BxPC-3, Panc-1 and SW-1990, a morphological assessment utilizing H&E staining was performed. Figure 6 shows that the BxPC-3 cells appear more elongated compared to the rounder Panc-1 cells. Furthermore, Panc-1 grows in a more clustered pattern compared to the BxPC-3 cells after PSC-CM treatment. On the other hand, SW-1990 cells appear larger and more circular in shape and contain larger nuclei compared to BxPC-3 and Panc-1. SW-1990 also grows more in singletons, in a similar manner to BxPC-3, compared to Panc-1. Figure 6 shows that there are considerably more cells when the cells are grown in the conditioned medium, compared to the serum free medium. Of the three PSC-CMs, HPaSteC stimulates strongest cell growth after both 24h and 72h.

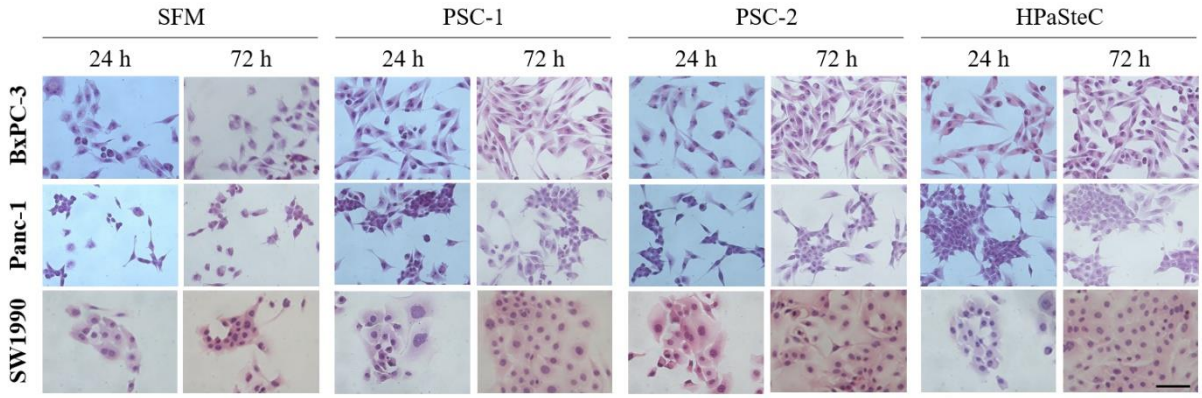

Figure 6: Morphological assessment. Representative images of H&E-stained PCC lines BxPC-3, Panc-1 and SW-1990. PCCs seeded in 96-well plates were incubated with SFM or PSC-CM for indicated times. Following incubation, the cells were stained by the H&E method. Pictures were taken at 40x magnification. Scale bar = 100 μm. H&E, hematoxylin and eosin; PC, pancreatic cancer; PCC, pancreatic cancer cells; PSC, pancreatic stellate cells; PSC-CM, PSC-conditioned medium; SFM, serum-free DMEM.

The H&E images were further investigated for cell number and cell growth area to further understand the impact of the PSC-CMs on the PCC phenotype. As shown in figure 7, BxPC-3 increased significantly in area coverage when treated with CM from PSC-1 and HPaSteC compared to the SFM control after 24h. After 72h, a significant increase in cell area

was seen for all three PSC-CMs compared to SFM. Moreover, no significant increase in cell numbers was observed for BxPC-3 when treated with PSC-CMs compared to SFM control after 24h. However, after 72h of growth, all three PSC-CMs had resulted in a significantly increased number of BxPC-3 cells. Both area coverage and cell number were significantly increased from 24h to 72h for all three PSC-CMs, except for the area coverage of BxPC-3 cells grown with CM from PSC-1, which was borderline significant (p-value = 0.06).

Panc-1 exhibited a different pattern than BxPC-3 in both area coverage and cell number (Figure 7). Treatment with all three PSC-CMs significantly increased both cell growth area and cell number in Panc-1 cells compared to SFM after 24h incubation, while only CM from PSC-1 and HPaSteC showed a similar significant increase after 72h incubation. Interestingly, both cell growth area and cell number decreased significantly from 24h to 72h in Panc-1 cells treated with HPaSteC. For both BxPC-3 and Panc-1 cells, CM from HPaSteC seemed to increase both area coverage and cell numbers the most compared to the effect of the other PSC-CMs.

Lastly, SW-1990 behaved differently from BxPC-3 and Panc-1 (Figure 7). Treatment of SW-1990 cells with all three PSC-CMs did neither increase cell growth area, nor cell number after 24h compared to the SFM control. After 72h of growth, there was a more than 2-fold decrease in cell growth area for SFM treated SW-1990 cells. Moreover, SW-1990 cells treated with CM from PSC-1 and PSC-2 significantly increased the cell growth area after 72h, while the increase was borderline significant in HPaSteC-CM treated cells. Regarding cell number, only CM from PSC-2 significantly increased SW-1990 cell numbers after 72h. From 24h to 72h, no significant change was observed across all three PSC-CMs, although the effect was borderline significant for SW-1900 treated with CM from PSC-2 (p-value 0.06). Interestingly, no significant increase in cell growth area was seen in PSC-CM treated SW-1990 cells after 72h compared to 24h, however, the cell number increased from 24h to 72h.

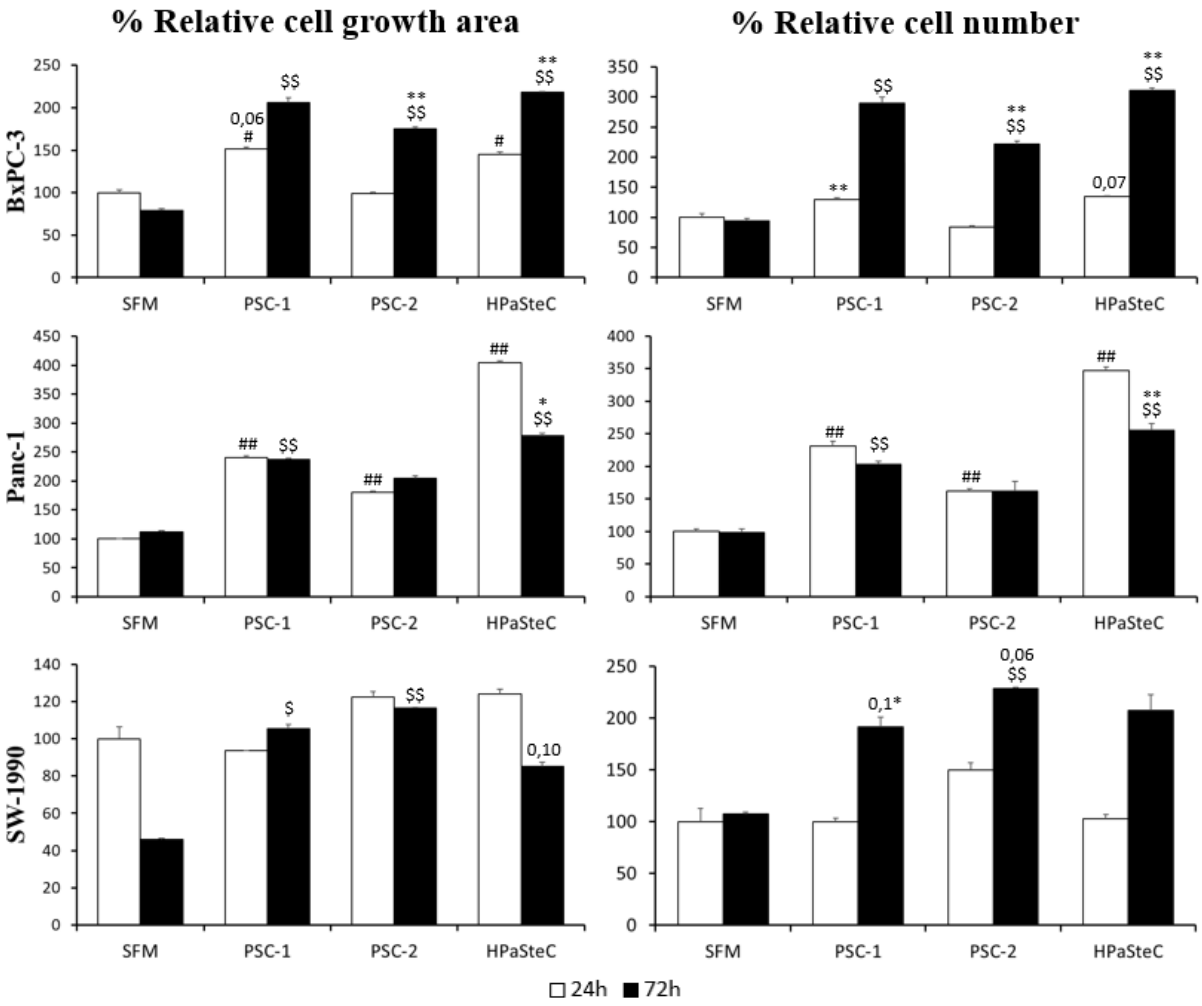

Figure 7: Cell growth area and cell number assessment. BxPC-3, Panc-1 and SW-1990 were incubated with SFM or three different PSC-CMs (PSC-1, PSC-2, and HPaSteC) for 24h and 72h and subsequently stained with H&E, as represented in Figure 6. Herein, 3-4 representative images for each condition and cell line were evaluated for cell growth area which was determined using ImageJ software (left panel) and manual counting of the cell number (right panel). Data are mean ± SEM of 3-4 replicates. *p<0.05, **p<0.01 comparing 24h to 72h SFM or PSC-CM. #p<0.05, ##p<0.01 comparing SFM vs PSC-CM at 24h. $p<0.05, $$p<0.01 comparing SFM vs PSC-CM at 72h. H&E, hematoxylin and eosin; PC, pancreatic cancer; PCC, pancreatic cancer cells; PSC, pancreatic stellate cells; PSC-CM, PSC-conditioned medium; SFM, serum-free DMEM.

3.2 Cell viability using MTT

The MTT assay was performed to investigate the impact of PSC-CM on the viability of the three PC cell lines BxPC-3, Panc-1 and SW-1990. Incubation with any of the three PSC-

CMs significantly increased the viability of the BxPC-3 cells at 24h and 72h compared to SFM control as seen in figure 8. Furthermore, BxPC-3 cells treated with all PSC-CMs significantly increased its viability from 24h to 72h.

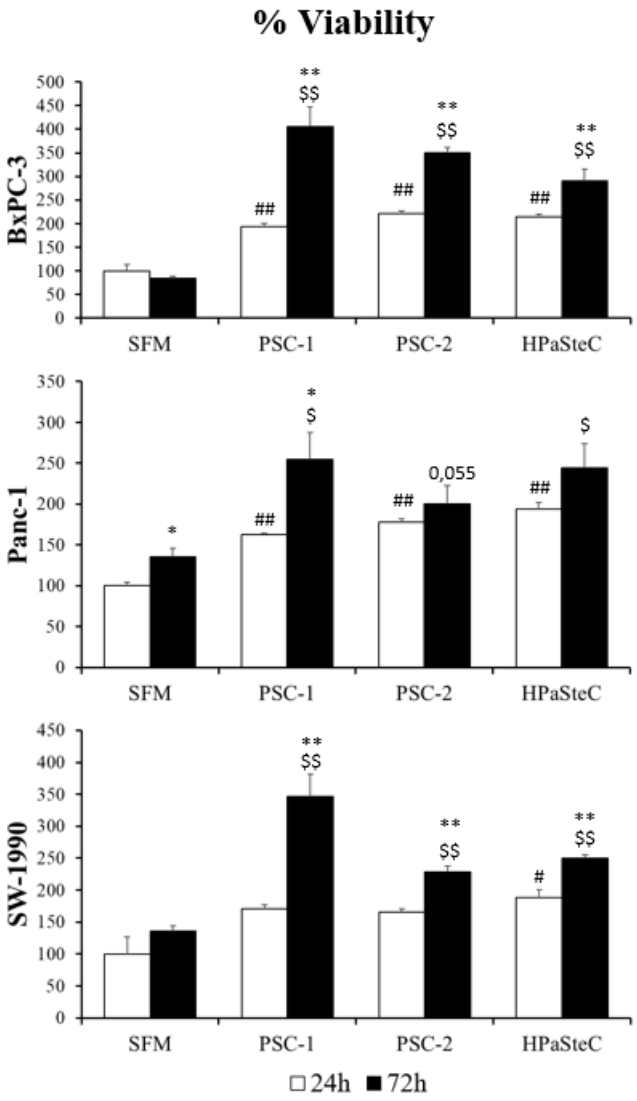

Figure 8: Assessment of cell viability using MTT assay. The PCCs were seeded in a 96-well plate and grown for 24h and 72h with either SFM or the conditioned media from PSC-1, PSC-2 or HPaSteC. Following incubation, an MTT assay was performed to determine the cell viability. Absorbance was measured at 570 nm using a spectrophotometer. Data are mean ± SEM of three replicates. *p<0.05, **p<0.01 comparing 24h to 72h SFM or PSC-CM. #p<0.05, ##p<0.01 comparing SFM vs. PSC-CM at 24h. $p<0.05, $$p<0.01 comparing SFM vs. PSC-CM at 72h. PCC, pancreatic cancer cells; PSC, pancreatic stellate cells; PSC-CM, PSC-conditioned medium; SFM, serum-free DMEM.

Panc-1 cells followed the same trend as BxPC-3, albeit with lower significance. All three PSC-CMs increased the viability of Panc-1 cells at 24h compared to SFM. However, only CM from PSC-1 and HPaSteC significantly increased the viability at 72h. The increase in viability of Panc-1 cells grown with CM from PSC-2 was only borderline significant. Moreover, from 24h to 72h, only SFM and CM from PSC-1 were associated with a significant increase in cell viability.

No significant increase in cell viability was observed for SW-1990 cells grown with CM from PSC-1 and PSC-2 after 24h compared to control SFM. SW-1990 cells grown with

HPaSteC-CM significantly increased the cell viability at 24h. On the other hand, a significant increase in cell viability was observed in SW-1990 cells treated with all three PSC-CMs after 72h of growth compared to SFM. A significant increase in viability for SW-1990 cells treated with all PSC-CMs from 24h to 72h was also observed. Noteworthy, CM from PSC-1 cause the highest increase in viability in all three PC lines. PSC-CM induced viability was variable between the three PCC lines as well as between the PSC-CMs.

3.3 BrdU cell proliferation assay

A BrdU cell proliferation assay was performed to investigate the impact of PSC-CMs on the cancer cell proliferation using BxPC-3, Panc-1 and SW-1990 cells. A significant increase in cell proliferation of BxPC-3 was seen after both 24h and 72h of incubation with all PSC-CMs compared to the SFM control (Figure 9). Moreover, a further, significant increase in proliferation from 24h to 72h was observed for all PSC-CMs. Notably, there was an over 6-fold decrease in cell proliferation of BxPC-3 cells grown in SFM at 72h compared to 24h.

In Panc-1 cells, there was no statistically significant increase in cell proliferation after 24h when treated with PSC-CM compared to SFM control, however, the effect of incubation with CM from both PSC-1 and PSC-2 was borderline significant with p-values of 0.059 and 0.058, respectively (Figure 9). After 72h of incubation, all three PSC-CMs significantly increased cell proliferation in Panc-1 cells compared to the SFM control. A significant increase in cell proliferation from 24h to 72h was only observed if Panc-1 cells were incubated with CM from PSC-2 and HPaSteC. Furthermore, Panc-1 cells treated with SFM significantly reduced cell proliferation from 24h to 72h.

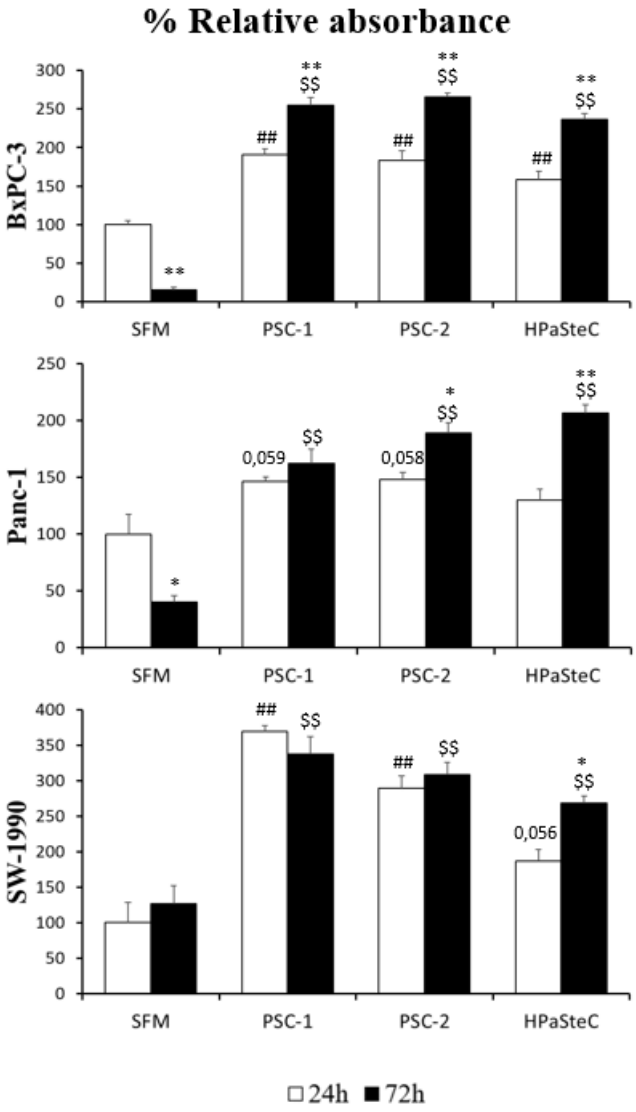

Figure 9: Assessment of cell proliferation using BrdU assay. 20 000 cells/well were seeded in 96-well plates and incubated for 24h and 72h with SFM or PSC-CMs (PSC-1, PSC-2 and HPaSteC). After incubation, the cells were processed for BrdU incorporation and detection. Actively replicating cells incorporate BrdU in their DNA and produce a turquoise color, the intensity of which is directly proportional with the amount of actively replicating cells. Absorbance was measured at 450 nm using a spectrophotometer. Data are mean ± SEM of three replicates. *p<0.05, **p<0.01 comparing 24h to 72h SFM or PSC-CM. #p<0.05, ##p<0.01 comparing SFM vs. PSC-CM at 24h. $p<0.05, $$p<0.01 comparing SFM vs. PSC-CM at 72h. PCC, pancreatic cancer cells; PSC, pancreatic stellate cells; PSC-CM, PSC-conditioned medium; SFM, serum-free DMEM.

SW-1990 showed a significant increase in cell proliferation after 24h in cells treated with CM from PSC-1 and PSC-2, while cells treated with HPaSteC-CM showed borderline significant change (p-value = 0.056) as compared to the SFM control (Figure 9). However, after 72h, all PSC-CMs significantly increased cell proliferation compared to SFM. Only SW-1990 cells treated with HPaSteC-CM significantly increased their proliferation from 24h to 72h, while it remained unchanged for CM from PSC-1 and PSC-2. Noteworthy, all PSC-CMs increased cell proliferation in all three PCCs at 72h compared to 24h, while the opposite effect was seen in SFM for both BxPC-3 and Panc-1 cells. Overall, a variability was observed between the PSC-CMs in their ability to influence cancer cell proliferation as well as between the individual PCC in their response to each PSC-CM.

3.4 Basal glucose transport

A glucose transport experiment was performed to investigate the time-dependent basal glucose transport in PCCs - BxPC-3, Panc-1 and SW-1990. No significant change in basal glucose transport was observed in BxPC-3 at any time point (Figure 10). In Panc-1, glucose transport increased from 8h to 24h, although this was not significant statistically. However, the glucose transport in Panc-1 cells at 72h was significantly reduced compared to both 8h and 24h. SW-1990 cells followed the same pattern for glucose transport as the Panc-1 cells. Glucose transport peaked at 24h, but was significantly reduced after 72h compared to both 8h and 24h

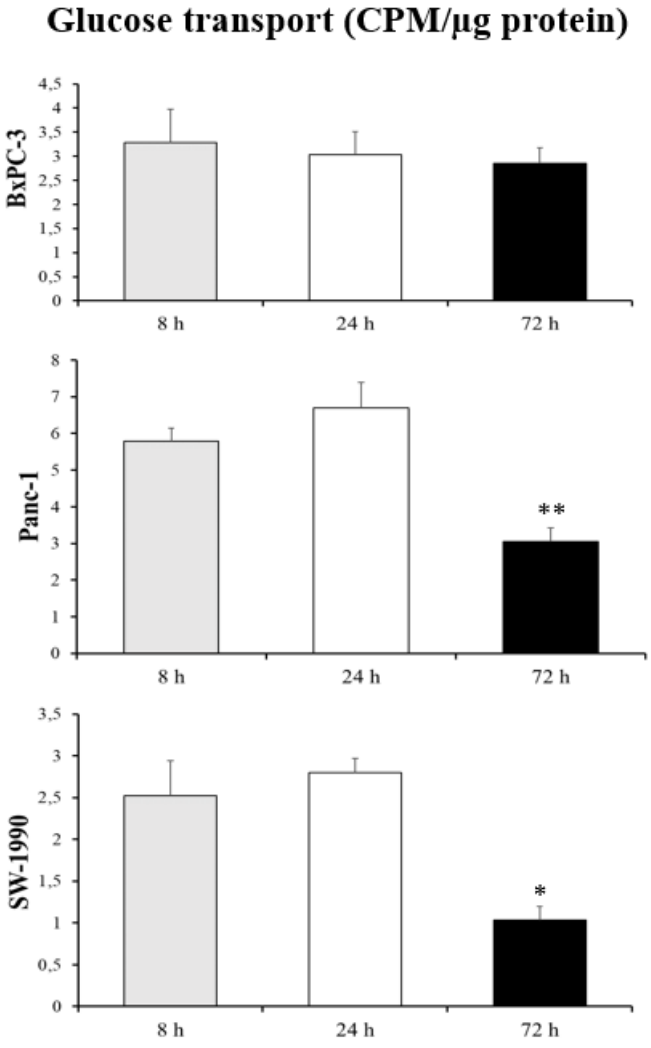

Figure 10: Assessment of basal glucose transport. Briefly, 10 000 cells/well seeded in 96-well plates were incubated with a KRH buffer containing radioactive ^{3}H-2-deoxy-DG for the indicated time points (8h, 24h and 72h). Intracellular ^{3}H-glucose was measured using a liquid scintillation counter, and the results were normalized to protein concentration. Data are mean ± SEM of four replicates. *p<0.05, **p<0.01 comparing 8h vs 72h. SFM, serum-free DMEM; CPM, counts per minute.

3.5 Glucose transport after PSC-CM exposure

Following the assessment of basal glucose transport, the glucose transport in PCC lines after exposure to PSC-CM was investigated. After a 24h incubation with any of the three PSC-CMs, BxPC-3 cells had significantly increased their glucose transport compared to the SFM control (Figure 11). After 72h of growth, only BxPC-3 cells treated with CM from PSC-2 and HPaSteC showed a significant increase compared to SFM. Furthermore, the only significant difference in glucose transport from 24h to 72h was observed in BxPC-3 cells treated with SFM, which was a reduction in glucose transport.

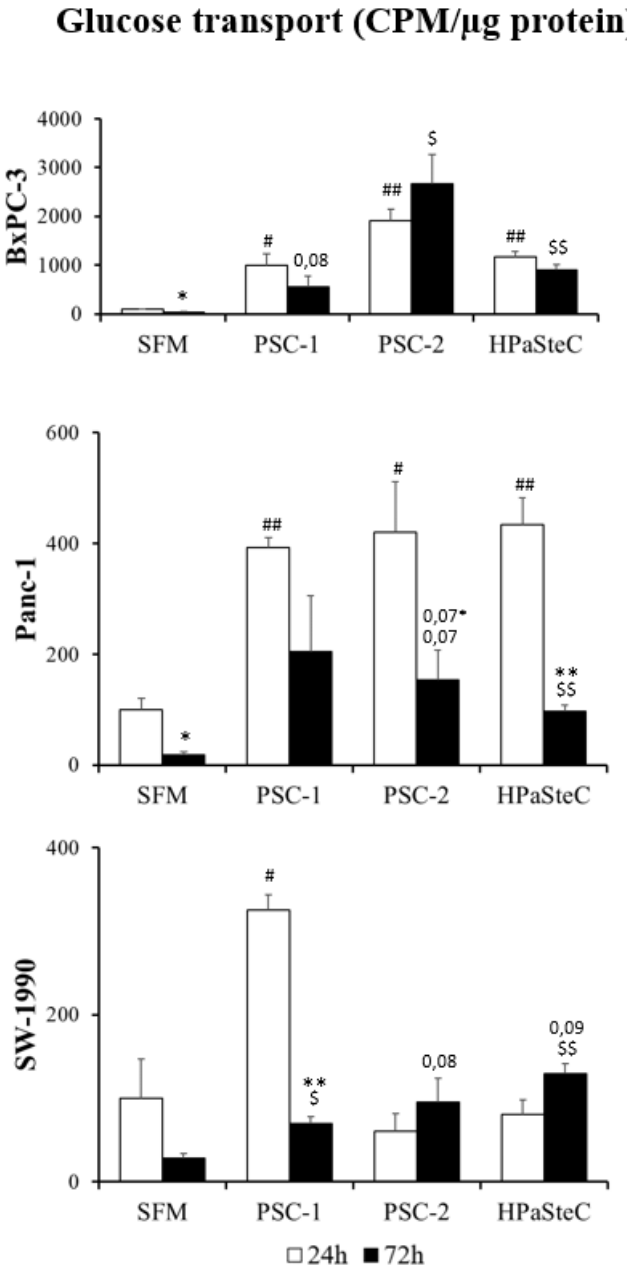

Figure 11: Assessment of glucose transport after PSC-CM exposure. Briefly, 10 000 cells/well were seeded in 96-well plates and incubated overnight. The following day, the media were changed to either SFM or any of the PSC-CMs and incubated for 24h and 72h. Subsequently, a KRH buffer containing radioactive ^{3}H-2-deoxy-DG was added to each well and incubated for 24h. Glucose transport was quantified using a liquid scintillation counter and normalized to the protein concentration. Data are mean ± SEM of three replicates. *p<0.05, **p<0.01 comparing 24h to 72h SFM or PSC-CM. #p<0.05, ##p<0.01 comparing SFM vs. PSC-CM at 24h. $p<0.05, $$p<0.01 comparing SFM vs. PSC-CM at 72h. PSC, pancreatic stellate cells; PSC-CM, PSC-conditioned medium; SFM, serum-free DMEM.

Panc-1 cells had an overall lower glucose transport compared to BxPC-3 (Figure 11). Panc-1 cells treated with any of the three PSC-CMs significantly increased glucose transport at 24h compared to the SFM control. However, after 72h, a significant difference was only seen in Panc-1 cells treated with HPaSteC-CM compared to SFM. From 24h to 72h, the only significant difference in glucose transport was seen in SFM and HPaSteC-CM treated Panc-1 cells, which reduced their glucose transport after 72h. Overall, all Panc-1 exhibited higher glucose transport after 24h, compared to 72h when treated SFM or any of the three PSC-CMs.

In SW-1990 cells, a significant increase in glucose transport was only seen after 24h when treated with CM from PSC-1 compared to the SFM control (Figure 11). In fact, CM from both PSC-2 and HPaSteC decreased the glucose transport after 24h compared to SFM, although the differences were not statistically significant. At 72h, only CM from PSC-1 and HPaSteC showed a significant difference in glucose transport compared to SFM. In contrast, from 24h to 72h, a significant decrease in glucose transport was only observed in SW-1990 cells treated with CM from PSC-1.

Noteworthy, glucose transport was reduced across all three cell lines from 24h to 72h upon incubation with SFM (Figure 11). Glucose transport was overall higher in BxPC-3, while Panc-1 and SW-1990 displayed similar levels. Furthermore, there was variability between the different PSC-CMs in their ability to induce glucose transport across the PCCs. Panc-1 was the only cell line that displayed higher glucose transport after 24h for all conditions. Overall, there was a trend that PSC-CM increased glucose transport after 24h and 72h in PCC lines compared to the control.

3.6 Lactate secretion following incubation with PSC-CM

Lactate secretion experiments were performed to assess the impact of PSC-CMs on glycolysis in PCCs. In BxPC-3 cells, a significant increase in lactate secretion was observed across all three PSC-CMs after both 24h and 72h, compared to the respective LGM controls (Figure 12). However, a significant increase in lactate secretion from 24h to 72h was only observed in HPaSteC-CM treated BxPC-3 cells. In Panc-1 cells, all three PSC-CMs significantly increased lactate secretion after 24h compared to the LGM control, while only CM from PSC-1 and HPaSteC significantly increased lactate secretion after 72h. Furthermore, from

24h to 72h, a significant decrease in lactate secretion was observed in Panc-1 cells treated with CM from PSC-1, while the opposite effect was observed following exposure to HPaSteC-CM.

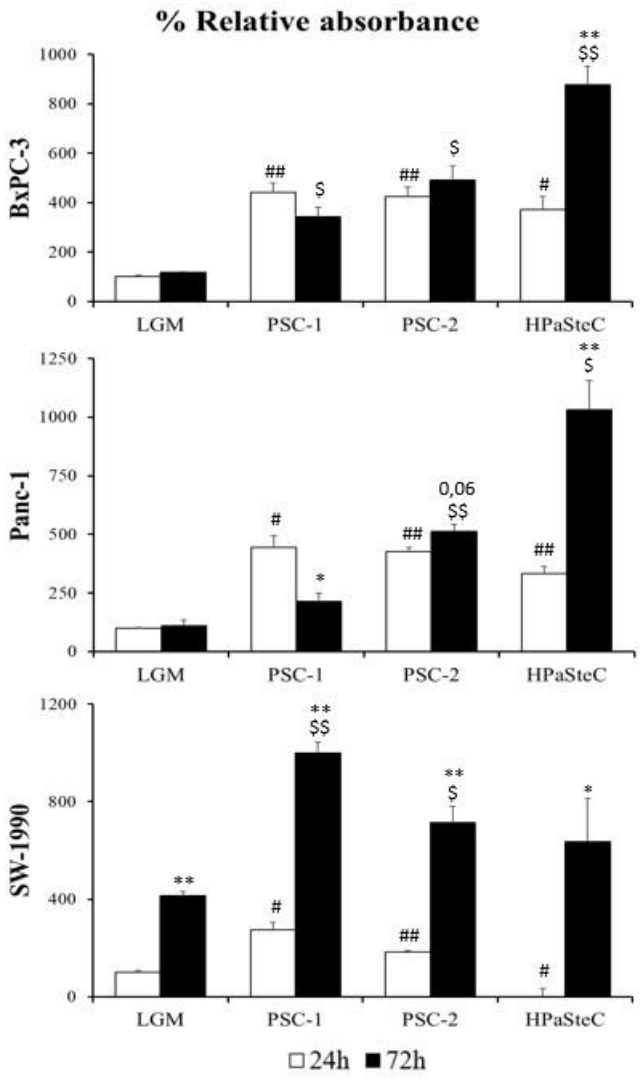

Figure 12: Assessment of lactate secretion in BxPC3, Panc-1 and SW-1990. Briefly 10 000 cells/well were seeded in a 96-well plate and incubated overnight. Next day, the cells were incubated with LGM for 2h to acclimatize the cells. After acclimatization, new medium, LGM or CM from PSC-1, PSC-2 and HPaSteC, was added, and the cells were incubated for 24h and 72h. To measure lactate secretion, a "Glycolysis Cell-Based Assay kit" was used according to the manufacturer's instructions. Data are ± SEM of three replicates. *p<0.05, **p<0.01 comparing 24h to 72h LGM or PSC-CM. #p<0.05, ##p<0.01 comparing 24h LGM vs. PSC-CM. $p<0.05, $$p<0.01 comparing 72h LGM vs. PSC-CM. PCC, pancreatic cancer cells; PSC, pancreatic stellate cells; PSC-CM, PSC-conditioned medium; LGM, low-glucose medium.

In SW-1990 cells, a significant increase in lactate secretion was observed for CM from PSC-1 and PSC-2, while a significant decrease in lactate secretion was observed for HPaSteC-CM after 24h compared to the LGM control (Figure 12). In contrast, after 72h, a significant increase in lactate secretion was only observed in SW-1990 cells treated with CM from PSC-1 and PSC-2. Interestingly, there was a highly significant increase in lactate secretion from 24h to 72h in SW-1990 cells growth in LGM. A significant increase was also observed with all three PSC-CMs from 24h to 72h. Overall, BxPC-3 and Panc-1 followed a similar pattern, where it appeared that HPaSteC-CM was most effective in inducing increased lactate secretion. Interestingly, HPaSteC-CM was the least effective in SW-1990 cells. SW-1990 cells treated

with LGM significantly increased their lactate secretion, an effect that was not apparent in BxPC-3 and Panc-1 cells. There was also variability between the different PSC-CMs regarding their induction of lactate secretion across all three cell lines.

3.7 Lactate secretion under nutrient-poor conditions

To see if the low-glucose medium had any impact on lactate secretion, PCCs pre-exposed to SFM or PSC-CM for 72h were further incubated with LGM for 24h and 48h, and lactate secreted in the medium was measured. For BxPC-3 cells, a significant increase in lactate secretion was seen with all PSC-CMs for both 24h and 48h compared to the respective SFM controls, as shown in figure 13. Moreover, from 24h to 48h, a significant increase in lactate secretion was seen in the BxPC-3 cells treated with all three PSC-CMs, but not in cells treated with SFM.

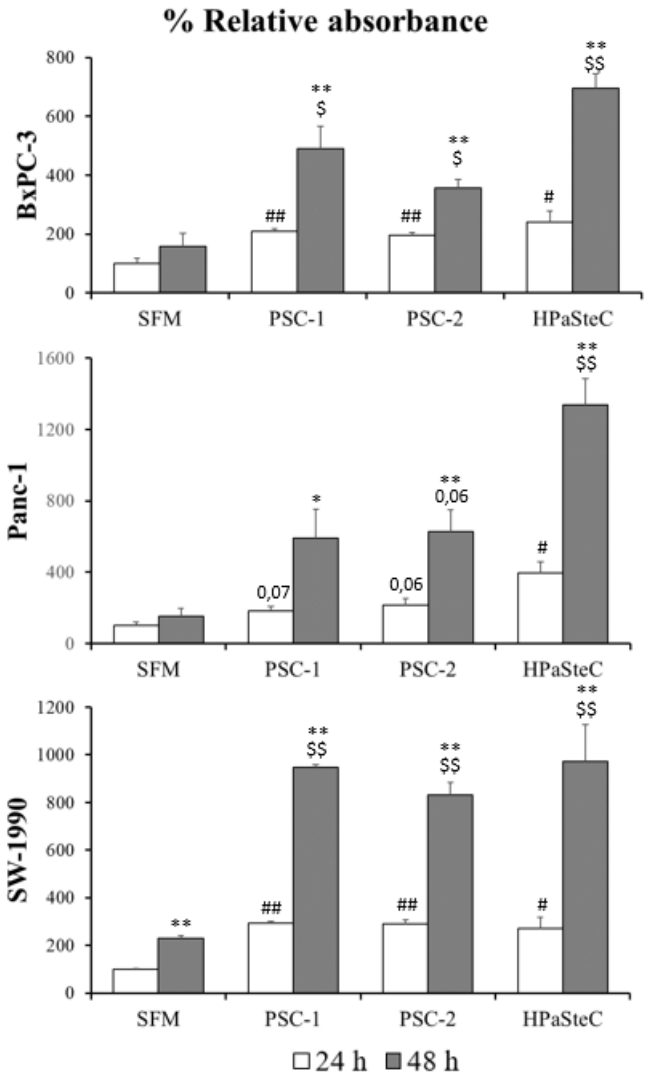

Figure 13: Assessment of lactate secretion under nutrient poor conditions. Briefly 10 000 cells/well were seeded in a 96-well plate and incubated overnight. Next day, the medium was changed to SFM and incubated for 24h and 48h. To measure lactate secretion, a "Glycolysis Cell-Based Assay kit" was used according to the manufacturer's instructions. Data are ± SEM of three replicates. *p<0.05, **p<0.01 comparing 24h to 48h SFM or PSC-CM. #p<0.05, ##p<0.01 comparing 24h SFM vs. PSC-CM. $p<0.05, $$p<0.01 comparing 48h SFM vs. PSC-CM. PCC, pancreatic cancer cells; PSC, pancreatic stellate cells; PSC-CM, PSC-conditioned medium; SFM, serum-free DMEM.

Interestingly, for Panc-1 cells, only treatment with HPaSteC-CM showed a significant increase in lactate secretion at 24h and 48h compared to the SFM controls. However, changes induced by CM from PSC-2 were borderline significant both at 24h and 48h, each with a p-value of 0.06. From 24h to 48h, the only difference was seen for exposure to HPaSteC-CM, which significantly increased lactate secretion from 24h to 48h.

SW-1990 cells showed an increase in lactate secretion when exposed to all three different PSC-CMs after both 24h and 48h compared to the SFM control. Noteworthy, lactate secretion was significantly increased in SW-1990 cells treated with SFM from 24h to 48h, this was similar to the trend seen in figure 12. Furthermore, all PSC-CMs induced a significantly increase in lactate secretion from 24h to 48h.

There was a clear trend in all three cell lines for lactate secretion to be increased from 24h to 48h. Furthermore, SFM seemed to affect lactate secretion only in SW-1990 cells. Noteworthy, there appeared to be an order in which PSC-CM increases the lactate secretion the most: cells exposed HPaSteC-CM seemed to increase lactate secretion the most, followed by CM from PSC-1 and PSC-2.

3.8 Gemcitabine sensitivity

To determine the effect of PSCs on gemcitabine sensitivity in PCCs, we assessed gemcitabine-induced cytotoxicity by measuring MTT-based cell viability in PCCs pre-exposed or not to PSC-CMs. As seen in figure 14, a significant reduction in cell viability, upon exposure to gemcitabine was observed in all three PCCs at SFM controls, albeit at variable levels, with BxPC-3 showing the most (51.6%) and Panc-1 showing the least (29.6%) reduction. The gemcitabine-induced reduction in cell viability was, however, reduced upon incubation with PSC-CM, as can be seen from the higher viability of cells exposed to PSC-CM to SFM following treatment with gemcitabine. The impact of the PSC-CMs on the PCCs was variable. This suggested that all three PSC-CMs induce resistance to gemcitabine at variable levels in different PCCs. Of the three PCCs, SW-1990 showed most resistance to gemcitabine upon incubation with PSC-CM. The results show that in all experiments there was a significant increase in cell viability when treated with all PSC-CMs compared to SFM control (white bars). Moreover, the PSC-CMs induce resistance to gemcitabine in all three PCCs.

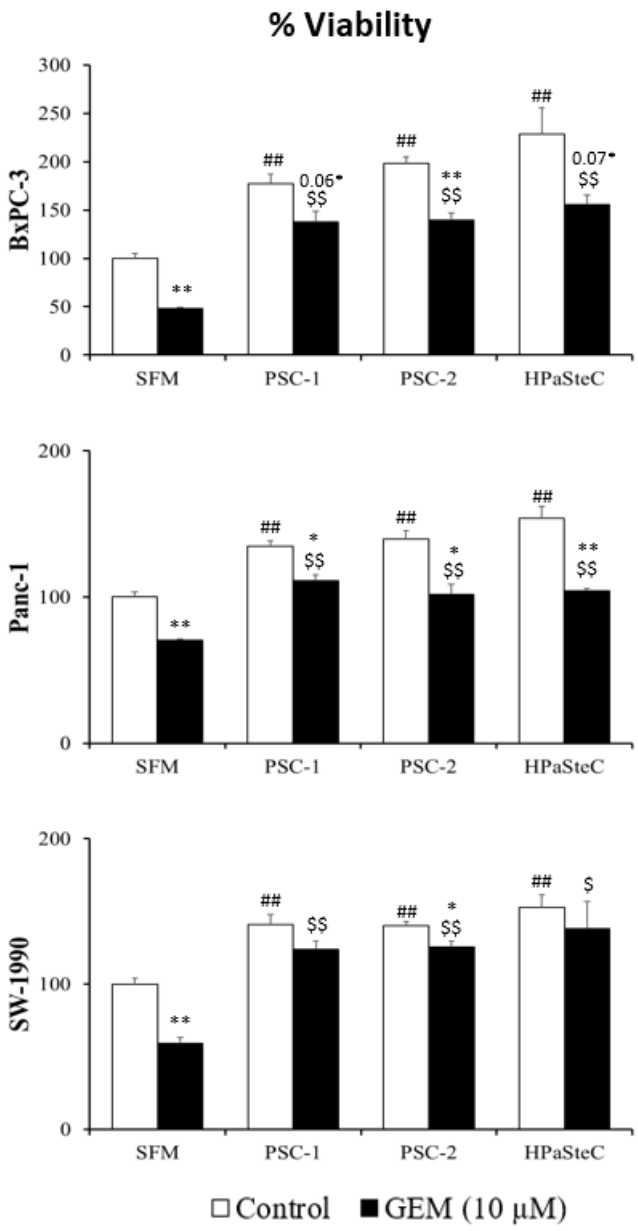

Figure 14: Assessment of gemcitabine cell sensitivity using MTT assay. The PCCs were seeded in a 96-well plate and grown for 72h with either SFM or the conditioned media from PSC-1, PSC-2 or HPaSteC. After the incubation, the PCCs were exposed to gemcitabine for 48h. Lastly, an MTT assay was performed to determine the cell viability following gemcitabine exposure. Absorbance was measured at 570 nm using a spectrophotometer. Data are mean ± SEM of three replicates. *p<0.05, **p<0.01 CTRL vs. gemcitabine. #p<0.05, ##p<0.01 comparing CTRL SFM vs. PSC-CM. $p<0.05, $$p<0.01 comparing gemcitabine SFM vs. PSC-CM. PCC, pancreatic cancer cells; PSC, pancreatic stellate cells; PSC-CM, PSC-conditioned medium; SFM, serum-free DMEM.

3.9 NV-5440 dose-response

To determine the optimal dosage for the glucose transport inhibitor NV-5440, a dose response curve experiment was performed in Panc-1 cells. Figure 15 shows that NV-5440 operates in a dose dependent manner. From 0 to 1 µM, there was no significant change in glucose transport. At 3 µM, glucose transport was almost halved compared to the blank, and it was further reduced by almost 4-fold at 10 µM NV-5440.

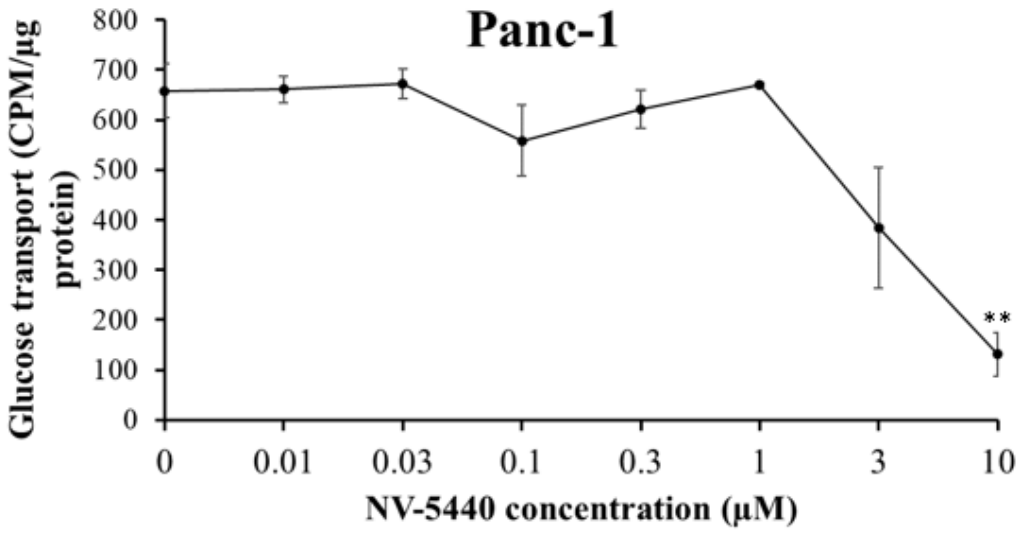

Figure 15: Dose response curve for NV-5440 on Panc-1 cells. Briefly, 10 000 Panc-1 cells/well in a 96-well plate were seeded and incubated overnight. The following day, the media were changed to SFM with indicated concentrations of NV-5440. DMSO (0,1%) was used as 0 concentration. After a 4h incubation, KRH buffer and start solution containing ^{3}H-2-deoxy-DG were added to each well and incubated for 24h. The next day, the experiment was stopped by adding a stop solution. Lastly, the cells were lysed with NaOH, and the CPM was quantified by using a liquid scintillation counter. The amount of ^{3}H-2-deoxy-DG taken up by the cells was directly proportional with the radioactivity from the cell lysates. Data are mean ± SEM of three replicates. **$p<0.01$.

3.10 Glucose transport after PSC-CM exposure *plus* NV5440 and gemcitabine

Next, the effect of NV-5440 and gemcitabine on glucose transport in PCCs pre-exposed to PSC-CM was assessed. BxPC-3 cells pre-exposed to SFM and all three PSCs significantly reduced their glucose transport upon exposure to NV-5440 (Figure 16). Moreover, no significant decrease in glucose transport was observed for BxPC-3 cells pre-incubated with SFM or any of the three PSC-CMs and subsequently exposed to gemcitabine. In Panc-1 cells, both SFM and PSC-CM treated cells, exposed to NV-5440, significantly decreased the glucose transport. Furthermore, only HPaSteC-CM treated Panc-1 cells exposed to gemcitabine showed a significant decrease in glucose transport compared to the DMSO control. Moreover, when comparing SFM and PSC-CM, no significant difference was observed in the ability of PSC-CM to affect glucose transport in control cells or in NV-5440 and gemcitabine treated cells.

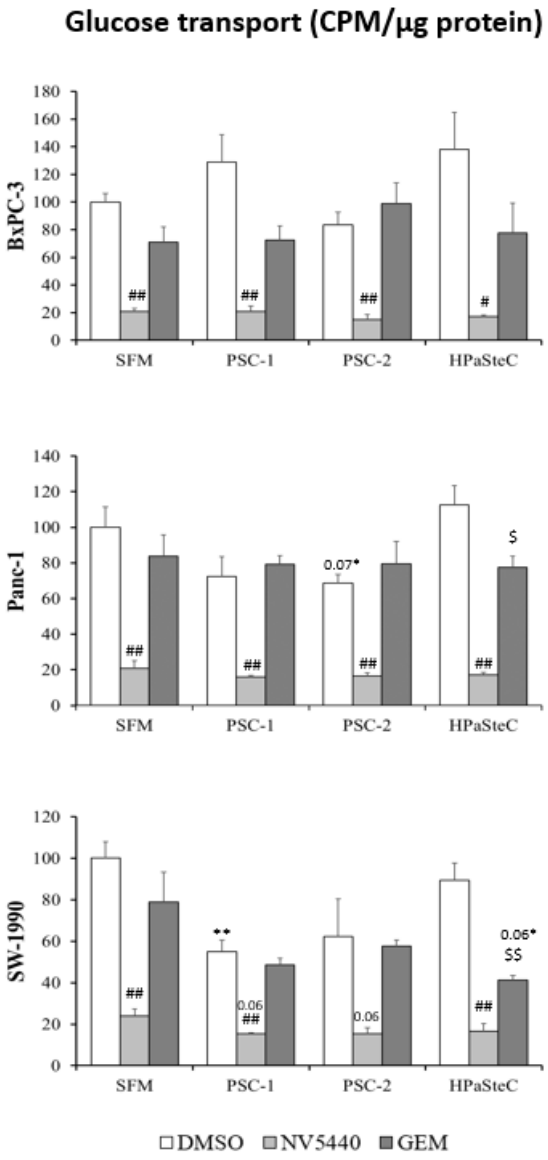

Figure 16: Assessment of glucose transport after PSC-CM exposure and treatment with NV-5440 and gemcitabine. Briefly, 10 000 cells/well of the three PCCs were seeded in three separate plates: control, NV-5440 and gemcitabine. After acclimatization with SFM, media were changed to SFM and the three PSC-CMs and incubated for 72h. Thereafter, media were changed to DMEM containing NV-5440, gemcitabine and DMSO and incubated for 4h. A start solution with ^{3}H-2-deoxy-DG and KRH buffer were then added to all wells and incubated for 24h. Lastly, the cells were lysed with NaOH and the intracellular glucose was quantified using a liquid scintillation counter. Data are mean ± SEM of three replicates. *p<0.05, **p<0.01 comparing SFM vs. PSC-CM for CTRL, NV and GEM. #p<0.05, ##p<0.01 comparing CTRL vs. NV. $p<0.05, $$p<0.01 comparing CTRL vs. GEM. PSC-CM, PSC-conditioned medium; GEM, gemcitabine; PCC, pancreatic cancer cells; PSC, pancreatic stellate cells; SFM, serum-free DMEM; CTRL, control.

SW-1990 cells incubated with SFM or CM from PSC-1 and HPaSteC and subsequently exposed to NV-5440, significantly decreased the glucose transport. In contrast, only SW-1990 cells pre-incubated with HPaSteC-CM and subsequently exposed to gemcitabine significantly decreased glucose transport (Figure 16). SW-1990 cells pre-exposed to CM from PSC-2 and treated with NV-5440 showed a borderline significant decrease in glucose transport. Overall, the glucose inhibitor NV-5440 appeared to be equally effective in decreasing glucose transport in all cell lines. Moreover, the inhibitory effect of NV-5440 on glucose transport was similar for all PSC-CMs and for SFM.

3.11 Western blot

A western blot analysis was performed on PCCs to detect proteins that play a major role in the regulation of metabolism, with a focus on carbon metabolism. In figure 17, BxPC-3 showed a high expression of the glycolysis enzyme Hexokinase-1 (HK-1), while the expression was lower in Panc-1 and SW-1990. All three cell lines exhibited a similar, yet low, expression of monocarboxylate transporter 1 (MCT-1).

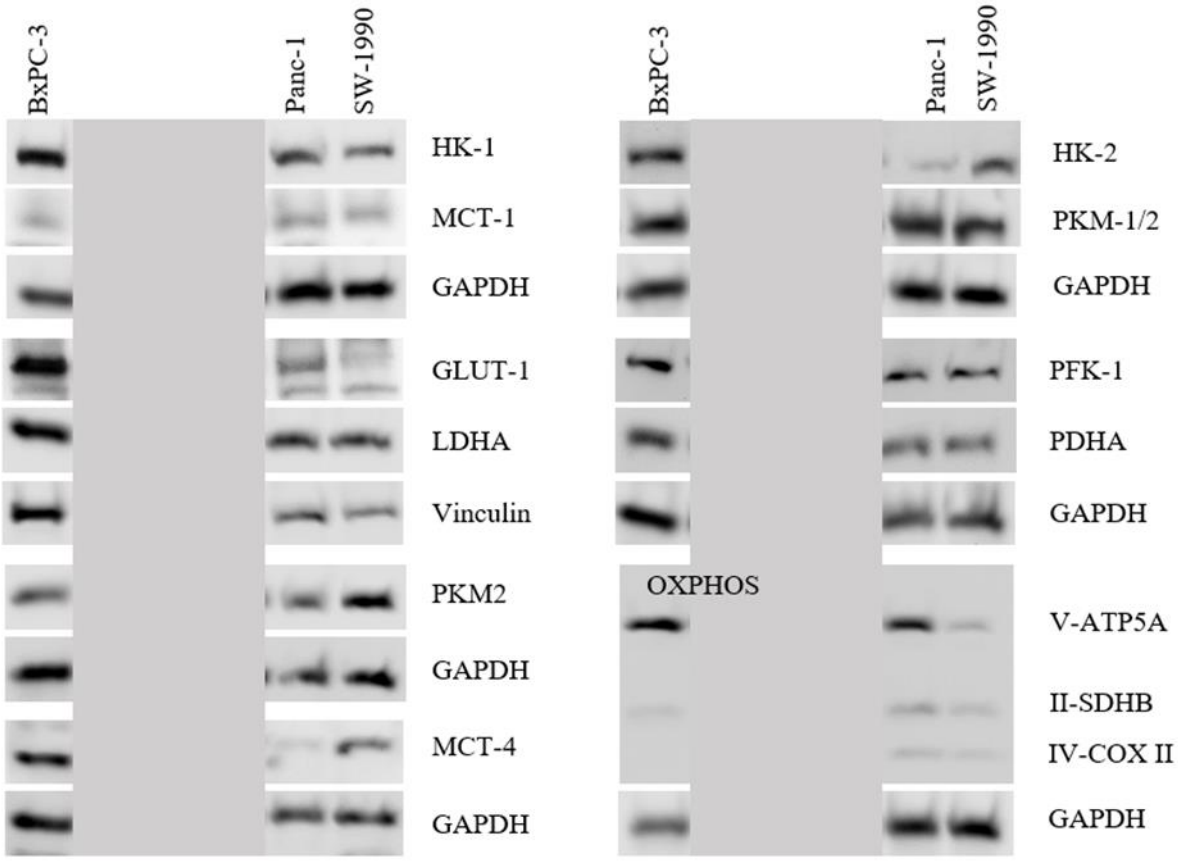

Figure 17: Western blot expression analysis of glucose metabolism related proteins in BxPC-3, Panc-1 and SW-1990 cells. The PCCs were lysed and immunoblotted by using antibodies against HK-1, MCT-1, GLUT-1, LDHA, PKM2, MCT-4, HK-2, PKM-1/2, PFK-1, PDHA, V-ATP5A, II-SDHB and IV-COX II. GAPDH was used as a loading control. PCC, pancreatic cancer cell; OXPHOS, oxidative phosphorylation. Panel marked in grey are three other PDAC cell lines and will not be included here.

Furthermore, BxPC-3 strongly expressed the glucose transporter GLUT-1, lactate dehydrogenase A (LDHA) and vinculin. Both Panc-1 and SW-1990 showed a lower expression of GLUT-1, similar levels of LDHA, while vinculin expression was lower in SW-1990 compared to Panc-1. Pyruvate kinase isozymes M2 (PKM2) on the other hand was strongly

expressed in SW-1990 cells and considerably lower in BxPC-3 and Panc-1 cells. Interestingly, the monocarboxylate transporter 4 (MCT-4) was strongly expressed in BxPC-3 but not expressed in Panc-1. The hexokinase-2 (HK-2) protein was very weakly expressed in Panc-1 cells, but detected in the other two cell lines. PKM-1/2, phosphofructokinase-1 (PFK-1) and pyruvate dehydrogenase A (PDHA) were equally expressed in all three cell lines. With regards to proteins involved in the oxidative phosphorylation pathway, only ATP synthase F1 subunit alpha in complex V (V-ATP5A) was detected, both in BxPC-3 and Panc-1 and at low level also in SW-1990. Complex II succinate dehydrogenase iron-sulfur subunit (II-SDHB) and complex IV cytochrome c oxidase subunit 2 (IV-COX II) were not expressed in BxPC-3 and only weakly expressed in Panc-1 and SW-1990.

3.12 Secretome analysis

Secretome analysis was performed for all three PSC-CMs to identify proteins that were differentially expressed between them. In brief, PSCs cultured to confluence in 10-cm^2 petri-dishes were incubated with SFM for 48h to obtain conditioned medium, as described in figure 18A. The aliquots of PSC-CM obtained from PSC-1, PSC-2 and HPaSteC (5 mL triplicates of each PSC) were subjected to proteomics-based secretome analysis by LC-MS/MS. Proteins were identified and quantified by using the programs Proteome discoverer 2.1 and Mascot 2.6. Furthermore, MaxQuant and Swiss-Prot were used as search engines and search databases, respectively. Ultimately, the secretome analysis was performed by GO annotation, KEGG pathway analysis and STRING network analysis.

From the secretome analysis, a total number of 685 proteins were identified (Figure 18B). Of these, 684 (99.9%) were detected in the CM from HPaSteC. A total of 332 (48.5%) proteins were detected in CM from PSC-1, while only 93 (13.6%) proteins were detected in CM from PSC-2. The difference between the number of proteins detected in the secretome indicates the differential secretive ability of PSCs originating from different sources. Most of these secretory proteins belonged to ECM proteins, for example, plectin, fibronectin, fibrillin, different types of collagen, filamin, myosin, vimentin, vinculin, thrombospondin, and laminin, to name a few.

KEGG pathway analysis was performed using the DAVID bioinformatics tool. All proteins were subjected to analysis, which focused on identifying proteins subgroups that are relevant to known pancreatic cancer related functions. The top five protein clusters were selected based on the protein count and are listed in figure 18C. Almost double the number of proteins were found to be related to metabolic pathways (n=78) as compared to the second pathway on the list - focal adhesion (n=40). Furthermore, a total of 36 proteins identified were linked to the PI3K-Akt signaling pathway, and 24 proteins played a role in ECM-receptor interaction. Interestingly, 25 proteins were identified that could be linked to the carbon metabolism pathway.

We further chose to take a closer look at the carbon metabolism related proteins identified in the secretome. The average label-free quantitation (LFQ) intensity for each of these proteins in CM from PSC-1, PSC-2 and HPaSteC is tabularized in figure 18D. Number zero indicates that expression was below detection level. We found that all 25 carbon metabolism proteins were present in CM from HPaSteC, but at different levels. In CM from PSC-2, only 4 proteins were detected - ALDOA, PSAT1, PKM and TPI1, whereas 17 proteins were identified in CM from PSC-1.

Lastly, a STRING network analysis was performed on these 25 carbon metabolism proteins as presented in figure 18E. Twelve of these proteins were found to be involved in glycolysis (cyan circles), seven proteins belonged to the TCA cycle and LDH activity (pink circles), and two proteins were found to be involved in serine biosynthesis (green circles) and the pentose-phosphate shunt/pathway (yellow circles).

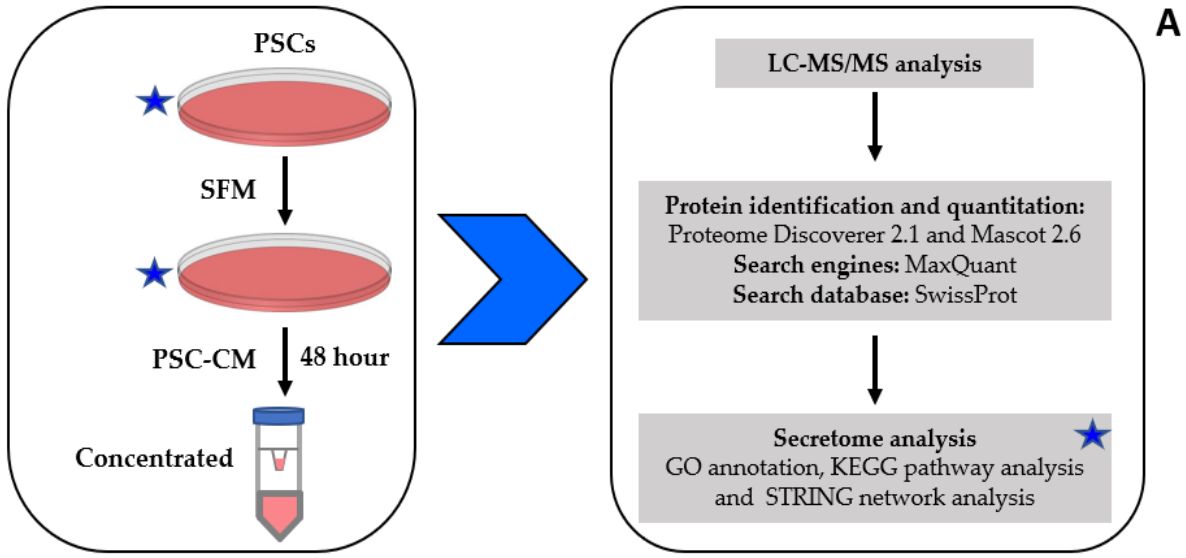

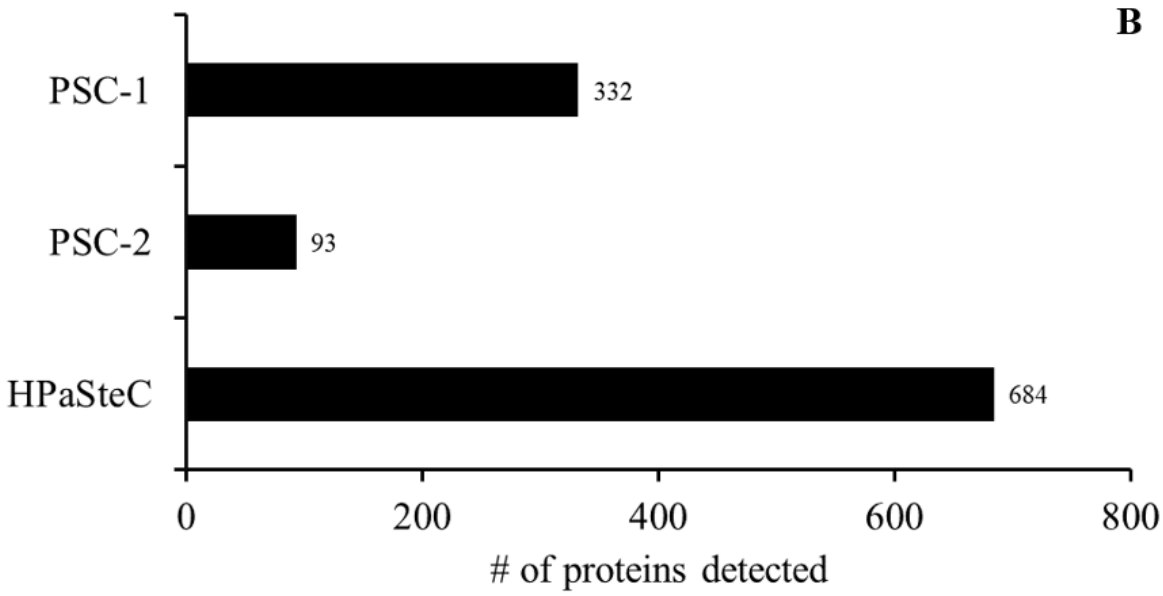

C

Pathway ID	Pathway description	Gene count	FDR
1100	Metabolic pathways	78	5.0E-1
4510	Focal Adhesion	40	3.0E-10
4151	PI3K-Akt signalling pathway	36	3.2E-3
1200	Carbon metabolism	25	9.2E-8
4512	ECM-receptor interaction	24	2.0E-9

D

Gene names	Average LFQ intensity PSC-1	Average LFQ intensity PSC-2	Average LFQ intensity HPaSteC
PGLS	0	0	4536933
ACAT2	0	0	2345533
ADH5	0	0	3522467
ALDOA	11710333	217240	57659333
ALDOC	3510667	0	18518667
ENO1	14796333	0	91468000
ENO2	457867	0	7096367
FH	0	0	8269567
GPI	17987000	0	25241667
GOT1	0	0	9197033
GOT2	0	0	13751333
GAPDH	1875567	0	30282000
IDH1	1015453	0	2736867
MDH1	2371140	0	17835600
MDH2	2281833	0	17741833
ME1	0	0	2103333
PGD	0	0	8200467
PGK1	3370433	0	20216667
PGAM1	11395200	0	31554467
PSAT1	4136267	604700	22630000
PSPH	1229167	0	6587100
PKM	5725500	954633	48629667
TALDO1	1921200	0	15381667
TKT	1008847	0	48787000
TPI1	24008333	9429833	53959900

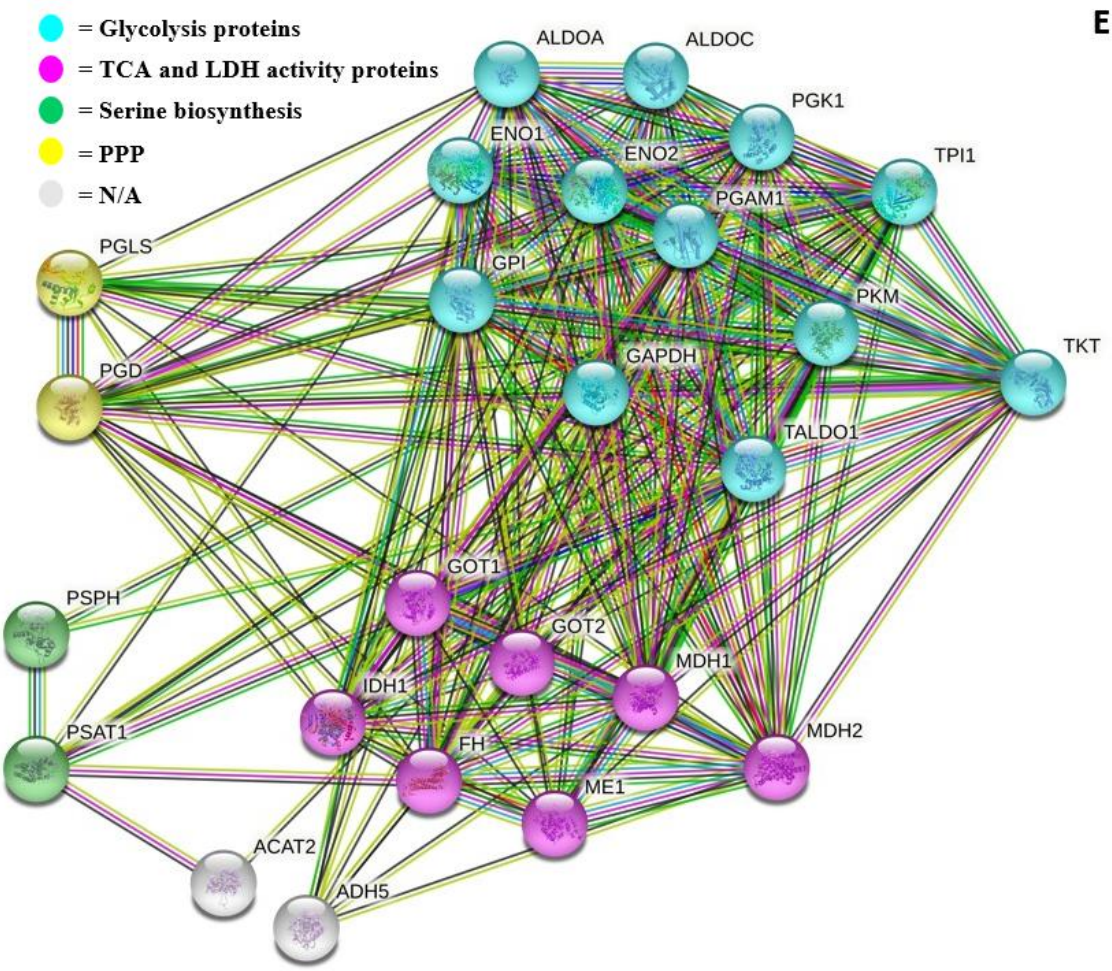

Figure 18: Proteome-based analysis of the pancreatic stellate cell secretome. **A.** A flow chart describing the procedure for sample collection, processing and proteome analysis of PSC-CMs. Blue stars represent steps done at the lab; other steps were performed by the proteomics core facility. **B.** A bar diagram representing the total number of proteins identified in each of the three PSC-CMs by secretome analysis. **C.** The top five enriched KEGG pathways of identified proteins of interest are listed. **D.** A list of 25 proteins involved in carbon metabolism, as identified by KEGG analysis in figure 18C. The table displays gene ID along with the average LFQ intensity in the conditioned medium from PSC-1, PSC-2 and HPaSteC. **E.** A STRING network of the 25 proteins involved in the carbon metabolism**.** PSC, pancreatic stellate cells; SFM, serum free DMEM; GO, gene ontology; KEGG, Kyoto encyclopedia of genes and genomes; PSC-CM, PSC-conditioned medium; STRING, search tool for the retrieval of interacting genes/proteins; PPP, pentose phosphate pathway; N/A, not accounted for.

4. Discussion

Pancreatic ductal adenocarcinoma (PDAC) is the most common type of pancreatic cancer and the deadliest of all cancers. The reported 5-year survival rate lies below 10% and is mostly due to late detection of PDAC, the high metastatic potential, high degree of heterogeneity and profound resistance to existing treatment options [9, 31]. In recent years, the pancreatic stellate cells (PSCs) have been found to be a contributing factor to the progression of PDAC. PSC are the main component in PDAC stroma and can constitute as much as 50% of the stroma [44, 45]. As discussed in section 1.5, activation of PSCs results in the development of the prominent tumor stroma. PSCs have been shown to remodel the tumor stroma in several ways, including mechanical reprogramming of the TME, metabolic remodeling, increased chemoresistance, metastasis, immune tolerance and angiogenesis [46].

The role of PSCs in PDAC progression is an evolving concept, however, over the last years, two main aspects of PDAC biology - the metabolic regulation and the response to existing therapy - have gathered attention. Knowledge about both processes is crucial for a better understanding of disease progression as well as for developing better therapeutics. Several studies have highlighted the role of PSCs in the development of chemoresistance in PDAC [46, 48, 65, 79], however, the exact mechanisms remain unknown. Moreover, some ways in which PSCs promote chemoresistance in PDAC are thought to be through physical barrier mechanisms, reduced bioavailability of drugs, drug scavenging effect and molecular changes induced by PSCs in PCCs [63-65, 80, 81].

Pancreatic tumor cells have high nutrient and energy demands to maintain their active proliferation, however, how they obtain nutrients in the challenging PDAC microenvironment remains to be elucidated [48, 82]. A few recent studies highlighted the importance of PSCs in this process, in which PSCs act as nutrient suppliers to the cancer cells through a process called metabolic rewiring, especially regulating amino acid [56] and lipid metabolism [83]. Moreover, glucose is one of the main cellular energy sources and therefore, the regulation of glucose metabolism is also critical to tumor progression [59]. Recent studies have shown that PDAC has an altered glucose metabolism, which helps cancer cells to grow and actively proliferate despite challenging restrains of the tumor microenvironment [59, 84]. However, the contribution of the PSCs to this process is not clearly understood. Therefore, in this study, we

aimed to investigate the effects of PSCs on PCCs in terms of phenotypic changes, cell proliferation, glucose metabolism, and chemosensitivity.

First, we wanted to investigate the PSC-induced changes in the morphological features and phenotype of the cancer cells, and for this purpose, three PCC lines, BxPC-3, Panc-1 and SW-1990, were exposed to three different CMs, namely from PSC-1, PSC-2 and HPaSteC (Figure 6). Morphological assessment revealed no significant change in the general appearance of any of the PCCs upon exposure with PSC-CMs compared to the SFM controls. In general, both BxPC-3 and Panc-1 appear elongated in shape, however, Panc-1 grows more clustered compared to BxPC-3. SW-1990 cells were circular in shape and appeared to be larger than BxPC-3 and Panc-1. We further analyzed the PCCs in relation to cell number and cell growth area (Figure 7). Noteworthy, this assessment revealed some sort of a pattern to which PSC-CMs induce an increase in cell growth area and numbers. Among the three PSC-CMs, HPaSteC-CM appears most effective in increasing both cell growth area and cell numbers, while PSC-2 was least effective in BxPC-3 and Panc-1 cells. Panc-1 treated with CM from PSC-2 for 72h did not display any change in either cell growth area nor cell numbers. Interestingly, no significant increase in cell growth area was seen in PSC-CM treated SW-1990 cells after 72h compared to 24h, although the cell number was increased during the same time interval. This suggests that SW-1990 cells became smaller from 24h to 72h with PSC-CM treatment. This is also reflected in figure 6. Moreover, PSC-2 was most effective in increasing cell growth area and cell numbers in SW-1990 cells.

The 10 hallmarks of cancer describe the processes that are known to overall increase the viability of cancers [85]. These hallmarks include the ability of cancer cells to sustain proliferative signaling, evasion of growth suppressors, resistance to cell death and attaining replicative immortality [85]. It is therefore no surprise that PCCs in general have increased viable abilities. However, the contribution of PSC-CMs to the growth of PCCs is still an evolving concept. In this context, we investigated the impact of PSC-CM on the PCC's viability (Figure 8). According to our findings, the viability of BxPC-3 significantly increased both at 24h and 72h, upon exposure to PSC-CM, compared to SFM. Moreover, the viability was further increased from 24h to 72h for all three PSC-CMs (Figure 8). Results were variable between Panc-1 and SW-1990, however, Panc-1 cells treated with all PSC-CMs significantly increased their viability after 24h, while SW-1990 cells treated with all PSC-CMs significantly increased their viability at 72h as well as from 24h to 72h. This is in accordance with the previous work

which showed that PSC-CM increases viability of PCCs [86, 87]. Interestingly, CM from PSC-1 increased viability the most across all three PSC-CMs. PSC-1 is considered the one "true and genuine" PSC as it comes from a treatment naïve PDAC patient. This suggests that PSCs from treatment naïve patients supports the increased growth of tumor until treatment is given. This is an interesting feature which needs more investigation.

Sustaining proliferative signaling is one of the hallmarks of cancer [85]. Indeed, all BxPC-3 cells significantly increased proliferation after 72h incubation with the three PSC-CMs, however, in the SFM control proliferation decreased significantly after 72h (Figure 9). This is most likely due to the fact that this is just SFM, which alone does not promote proliferation. Furthermore, SFM alone are unable to keep the cells alive after 72h. The same trend was observed in both Panc-1 and SW-1990 cells, while in SW-1990 cells, no significant difference was seen after 72h incubation with the SFM control. These results suggest that PSC-CM promoted proliferation in PCCs. Interestingly, this effect appeared to be time dependent. After 72h, all PSC-CMs significantly increased the proliferation compared to the SFM control, whereas after 24h, the results were variable. In 2016, Wu et al. showed that PSCs secrete soluble factors such as interleukin-6 (IL-6) and stromal-derived factor 1 alpha (SDF-1α) which induce PDAC cell proliferation in a dose- and time-dependent manner via Nrf2, which activates metabolic reprogramming and detoxification of reactive oxygen species (ROS) [86]. In fact, Nrf2 is upregulated in certain PCC lines, which has proved to have an effect on both proliferation and resistance to drugs [88].

PDAC is increasingly known for its reprogrammed metabolism, therefore, it is of utmost importance to study the contribution of PSCs in the metabolic context of PDAC [48]. Glucose is one of the key metabolites that cancer cells use as an energy source [89]. Among other significant metabolic changes occurring during PDAC development and progression, an alteration of glucose metabolism is increasingly considered critical for pancreatic tumors [59]. However, the contribution of PSCs in the altered glucose metabolism in PDAC tumors is only partially investigated to date [48]. In this context, we first investigated the basal level of glucose transport (i.e., in absence of PSC-CM) over a period of up to 72h in three different PCCs (Figure 10). According to our findings, there was no significant difference in glucose transport for BxPC-3 cells between 8h, 24h and 72h. However, both Panc-1 and SW-1990 showed a significant reduction of glucose transport after 72h. This indicates that after 72h, both Panc-1 and SW-1990 either transport less glucose intracellularly or these cells have reached saturation

at some point thereby decreasing the demand for further glucose transport. Interestingly, the expression of GLUT-1 was higher in BxPC-3 cells compared to Panc-1 and SW-1990, which may explain why BxPC-3 retained similar levels of glucose transport from 8h to 72h (Figure 17).

In general, the glucose transport appeared to peak at 24h (albeit not statistically significant compared to 8h), hence the 24h time-point was chosen for further experiments in the next step, when we investigated whether the exposure to PSC-CM promoted glucose transport in PCCs. Overall, the results showed a great variability both between PSC-CMs and between PCC lines in terms of glucose transport after PSC-CM exposure (Figure 11). After 24h incubation, all PSC-CMs significantly increased glucose transport in both BxPC-3 and Panc-1 cells compared to SFM control. This effect was only seen for CM from PSC-1 in SW-1990 cells. Interestingly, the general notion seems to be that glucose transport decreased with longer incubation time with PSC-CMs (comparing 24h and 72h) In fact, in BxPC-3 and SW-1990, only CM from PSC-2 increased glucose transport after 72h (but the change was significant only in BxPC-3), and in SW-1990 cells this effect was observed only for HPaSteC-CM. Noteworthy, all cells treated with HPaSteC-CM for 72h showed a significant increase in glucose transport compared to SFM control. Interestingly, BxPC-3 had a much higher rate of glucose transport compared to Panc-1 and SW-1990. The difference in the glucose transport between the PCCs could be partially explained by high expression of GLUT1 in BxPC-3 compared to Panc-1 and SW-1990 at basal level (Figure 17). However, the impact of PSCs on the expression of glucose transporters needs to be further investigated. Moreover, the variability between different PSC-CMs in inducing glucose transport in PCCs can be explained by the divergence in numbers and levels of different proteins in the PSC-CMs, which can impact the PCCs in multi-faceted way (Figure 18C). However, this also needs to be further investigated.

Following its transport into the cancer cells, glucose first needs to undergo glycolysis to produce certain breakdown products such as pyruvate, by a process called glycolysis, in order to be utilized for energy production [90]. The Warburg effect is a known phenomenon in cancer, which is an effective way for cancer cells to meet their increased energy demand to maintain proliferation, invasion and metastasis [50]. Normal cells will primarily convert glucose to pyruvate which enters the oxidative phosphorylation and generates ATP for energy in the presence of oxygen, and they will only convert pyruvate to lactate in hypoxic conditions.

However, cancer cells convert almost all pyruvate to lactate, even in the presence of oxygen, which is called the “Warburg effect” (Figure 4) [53].

We therefore aimed to investigate if PSC-CM has an impact on lactate secretion in PCCs. In our findings, all three PSC-CMs significantly increased lactate secretion both after 24h and 72h in both BxPC-3 and Panc-1 cells (Figure 12). In fact, BxPC-3 and Panc-1 followed exactly the same pattern. CM from PSC-1 increased lactate secretion after 24h, while it decreased lactate secretion after 72h (compared to 24h), although only significantly for Panc-1 cells. Furthermore, no significant difference was observed with CM from PSC-2, although lactate secretion was slightly higher after 72h. HPaSteC-CM induced significantly higher lactate secretion after 72h (compared to 24h) in both BxPC-3 (almost 2.5-fold increase) and Panc-1 cells (3-fold increase). Again, there appeared to be some kind of hierarchy as to which extent the PSC-CMs induced a higher rate of lactate secretion. It appeared that HPaSteC-CM was the most effective, while CM from PSC-1 was the least effective in increasing lactate secretion in both BxPC-3 and Panc-1 cells. While lactate secretion was similar for BxPC-3 and Panc-1 cells grown in nutrient-poor LGM, there was a significant increase in lactate secretion after 72h in SW-1990 cells treated with LGM. Moreover, lactate secretion had actually significantly decreased in SW-1990 cells treated with HPaSteC-CM, compared to CM from PSC-1 and PSC-2. Furthermore, the latter significantly increased lactate secretion after 72h compared to LGM, while no significant difference was seen for HPaSteC. However, the change in lactate secretion from 24h to 72h had significantly increased for all three PSC-CMs. Interestingly, the reverse effect was seen in SW-1990, in which HPaSteC-CM was the least effective in inducing lactate secretion, while CM from PSC-1 was most effective. Overall, lactate secretion was highly increased in PCCs treated with PSC-CMs.

The expression of MCT-1 was similar across the three PCCs. However, the expression of MCT-4 was highest in BxPC-3 and lowest in Panc-1 and SW-1990 in between the two (Figure 17). MCTs are responsible for the transport of lactate from inside to outside the cell. However, the amount of lactate secreted was similar between the three PCCs. This indicates that the difference in lactate secretion is seen both between the PCCs, and in PSC-CMs, which was variable in increasing lactate secretion between the PSCs, due to the effect and impact of PSCs on the PCCs. Moreover, lactate secretion was linked with the glucose transport experiment in figure 11. A higher rate of intracellular glucose transport in PCCs would be expected to result in increased lactate secretion. When comparing glucose transport (Figure 11)

and lactate secretion (Figure 12), BxPC-3 reflected this notion for CM from both PSC-1 and PSC-2 but not for HPaSteC-CM. In Panc-1, this was only seen for CM from PSC-1, whereas in SW-1990, this was reflected in the effect of the CM from both PSC-2 and HPaSteC. Interestingly, comparing glucose transport and lactate secretion following exposure of SW-1990 cells to CM from PSC-1, glucose transport was much higher at 24h, while lactate secretion was much higher at 72h. Another interesting theme is the reverse Warburg effect. This states that the cancer cells induce PSC to secrete pyruvate/lactate, which again can be used by the PCCs as fuel required for biological processes [55]. The high lactate secretion seen in BxPC-3 and Panc-1 cells treated with HPaSteC-CM, and in SW-1990 cells exposed to CM from PSC-1 could indicate that these PCCs utilize the reverse Warburg effect. In fact, MCT-4 is found to be upregulated when the reverse Warburg effect is active [53]. However, MCT-4 was differentially expressed in all three PCCs (Figure 17). This again indicates that PSCs affect PCCs in a way that increases the PCCs ability to secrete lactate; this, however, needs to be further investigated.

Next, we wanted to check how PSC-CM affects lactate secretion by PCCs in nutrient-poor conditions - a hallmark of PDAC -, using a low-glucose medium (LGM) for up to 48h. Indeed, in BxPC-3 and SW-1990 cells treated with PSC-CMs, lactate secretion after 24h, 48h and the difference from 24-48h were all significantly elevated (Figure 13). Furthermore, SW-1990 cells treated with SFM instead of PSC-CM also showed elevated levels of lactate secretion after 48h compared to 24h, which is consistent with the results from figure 12. Panc-1 displayed more variability than the other two cell lines, however, Panc-1 cells treated with HPaSteC-CM showed a significant increase in lactate secretion after 24h, 48h and between 24h and 48h. Moreover, there seemed to be a consistent difference between the PSC-CMs in their ability to increase lactate secretion. In all three PCCs, HPaSteC-CM was most efficient in increasing lactate secretion, while PSC-2 was least effective (HPaSteC > PSC-1 > PSC-2). We propose that this is connected with the number of proteins found in the three PSC-CMs, with HPaSteC clearly secreting the most proteins out of the three PSCs. These results corroborate the results in figure 12, demonstrating that PSCs have a profound impact on lactate secretion in PCCs.

It is a known fact that gemcitabine remains the standard drug when it comes to chemotherapeutic treatment of PDAC [32]. However, the benefits are limited due to the rapid development of resistance to gemcitabine [91]. Over the years, several studies have reported how PDAC develops resistance to gemcitabine in respect to cellular pathways and PSCs [62,

91, 92]. However, few studies have focused on gemcitabine resistance in connection with metabolism, particularly, few have investigated whether PSCs affect gemcitabine resistance in the context of glucose metabolism. We therefore performed first, a gemcitabine sensitivity assay to investigate if PSCs affected gemcitabine chemosensitivity in PCCs (Figure 14). All three PCCs showed gemcitabine-induced reduction in cell viability in SFM controls, albeit at variable levels (Panc-1 < SW-1990 < BxPC-3). The gemcitabine sensitivity was reduced upon exposure to PSC-CMs in all PCCs, with a maximum reduction seen in SW-1990 cells. These results indicated PSC-induced resistance to gemcitabine in PCCs. Available literature suggests that factors secreted by PSCs induce resistance to gemcitabine in cancer cells [64, 81, 93]. Our lab has previously shown that PSCs secrete fibronectin which promotes gemcitabine chemoresistance in PCCs by upregulating the activity of the ERK1/2 pathway [65]. In fact, fibronectin was one of the most abundant proteins found in the PSC-CMs as according to the secretome data (data not shown). We therefore propose that the decrease in viability and thus the reduction in sensitivity for gemcitabine in PCCs is partially due to fibronectin secreted by the PSCs. However, more research is needed to further understand how PSCs affect PCCs sensitivity to gemcitabine.

Next, we used the small molecule inhibitor NV-5440 for glucose transport inhibition [94]. The molecular target of NV-5440 is the GLUT-1 transporter, which also selectively inhibits the mTORC1 complex by inhibiting glucose transport [94, 95]. To the best of our knowledge, this is the first investigation into how NV-5440 affects glucose metabolism in PDAC cell lines. The dose response curve showed that NV-5440 operates in a dose-dependent manner in Panc-1 cells (Figure 15). At a concentration of 10 µM, NV-5440 significantly reduced glucose transport by 5.05-fold compared to blank. We therefore chose to use this concentration for further experiments.

Knowing that gemcitabine reduces chemosensitivity in PCCs after being cultured with PSC-CM and that NV-5440 inhibits glucose transport effectively at 10 µM, we wanted to check how NV-5440 and gemcitabine affect glucose transport after exposure to PSC-CM (Figure 16). We expected that glucose transport would be highly reduced in cells treated with NV-5440 after exposure to PSC-CM, due to the fact that NV-5440 selectively inhibits glucose transport. However, gemcitabine works in a different way. Gemcitabine works by inhibiting DNA synthesis and inducing apoptosis [48, 62]. Furthermore, Amrutkar et al. showed in 2020 that PSCs have a minimal uptake of gemcitabine and that PCCs are chemosensitive to gemcitabine

[33]. Therefore, we expected the effect of gemcitabine to be considerably lower than the effect of NV-5440, however, some effect might be seen due to its cytotoxic abilities. The results were clear: in all PCCs treated with NV-5440 after exposure to either SFM or PSC-CM, glucose transport was significantly reduced in all cases except one (PSC-2 SW-1990) as seen in figure 16. However, gemcitabine was not effective in reducing glucose transport, which was as expected. These results show for the first time that the NV-5440 is effective at inhibiting glucose transport in PCCs, even in the presence of PSC-CM. It also shows that gemcitabine does not inhibit glucose transport in PCCs, but by other mechanisms. In fact, in some cases, the glucose transport increased during gemcitabine exposure, albeit insignificantly. Furthermore, a combination of NV-5440 and gemcitabine may prove being an effective treatment option for PDAC in the future due to NV-5440s effect to inhibit glucose transport in PCCs and the ability of gemcitabine to inhibit DNA synthesis and promote apoptosis. However, much further investigation is still needed, both regarding NV-5440 and the impact of PSCs on glucose metabolism.

Glycolysis is the main pathway by which cancer cells acquire cellular energy, by a process named the Warburg effect [54]. Hence, this area of study ought to receive more attention. We therefore explored if any of the key glycolytic enzymes were expressed differently in the PCC lines BxPC-3, Panc-1 and SW-1990. We analyzed by western blot enzymes and proteins that play a key role in glycolysis as well as oxidative phosphorylation (Figure 17): HK-1, MCT-1, GLUT-1, LDHA, PKM2, MCT-4, HK-2, PKM-1/2, PFK-1, PDHA, V-ATP5A, II-SDHB and IV-COX II.

HK-1 and HK-2 regulate the rate limiting first step in the glucose metabolism pathway. HK-2 is in fact known to be elevated in most cancers [96]. HK-1 and HK-2 phosphorylate glucose to glucose-6-phosphate (G6P) [97, 98], In our experiments, we used ^{3}H-2-deoxy-D-glucose, a glucose analog that accumulates intracellularly after being modified by HK-1. HK-1 was expressed higher in BxPC-3 than in Panc-1 and SW-1990, whereas HK-2 was below detectable levels in Panc-1, but strongly expressed in BxPC-3 and expressed in SW-1990 (Figure 17). This could reflect the fact that glucose transport is more elevated in BxPC-3 cells after PSC-CM exposure. HKs may prove to be a valid target for treatment of PDAC due to their key role in glucose metabolism. However, inhibitors that target HKs will also target the HKs of normal cells. In this way, HKs as molecular targets for treatment may prove to be challenging, unless one can find a way to target cancer-specific HKs.

MCT-1 and -4 are responsible for the transport of monocarboxylates across cell membranes via H+ coupled transport, among these monocarboxylates, lactate [99]. The expression of MCT-1 was similarly low in all PCCs, while the expression of MCT-4 was elevated in BxPC-3 cells, present in SW-1990, but not detected in Panc-1 (Figure 17). The differential expression of MCT-4 did not appear to have any striking effect in our experiments. GLUT-1 expression was significantly higher in BxPC-3 cells, low in Panc-1 and even lower in SW-1990 (Figure 17). The high expression in BxPC-3 is backed by the results in figure 11, which show that BxPC-3 has an overall higher transport of glucose.

LDHA is an enzyme that catalyzes the final step in anaerobic glycolysis by converting L-lactate to pyruvate, with the simultaneous conversion of NAD to NADH [100, 101]. LDHA has been known to be upregulated in PDAC and to affect the c-Myc and mTOR pathways [102]- Moreover, a previous study established that LDHA is present in SW-1990 [103]. In our experiments, LDHA was highly expressed in all three PCC lines, albeit highest in BxPC-3 cells (Figure 17). Interestingly, lactate secretion in low glucose medium was higher for both Panc-1 and SW-1990. The presence of LDHA further confirms that PCCs have the ability to convert lactate to pyruvate and use it as energy for biological processes that promote PDAC survival.

PKM2 and PKM1/2 are different isoenzymes of the enzyme pyruvate kinase. PKM2 regulates the last rate limiting step in glycolysis, the conversion of phosphoenolpyruvate (PEP) to pyruvate, but it also functions as a kinase, which is important in tumorigenesis [104]. Furthermore, PKM2 is known to be highly expressed in proliferative tissue, such as cancers, and therefore it may be considered as a biological marker [104-106]. PKM2 was highly expressed in SW-1990, but expression was lower in BxPC-3 and Panc-1 cells (Figure 17). PKM-1/2 were equally highly expressed across all three PCCs. In cancer cells, PKM2 functions as a low catalytic activity dimer. The dimer form promotes synthesis of macromolecules, thereby promoting cancer cell growth and proliferation [104]. As PKM2 plays a role in cancer progression, PKM2 may be a useful target for further treatment options, especially for PDACs that, similar to SW-1990, show a high-level expression of PKM2.

PFK-1 catalyzes the third step in glycolysis, which phosphorylates fructose-6-phosphate (F6P) into fructose-1,6-bisphosphate (F16BP) [107]. PFK have been found to be upregulated in PDAC epithelia and plays a role in the hypoxia-inducible factor (HIF) pathway [102]. PDHA

functions as the bridge and link between glycolysis and the tricarboxylic acid (TCA) cycle and catalyzes the formation of acetyl-CoA from pyruvate [108]. PDHA also implicates the HIF pathway, but could prove to be a much more valuable target for future treatment. PDHA is a part of the pyruvate dehydrogenase complex (PDC), and PDC is directly regulated and inhibited by pyruvate dehydrogenase kinase (PDK) [102]. In fact, a study by Anderson et al. showed that inhibition of PDK in Panc-1 cells proved to activate metabolism via the TCA cycle which reversed the Warburg effect, PDACs main source of energy [102, 109]. This also reduces PDAC viability and proliferation. Both PFK-1 and PDHA are expressed at similar levels in the PCCs, albeit at a higher level in BxPC-3 (Figure 17). Inhibition of PDHA could prove to effectively inhibit PDAC with a high expression of PDHA in the future, however, further research is needed to find out if inhibition of PDHA and activation of the TCA cycle can reverse the Warburg effect and thereby reduce/deny energy available to PCCs.

Lastly, we checked the expression of selected proteins of the OXPHOS. Only V-ATP5A was expressed in considerable amounts in BxPC-3 and Panc-1 cells (Figure 17). V-ATP5A is a subunit of the mitochondrial ATP synthase complex, which generates ATP during OXPHOS by utilizing a proton gradient in the inner membrane of the mitochondria [110]. The presence of V-ATP5A indicates a functional ATP synthase complex. Momose et al. reported that inhibitors of mitochondrial OXPHOS had a cytotoxic effect on Panc-1 cells in nutrient deprived and glucose limiting conditions [102, 111]. This suggests that targeting the mitochondrial OXPHOS may offer a promising antitumor therapy in PDAC cells that express V-ATP5A.

In the end, we performed a secretome analysis on all three PSC-CMs to detect proteins in the CM and to reveal if any proteins are differentially expressed between the CMs (Figure 18A). The PSCs were obtained from two different human PDACs - treatment naive (PSC-1) and neoadjuvantly treated (PSC-2) - and from a healthy donor (HPaSteC). In CM from the three PSCs, we detected a total of 685 proteins (Figure 18B). Out of these, 684 (99.9%) were detected in the CM from HPaSteC. A total of 332 (48.5%) proteins were detected in CM from PSC-1, while only 93 (13.6%) proteins were detected in CM from PSC-2. These results mirror the findings of this study. In general, it seems that HPaSteC-CM had a more profound effect on morphology, proliferation, glucose transport and lactate secretion, while PSC-1 had the most effect on viability. This is most likely due to the fact that HPaSteC secretes over 50% more proteins than PSC-1, and over 85% more proteins than PSC-2. As we do not know exactly how

these proteins in the PSC-CM affect glucose metabolism and chemosensitivity in PCCs, more research is needed.

Next, we performed a KEGG pathway analysis of the secretome proteins and identified the top 5 protein cluster pathways that have implications for PC (Figure 18C). Indeed, 78 out of 685 proteins were identified to be involved in metabolic pathways. A majority of proteins were also found to be involved in focal adhesion and ECM-receptor interaction, these included proteins like fibronectin and collagen, which are crucial to the normal functioning of the cancer cells. Surprisingly, a total of 25 proteins were identified to be involved in carbon metabolism, which involves the glycolysis. This indicates that PSC-CMs express and secrete proteins that are crucial for carbon metabolism. In other words, PSC-CMs may aid cancer cells in positively regulating their carbon metabolism to promote PDAC survival and proliferation. Our lab has previously investigated the secretome of PSC-CMs, however, the focus was not on proteins related to carbon metabolism [65].

We therefore wanted to explore this closer. We generated a table with the average LFQ intensity (i.e., expression) for the 25 proteins identified in each PSC-CM (Figure 18D). As expected, all 25 proteins were detected in HPaSteC-CM, albeit in variable amounts. In CM from PSC-2, only 4 proteins were identified - ALDOA, PSAT1, PKM and TPI1 -, whereas 17 proteins were found in CM from PSC-1. This reflects the results seen in figure 18B, indicating that HPaSteC generally secretes more proteins than the other two PSCs. This is also interesting, as HPaSteC comes from a healthy donor (22-week fetus). At 22 weeks, the pancreas and its stroma are very different from an adult pancreas. The stroma is more voluminous with a different ECM composition, mainly including proteins involved in development of the organ. Hence, it makes sense that CM from HPaSteC contains more proteins than CMs from PSCs form PDAC. Therefore, the types of proteins found in HPaSteC will differ from that found in the PSCs. For instance, cancer-related proteins are not expected to be expressed in HPaSteC-CM. PSC-2, which overall seems to be the least effective, was isolated from a neoadjuvantly treated PDAC (exposed to 4 rounds of FOLFIRINOX), and its CM contained a significantly lower number of proteins compared to the CM from PSC-1. Whether or not exposure to chemotherapy is the reason for the observed limited secretion of proteins into the medium we do not know, but it could be an explanation. Another explanation could be that the TME has been replaced by a non-specific stroma, in which PSCs are less active, due to the regression of the cancer due to chemotherapeutic treatment. PSC-1 originated from treatment-naive PDAC

and it seems to be more active than PSC-2. This makes PSC-1 the only "genuine" PSC, which would probably make the results from this PSC culture the most relevant for understanding the true impact of PSCs on PCCs glucose metabolism and chemosensitivity and for future studies. This is an interesting phenomenon and further investigations are necessary in a larger sample size to know if neoadjuvant treatment actually reduces the secretive ability of PSC. Further investigations are also necessary to understand how "genuine" PSCs, such as PSC-1, effect PCC metabolism and chemosensitivity.

From this list of 25 carbon metabolism proteins, we wanted to see in what branch of carbon metabolism the different proteins group into. Thus, we generated a network map of proteins involved in carbon metabolism and their categories based on their molecular function (Figure 18E). Twelve of the 25 carbon metabolism proteins were found to be involved in glycolysis: ALDOA, ALDOC, ENO1, ENO2, GAPDH, GPI, PGAM1, PGK1, PKM, TALDO1, TKT and TPI1.

Both ALDOA and ALDOC are isozymes of aldolase, which catalyzes the conversion of F16BP to dihydroxyacetone phosphate and glyceraldehyde-3-phosphate (GA3P) [112, 113]. ENO1 and ENO2 are isozymes of enolase, which catalyzes the conversion of 2-phosphoglycerate to phosphoenolpyruvate, the penultimate product of the glycolysis [114-116]. Glyceraldehyde-3-phosphate dehydrogenase (GAPDH) catalyzes the sixth step in glycolysis, which is the conversion of GA3P to 1,3-bisphosphoglycerate (1,3BPG), which also generates two NADH molecules [117]. Glucose-6-phosphate isomerase (GPI) catalyzes the second step in the glycolysis, in which G6P is converted to F6P [118]. Phosphoglycerate mutase (PGAM1) catalyzes the eighth step in glycolysis, the conversion of 3-phosphoglycerate (3PG) to 2-phosphoglycerate (2PG) [119]. Phosphoglycerate kinase 1 (PGK1) catalyzes the seventh and one of the energy generating steps in glycolysis, the conversion of 1,3BPG to 3PG [120]. The common denominator for all these enzymes is that they are key regulators of several steps in the glycolysis.

We hypothesize that these enzymes may be involved in the "reverse Warburg effect" as proposed by Pavlides et al. in 2009 [55]. The reverse Warburg effect postulates that ROS from cancer cells induce aerobic glycolysis in adjacent PSCs. This could also be one reason to why we saw a higher expression of glycolytic enzymes in the PSCs. This ultimately leads to secretion of pyruvate and lactate from the PSCs, which subsequently can be used by the cancer

cells that released the ROS. However, pyruvate and lactate will now enter the TCA cycle in mitochondria where ATP is generated by OXPHOS. In this way, cancer cells bypass the less energy generating glycolysis and use the high energy compounds pyruvate and lactate to generate ATP in a greater yield than by glycolysis [48, 55, 56]. The expression of glycolytic enzymes in the PSCs may also reflect back on to the origin of the PSC cultures in the first place, in which the CM from HPaSteC comes from a 22-week-old fetal donor. This PSC is in the middle of a developmental phase and require energy for developing its organ and other features. This may explain why the expression of glycolytic enzymes was highest in this PSC-CM.

Lastly, we need to interpret the results of our experiments in the light of tumor heterogeneity. Tumor heterogeneity is one of the main reasons why treatment of PDAC is so challenging. Inter-tumor heterogeneity refers to differences between the tumors of individual patients despite the fact that these patients suffer from the same cancer type (e.g. PDAC) [41]. This kind of heterogeneity can be manifest at different levels, including at the metabolomic and stromal level [41]. Indeed, a classification to distinguish metabolic subtypes of PDAC has been proposed. One of these is a glycolytic subtype [121]. These tumors constitute a higher level of intermediates from the glycolytic cycle and would therefore be sensitive to glycolytic and glutamine inhibitors. As Daemen et al.[121] describe, the different subgroups are sensitive to different drugs, depending on the metabolic profile of the tumor [121]. By classifying PDAC tumors into subtypes based on their metabolic profile, one can target each tumor with a specific drug, for which the tumor is known to be sensitive. This could be exploited clinically: If the metabolic subtype is known, one might predict that the tumor is sensitive to a certain type of metabolic inhibitor. In this way, drug targeting various metabolic pathways may become a part of the tool kit on the road to achieve personalized medicine.

Intra-tumor heterogeneity refers to diversity within the same tumor. Intra-tumor heterogeneity can occur within the primary tumor, in the metastases, and even between metastases [42]. In 2007, Nakamura and colleagues even showed that zonal heterogeneity of gene expressions exist in primary tumors [43]. This could indicate that drugs effective against the peripheral part of the tumor, might be ineffective against the central part or vice versa. Even tumor glands lying immediately adjacent to each other have been shown to have different genomic profiles [122]. In the end, tumor heterogeneity is a major problem when it comes to PDAC. Heterogeneity may also be one of the explanations for the substantial degree of variability that was observed between the PSC-CMs in terms of the induction of proliferation,

glucose transport and chemosensitivity. If there was a way to classify all PDACs based on certain characteristics and then administer the best possible treatment option tailored to that particular PDAC, that would be ideal. However, this requires much more extensive investigation and it might not even be possible, due to the profound heterogeneity in PDAC.

Briefly, there are a few limitations to this study. The main limitation is the selection PSCs and PCCs. This is reflected in the results as there are variation between the different PCC lines and a lot of variation between the PSC-CMs especially. *KRAS* is the most common gene that is found to be mutated in PDAC [67]. However, in this study, the PCC line BxPC-3 does not have a *KRAS* mutation and are considered wild type (WT) [67]. On the other hand, Panc-1 and SW-1990 both have KRAS mutations, albeit different mutations [67, 123].

Overall, we have shown that PSC-CMs increase proliferation and viability in PCCs in a way that supports cancer cell survival and tumor growth. Furthermore, PSC-CMs were observed to have a profound effect on the glucose metabolism by secretory proteins that stimulate and promote metabolism in PCCs. Of the three PSC-CMs investigated, the CM from HPaSteC, the PSCs derived from a healthy individual, seems to have the strongest ability to induce proliferation, chemosensitivity and increased glucose transport in PCCs. Moreover, PSC-CMs were shown to induce resistance to gemcitabine in PCCs, thereby altering the chemosensitivity of PCCs for gemcitabine. However, to the best of our knowledge, we demonstrated for the first time that NV-5440 was effective in reducing glucose transport in all PCCs, even when the PCCs were pre-exposed to PSC-CMs. This indicates that NV-5440 may be a potential treatment option, alone or together with other therapeutic agents. This study forms the basis for future investigations into how PSCs affect PCCs metabolism and chemosensitivity. However, more research is needed to truly understand how PSCs affect PCCs metabolism and chemosensitivity and how we can exploit the PSCs to develop better and more effective treatments.

5. References

1. Columbiasurgery. *The pancreas and its functions*. 2016 [cited 2021 Jan]; Available from: https://columbiasurgery.org/pancreas/pancreas-and-its-functions.
2. Britannica, T.E.o.E. *Islets of langerhans*. 1998 26 May 2020 [cited 2021 Jan]; Available from: https://www.britannica.com/science/islets-of-Langerhans.
3. Hopskinsmedicine. *The Pancreas*. 2021 [cited 2021; Available from: https://www.hopkinsmedicine.org/health/conditions-and-diseases/the-pancreas.
4. Yao, W., A. Maitra, and H. Ying, *Recent insights into the biology of pancreatic cancer.* EBioMedicine, 2020. **53**: p. 102655.
5. Rawla, P., T. Sunkara, and V. Gaduputi, *Epidemiology of Pancreatic Cancer: Global Trends, Etiology and Risk Factors.* World J Oncol, 2019. **10**(1): p. 10-27.
6. De Angelis, R., et al., *Cancer survival in Europe 1999-2007 by country and age: results of EUROCARE--5-a population-based study.* Lancet Oncol, 2014. **15**(1): p. 23-34.
7. Hopskinsmedicine. *Pancreatic neuroendocrine tumor*. [cited 2021 Jan]; Available from: https://www.hopkinsmedicine.org/health/conditions-and-diseases/pancreatic-cancer/islet-cell-carcinoma.
8. Hopskinsmedicine. *Pancreatic cancer types*. [cited 2021 Jan]; Available from: https://www.hopkinsmedicine.org/health/conditions-and-diseases/pancreatic-cancer/pancreatic-cancer-types.
9. Sarantis, P., et al., *Pancreatic ductal adenocarcinoma: Treatment hurdles, tumor microenvironment and immunotherapy.* World J Gastrointest Oncol, 2020. **12**(2): p. 173-181.
10. Collaborators, G.B.D.P.C., *The global, regional, and national burden of pancreatic cancer and its attributable risk factors in 195 countries and territories, 1990-2017: a systematic analysis for the Global Burden of Disease Study 2017*. Lancet Gastroenterol Hepatol, 2019. **4**(12): p. 934-947.
11. The Norwegian Cancer Society. *Pancreatic cancer*. 2021 07 Jan 2021 [cited 2021 Jan]; Available from: https://kreftforeningen.no/om-kreft/kreftformer/bukspyttkjertelkreft/.
12. Cancer Registry of Norway. *Key numbers about cancer*. 2019 March 2021 [cited 2021 Jan]; Available from: https://www.kreftregisteret.no/Temasider/om-kreft/.

13. Caner Registry of Norway. *Cancer in Norway 2019 - Cancer incidence, mortality, survival and prevalence in Norway*. 2020 [cited 2021 Jan]; Available from: https://www.kreftregisteret.no/globalassets/cancer-in-norway/2019/cin_report.pdf.
14. Paluszkiewicz, P., et al., *Main dietary compounds and pancreatic cancer risk. The quantitative analysis of case-control and cohort studies.* Cancer Epidemiol, 2012. **36**(1): p. 60-7.
15. Wang, H., et al., *Survival of pancreatic cancer patients is negatively correlated with age at diagnosis: a population-based retrospective study.* Sci Rep, 2020. **10**(1): p. 7048.
16. Batabyal, P., et al., *Association of diabetes mellitus and pancreatic adenocarcinoma: a meta-analysis of 88 studies.* Ann Surg Oncol, 2014. **21**(7): p. 2453-62.
17. Pezzilli, R. and N. Pagano, *Is diabetes mellitus a risk factor for pancreatic cancer?* World J Gastroenterol, 2013. **19**(30): p. 4861-6.
18. McAuliffe, J.C. and J.D. Christein, *Type 2 diabetes mellitus and pancreatic cancer.* Surg Clin North Am, 2013. **93**(3): p. 619-27.
19. Haugvik, S.P., et al., *Diabetes, smoking, alcohol use, and family history of cancer as risk factors for pancreatic neuroendocrine tumors: a systematic review and meta-analysis.* Neuroendocrinology, 2015. **101**(2): p. 133-42.
20. Stevens, R.J., A.W. Roddam, and V. Beral, *Pancreatic cancer in type 1 and young-onset diabetes: systematic review and meta-analysis.* Br J Cancer, 2007. **96**(3): p. 507-9.
21. Kim, V.M. and N. Ahuja, *Early detection of pancreatic cancer.* Chin J Cancer Res, 2015. **27**(4): p. 321-31.
22. MayoClinic. *Pancreatic cancer - Diagnosis and Treatment*. 2020 [cited 2021 Jan]; Available from: https://www.mayoclinic.org/diseases-conditions/pancreatic-cancer/diagnosis-treatment/drc-20355427.
23. Pal, T., et al., *Points to consider: is there evidence to support BRCA1/2 and other inherited breast cancer genetic testing for all breast cancer patients? A statement of the American College of Medical Genetics and Genomics (ACMG).* Genet Med, 2020. **22**(4): p. 681-685.
24. Patel, H., et al., *Current Advances in the Treatment of BRAF-Mutant Melanoma.* Cancers (Basel), 2020. **12**(2).
25. Amundadottir, L.T., *Pancreatic Cancer Genetics.* Int J Biol Sci, 2016. **12**(3): p. 314-25.

26. Pancreatic Cancer Action Network. *Treatment types*. [cited 2021 Jan]; Available from: https://www.pancan.org/facing-pancreatic-cancer/treatment/treatment-types/.
27. Springfeld, C., et al., *Chemotherapy for pancreatic cancer*. Presse Med, 2019. **48**(3 Pt 2): p. e159-e174.
28. Hopskinsmedicine. *Chemotherapy for pancreatic cancer*. [cited Jan 2021; Available from: https://www.hopkinsmedicine.org/health/conditions-and-diseases/pancreatic-cancer/chemotherapy-for-pancreatic-cancer.
29. Conroy, T., et al., *FOLFIRINOX versus gemcitabine for metastatic pancreatic cancer*. N Engl J Med, 2011. **364**(19): p. 1817-25.
30. Von Hoff, D.D., et al., *Increased survival in pancreatic cancer with nab-paclitaxel plus gemcitabine.* N Engl J Med, 2013. **369**(18): p. 1691-703.
31. Mizrahi, J.D., et al., *Pancreatic cancer.* Lancet, 2020. **395**(10242): p. 2008-2020.
32. Burris, H.A., 3rd, et al., *Improvements in survival and clinical benefit with gemcitabine as first-line therapy for patients with advanced pancreas cancer: a randomized trial.* J Clin Oncol, 1997. **15**(6): p. 2403-13.
33. Amrutkar, M., et al., *Differential Gemcitabine Sensitivity in Primary Human Pancreatic Cancer Cells and Paired Stellate Cells Is Driven by Heterogenous Drug Uptake and Processing.* Cancers (Basel), 2020. **12**(12).
34. Pancreatic Cancer Action Network. *Radiation Therapy*. [cited 2021 Jan]; Available from: https://www.pancan.org/facing-pancreatic-cancer/treatment/treatment-types/radiation-therapy/.
35. American Cancer Society. *Radiation therapy for pancreatic cancer*. 2019 [cited Jan 2021]; Available from: https://www.cancer.org/cancer/pancreatic-cancer/treating/radiation-therapy.html.
36. Hopskinsmedicine. *Radiation therapy for pancreatic cancer*. [cited 2021 Jan]; Available from: https://www.hopkinsmedicine.org/health/conditions-and-diseases/pancreatic-cancer/radiation-therapy-for-pancreatic-cancer.
37. Amrutkar, M., et al., *Establishment and Characterization of Paired Primary Cultures of Human Pancreatic Cancer Cells and Stellate Cells Derived from the Same Tumor*. Cells, 2020. **9**(1).
38. Liang, C., et al., *Complex roles of the stroma in the intrinsic resistance to gemcitabine in pancreatic cancer: where we are and where we are going.* Exp Mol Med, 2017. **49**(12): p. e406.

39. Murakami, T., et al., *Role of the tumor microenvironment in pancreatic cancer.* Ann Gastroenterol Surg, 2019. **3**(2): p. 130-137.
40. Ho, W.J., E.M. Jaffee, and L. Zheng, *The tumour microenvironment in pancreatic cancer - clinical challenges and opportunities.* Nat Rev Clin Oncol, 2020. **17**(9): p. 527-540.
41. Cros, J., et al., *Tumor Heterogeneity in Pancreatic Adenocarcinoma.* Pathobiology, 2018. **85**(1-2): p. 64-71.
42. Verbeke, C., *Morphological heterogeneity in ductal adenocarcinoma of the pancreas - Does it matter?* Pancreatology, 2016. **16**(3): p. 295-301.
43. Nakamura, T., et al., *Zonal heterogeneity for gene expression in human pancreatic carcinoma.* Cancer Res, 2007. **67**(16): p. 7597-604.
44. Phillips, P., *Pancreatic stellate cells and fibrosis*, in *Pancreatic Cancer and Tumor Microenvironment*, P.J. Grippo and H.G. Munshi, Editors. 2012: Trivandrum (India).
45. Schnittert, J., R. Bansal, and J. Prakash, *Targeting Pancreatic Stellate Cells in Cancer.* Trends Cancer, 2019. **5**(2): p. 128-142.
46. Wu, Y., et al., *The Role of Stellate Cells in Pancreatic Ductal Adenocarcinoma: Targeting Perspectives.* Front Oncol, 2020. **10**: p. 621937.
47. Bynigeri, R.R., et al., *Pancreatic stellate cell: Pandora's box for pancreatic disease biology.* World J Gastroenterol, 2017. **23**(3): p. 382-405.
48. Amrutkar, M. and I.P. Gladhaug, *Stellate Cells Aid Growth-Permissive Metabolic Reprogramming and Promote Gemcitabine Chemoresistance in Pancreatic Cancer.* Cancers (Basel), 2021. **13**(4).
49. D. Nelson and M. Cox, *Principles of metabolic regulation*, in *Lehninger - Principles of biochemistry*. 2017. p. 575-618.
50. Amoedo, N.D., et al., *How does the metabolism of tumour cells differ from that of normal cells.* Biosci Rep, 2013. **33**(6).
51. Kalyanaraman, B., *Teaching the basics of cancer metabolism: Developing antitumor strategies by exploiting the differences between normal and cancer cell metabolism.* Redox Biol, 2017. **12**: p. 833-842.
52. D. Nelson and M. Cox, *Oxidative Phosphorylation*, in *Lehninger - Principles of Biochemistry*. 2017. p. 711-754.
53. Paolicchi, E., et al., *Targeting hypoxic response for cancer therapy.* Oncotarget, 2016. **7**(12): p. 13464-78.

54. Liberti, M.V. and J.W. Locasale, *The Warburg Effect: How Does it Benefit Cancer Cells?* Trends Biochem Sci, 2016. **41**(3): p. 211-218.
55. Pavlides, S., et al., *The reverse Warburg effect: aerobic glycolysis in cancer associated fibroblasts and the tumor stroma.* Cell Cycle, 2009. **8**(23): p. 3984-4001.
56. Fu, Y., et al., *The reverse Warburg effect is likely to be an Achilles' heel of cancer that can be exploited for cancer therapy.* Oncotarget, 2017. **8**(34): p. 57813-57825.
57. Qin, C., et al., *Metabolism of pancreatic cancer: paving the way to better anticancer strategies.* Mol Cancer, 2020. **19**(1): p. 50.
58. Camelo, F. and A. Le, *The Intricate Metabolism of Pancreatic Cancers.* Adv Exp Med Biol, 2018. **1063**: p. 73-81.
59. Yan, L., et al., *Glucose Metabolism in Pancreatic Cancer.* Cancers (Basel), 2019. **11**(10).
60. Sousa, C.M., et al., *Pancreatic stellate cells support tumour metabolism through autophagic alanine secretion.* Nature, 2016. **536**(7617): p. 479-83.
61. Weinberg, R., *The Rational Treatment of Cancer*, in *The biology of Cancer*. 2014, Garland Science. p. 832.
62. Amrutkar, M. and I.P. Gladhaug, *Pancreatic Cancer Chemoresistance to Gemcitabine.* Cancers (Basel), 2017. **9**(11).
63. Hessmann, E., et al., *Fibroblast drug scavenging increases intratumoural gemcitabine accumulation in murine pancreas cancer.* Gut, 2018. **67**(3): p. 497-507.
64. Hesler, R.A., et al., *TGF-beta-induced stromal CYR61 promotes resistance to gemcitabine in pancreatic ductal adenocarcinoma through downregulation of the nucleoside transporters hENT1 and hCNT3.* Carcinogenesis, 2016. **37**(11): p. 1041-1051.
65. Amrutkar, M., et al., *Secretion of fibronectin by human pancreatic stellate cells promotes chemoresistance to gemcitabine in pancreatic cancer cells.* BMC Cancer, 2019. **19**(1): p. 596.
66. American Type Culture Collection. [cited 2021 Feb]; Available from: https://www.lgcstandards-atcc.org/?geo_country=no.
67. Deer, E.L., et al., *Phenotype and genotype of pancreatic cancer cell lines.* Pancreas, 2010. **39**(4): p. 425-35.
68. Lenggenhager, D., et al., *Commonly Used Pancreatic Stellate Cell Cultures Differ Phenotypically and in Their Interactions with Pancreatic Cancer Cells.* Cells, 2019. **8**(1).

69. ThermoFisher. *Freezing cells*. [cited 2021; Available from: https://www.thermofisher.com/no/en/home/references/gibco-cell-culture-basics/cell-culture-protocols/freezing-cells.html.
70. Sciencedirect. *3-(4,5-dimethylthiazol-2-yl)-2,5-diphenyltetrazolium Bromide (MTT)*. [cited 2021; Available from: https://www-sciencedirect-com.ezproxy.uio.no/topics/chemistry/3-4-5-dimethylthiazol-2-yl-2-5-diphenyltetrazolium-bromide.
71. Abcam. *ab126556 BrdU Cell Proliferation ELISA Kit (Colorimetric)*. 2020 16 Nov 2020 [cited 2021; 9:[Available from: https://www.abcam.com/ps/products/126/ab126556/documents/brdu-cell-proliferation-elisa-kit-protocol-book-v9-ab126556%20(website).pdf.
72. Tanti, J.F., et al., *Assays of glucose entry, glucose transporter amount, and translocation.* Methods Mol Biol, 2001. **155**: p. 157-65.
73. PerkinElmer. *Liquid Scintillation Counting*. [cited 2021; Available from: https://www.perkinelmer.com/no/lab-products-and-services/application-support-knowledgebase/radiometric/liquid-scintillation-counting.html.
74. CaymanChemical. *Glycolysis Cell-Based Assay kit*. 2017; Available from: https://www.caymanchem.com/pdfs/600450.pdf.
75. CaymanChemical. *Glucose Colorimetric Assay Kit*. 2017; Available from: https://www.caymanchem.com/pdfs/10009582.pdf.
76. Kanehisa, M. and S. Goto, *KEGG: kyoto encyclopedia of genes and genomes.* Nucleic Acids Res, 2000. **28**(1): p. 27-30.
77. Dennis, G., Jr., et al., *DAVID: Database for Annotation, Visualization, and Integrated Discovery.* Genome Biol, 2003. **4**(5): p. P3.
78. Huang da, W., B.T. Sherman, and R.A. Lempicki, *Systematic and integrative analysis of large gene lists using DAVID bioinformatics resources.* Nat Protoc, 2009. **4**(1): p. 44-57.
79. McCarroll, J.A., et al., *Role of pancreatic stellate cells in chemoresistance in pancreatic cancer.* Front Physiol, 2014. **5**: p. 141.
80. Adamska, A., et al., *Molecular and cellular mechanisms of chemoresistance in pancreatic cancer.* Adv Biol Regul, 2018. **68**: p. 77-87.
81. Dalin, S., et al., *Deoxycytidine Release from Pancreatic Stellate Cells Promotes Gemcitabine Resistance.* Cancer Res, 2019. **79**(22): p. 5723-5733.

82. Derle, A., et al., *The role of metabolic adaptation to nutrient stress in pancreatic cancer.* Cell Stress, 2018. **2**(12): p. 332-339.
83. Sunami, Y., A. Rebelo, and J. Kleeff, *Lipid Metabolism and Lipid Droplets in Pancreatic Cancer and Stellate Cells.* Cancers (Basel), 2017. **10**(1).
84. Stopa, K.B., et al., *Pancreatic Cancer and Its Microenvironment-Recent Advances and Current Controversies.* Int J Mol Sci, 2020. **21**(9).
85. Hanahan, D. and R.A. Weinberg, *Hallmarks of cancer: the next generation.* Cell, 2011. **144**(5): p. 646-74.
86. Wu, Y.S., et al., *Soluble factors from stellate cells induce pancreatic cancer cell proliferation via Nrf2-activated metabolic reprogramming and ROS detoxification.* Oncotarget, 2016. **7**(24): p. 36719-36732.
87. Marzoq, A.J., et al., *Impact of the secretome of activated pancreatic stellate cells on growth and differentiation of pancreatic tumour cells.* Sci Rep, 2019. **9**(1): p. 5303.
88. Lister, A., et al., *Nrf2 is overexpressed in pancreatic cancer: implications for cell proliferation and therapy.* Mol Cancer, 2011. **10**: p. 37.
89. Lin, X., et al., *Glucose Metabolism on Tumor Plasticity, Diagnosis, and Treatment.* Front Oncol, 2020. **10**: p. 317.
90. Cao, L., et al., *Glycometabolic rearrangements--aerobic glycolysis in pancreatic cancer: causes, characteristics and clinical applications.* J Exp Clin Cancer Res, 2020. **39**(1): p. 267.
91. Quinonero, F., et al., *The challenge of drug resistance in pancreatic ductal adenocarcinoma: a current overview.* Cancer Biol Med, 2019. **16**(4): p. 688-699.
92. Zhang, H., et al., *Paracrine SDF-1alpha signaling mediates the effects of PSCs on GEM chemoresistance through an IL-6 autocrine loop in pancreatic cancer cells.* Oncotarget, 2015. **6**(5): p. 3085-97.
93. Liu, Y., et al., *Periostin promotes the chemotherapy resistance to gemcitabine in pancreatic cancer.* Tumour Biol, 2016. **37**(11): p. 15283-15291.
94. Kang, S.A., et al., *Discovery of Small-Molecule Selective mTORC1 Inhibitors via Direct Inhibition of Glucose Transporters.* Cell Chem Biol, 2019. **26**(9): p. 1203-1213 e13.
95. Reckzeh, E.S. and H. Waldmann, *Development of Glucose Transporter (GLUT) Inhibitors.* European J Org Chem, 2020. **2020**(16): p. 2321-2329.

96. Patra, K.C., et al., *Hexokinase 2 is required for tumor initiation and maintenance and its systemic deletion is therapeutic in mouse models of cancer.* Cancer Cell, 2013. **24**(2): p. 213-228.
97. Okur, V., et al., *De novo variants in HK1 associated with neurodevelopmental abnormalities and visual impairment.* Eur J Hum Genet, 2019. **27**(7): p. 1081-1089.
98. Cheung, E.C., R.L. Ludwig, and K.H. Vousden, *Mitochondrial localization of TIGAR under hypoxia stimulates HK2 and lowers ROS and cell death.* Proc Natl Acad Sci U S A, 2012. **109**(50): p. 20491-6.
99. Fisel, P., E. Schaeffeler, and M. Schwab, *Clinical and Functional Relevance of the Monocarboxylate Transporter Family in Disease Pathophysiology and Drug Therapy.* Clin Transl Sci, 2018. **11**(4): p. 352-364.
100. Nelson, D.C., M, *14.3 Fates of pyruvate under anaerobic conditions: Fermentation*, in *Lehninger - Principles of biochemistry*. 2017: W.H Freeman and company. p. 553.
101. Cui, B., et al., *Stress-induced epinephrine enhances lactate dehydrogenase A and promotes breast cancer stem-like cells.* J Clin Invest, 2019. **129**(3): p. 1030-1046.
102. Chan, A.K., J.I. Bruce, and A.K. Siriwardena, *Glucose metabolic phenotype of pancreatic cancer.* World J Gastroenterol, 2016. **22**(12): p. 3471-85.
103. Kyriazis, A.P., et al., *Establishment and characterization of human pancreatic adenocarcinoma cell line SW-1990 in tissue culture and the nude mouse.* Cancer Res, 1983. **43**(9): p. 4393-401.
104. Zahra, K., et al., *Pyruvate Kinase M2 and Cancer: The Role of PKM2 in Promoting Tumorigenesis.* Front Oncol, 2020. **10**: p. 159.
105. Nandi, S., et al., *Structural basis for allosteric regulation of pyruvate kinase M2 by phosphorylation and acetylation.* J Biol Chem, 2020. **295**(51): p. 17425-17440.
106. Prakasam, G., et al., *Posttranslational Modifications of Pyruvate Kinase M2: Tweaks that Benefit Cancer.* Front Oncol, 2018. **8**: p. 22.
107. Nelson, D.C., M, *14.1 Glycolysis*, in *Lehninger - Principles of biochemistry*. 2017, W.H Freeman and Company. p. 539.
108. Lazzarino, G., et al., *Pyruvate Dehydrogenase and Tricarboxylic Acid Cycle Enzymes Are Sensitive Targets of Traumatic Brain Injury Induced Metabolic Derangement.* Int J Mol Sci, 2019. **20**(22).
109. Anderson, K.M., et al., *In vitro effects of dichloroacetate and CO2 on hypoxic HeLa cells.* Anticancer Res, 2009. **29**(11): p. 4579-88.

110. NCBI. *ATP5F1A ATP synthase F1 subunit alpha [Homo sapiens (human)]*. [cited 2021 02 may]; Available from: https://www.ncbi.nlm.nih.gov/gene/498.
111. Momose, I., et al., *Mitochondrial inhibitors show preferential cytotoxicity to human pancreatic cancer PANC-1 cells under glucose-deprived conditions.* Biochem Biophys Res Commun, 2010. **392**(3): p. 460-6.
112. NCBI. *ALDOC aldolase, fructose-bisphosphate C [Homo sapiens (human)]*. [cited 2021 30 apr]; Available from: https://www.ncbi.nlm.nih.gov/gene/230.
113. NCBI. *ALDOA aldolase, fructose-bisphosphate A [Homo sapiens (human)]*. [cited 2021 30 apr]; Available from: https://www.ncbi.nlm.nih.gov/gene/226.
114. Uniprot. *UniProtKB - P06733 (ENOA_HUMAN)*. [cited 2021 30 apr]; Available from: https://www.uniprot.org/uniprot/P06733.
115. NCBI. *ENO1 enolase 1 [Homo sapiens (human)]*. [cited 2021 30 apr]; Available from: https://www.ncbi.nlm.nih.gov/gene/2023.
116. NCBI. *ENO2 enolase 2 [Homo sapiens (human)]*. [cited 2021 30 apr]; Available from: https://www.ncbi.nlm.nih.gov/gene/2026.
117. Nelson, D.C., M, *The payoff phase of glycolysis yields ATP and NADH*, in *Lehninger - Principles of biochemistry*. 2017, W.H Freeman and company. p. 541-542.
118. Uniprot. *UniProtKB - P06744 (G6PI_HUMAN)*. [cited 2021 30 apr]; Available from: https://www.uniprot.org/uniprot/P06744.
119. Nelson, D.C., M, *The payoff phase of glycolysis yields ATP and NADH*, in *Lehninger - Principles of biochemistry*. 2017, W.H Freeman and company. p. 544.
120. Nelson, D.C., M, *The payoff phase of glycolysis yields ATP and NADH*, in *Lehninger - principles of biochemistry*. 2017, W.H Freeman and company. p. 542-543.
121. Daemen, A., et al., *Metabolite profiling stratifies pancreatic ductal adenocarcinomas into subtypes with distinct sensitivities to metabolic inhibitors.* Proc Natl Acad Sci U S A, 2015. **112**(32): p. E4410-7.
122. Harada, T., et al., *Interglandular cytogenetic heterogeneity detected by comparative genomic hybridization in pancreatic cancer.* Cancer Res, 2002. **62**(3): p. 835-9.
123. Fujimura, K., et al., *KRAS Oncoprotein Expression Is Regulated by a Self-Governing eIF5A-PEAK1 Feed-Forward Regulatory Loop.* Cancer Res, 2018. **78**(6): p. 1444-1456.